

Medical University of South Carolina

MEDICA

MUSC Theses and Dissertations

Fall 11-14-2023

PCBP1 Regulates LIFR Through FAM3C to Maintain Breast Cancer Stem Cell Self-Renewal and Invasiveness

William S. Streitfeld

Medical University of South Carolina

Follow this and additional works at: <https://medica-musc.researchcommons.org/theses>



Part of the [Cancer Biology Commons](#), and the [Cell Biology Commons](#)

Recommended Citation

Streitfeld, William S., "PCBP1 Regulates LIFR Through FAM3C to Maintain Breast Cancer Stem Cell Self-Renewal and Invasiveness" (2023). *MUSC Theses and Dissertations*. 824.

<https://medica-musc.researchcommons.org/theses/824>

This Dissertation is brought to you for free and open access by MEDICA. It has been accepted for inclusion in MUSC Theses and Dissertations by an authorized administrator of MEDICA. For more information, please contact medica@musc.edu.

PCBP1 Regulates LIFR Through FAM3C to Maintain
Breast Cancer Stem Cell Self-Renewal and Invasiveness

By

William Scott Streitfeld

A dissertation submitted to the faculty of the Medical University of South Carolina in
partial fulfillment of the requirements for the degree of Doctor of Philosophy in the
College of Graduate Studies.

Department of Biochemistry and Molecular Biology

November 14, 2023

Approved by:

Chairman:

Philip Howe

Advisory Committee:

Joseph Delaney

Jorge Munera

Lauren Ball

Visu Palanisamy

Acknowledgements

I spent a considerable amount of time pursuing my academic degrees. On multiple occasions, I decided to continue my education by enrolling in yet another academic program. Although I will never stop learning, I would like to take this opportunity to reflect on the fact that the completion of this degree signifies the end of my formal education, and I would like to thank some of the people who were integral to my reaching this milestone.

I would like to thank my PhD mentor, Dr. Philip Howe, for his generous support during the time I worked in his lab. Dr. Howe provided a laboratory environment that was like a dream come true for an aspiring student such as myself. I was allowed to explore independent experimentation, and received scientific guidance and financial support that allowed me to provide a substantial body of work. Dr. Howe also provided an excellent example of success in biomedical science research and frequently took the time to discuss my progress and provide input in both scientific and professional arenas. I learned how to observe “between the lines” from Dr. Howe. I would also like to thank the other members of the Howe lab for providing an excellent level of scientific and professional support. I would like to give special thanks to Dr. Annamarie Dalton for providing one-on-one mentoring during some of the more challenging moments in my studies. Thank you for your patience, Dr. Dalton. I would like to thank all the members of my supervisory committee, both in the past and present. Sometimes, we have to learn how to fail so that we can expose the path to success. Sometimes, we have to learn from our failures, so we do not repeat them. Sometimes we just fail. I thank my committee for teaching me how to succeed by doing so. I would like to thank Dr. Kevin Brown, my master’s degree mentor. He never sugar-coated anything. Finally, I would like to thank my family for always being there when I needed them.

Table of Contents

Acknowledgements	ii
Table of Contents	iii
List of Tables	v
List of Figures	vi
Abbreviations Key	vii
Abstract	ix
Chapter 1: Introduction	1
1.1 Intracellular function of PCBP1 in mammary epithelium	1
1.2 The FAM3C gene and the “ILE1” protein	9
1.3 An introduction to LIFR and its role in mammary carcinoma	16
1.4 Pathological and clinical implications of FAM3C/LIFR/STAT3	24
i. Clinical characterization of FAM3C	24
ii. Clinical characterization of LIFR	27
iii. The identification of STAT3 as an oncogene	34
iv. The development of STAT3 as an anticancer drug target	36
v. Clinical use of STAT3 inhibitor drugs	40
vi. Characterization of STAT3 activation: impact on prognosis	43
1.5 Central hypothesis and specific aims	47
i. Aim 1: Characterize PCBP1-mediated increase in LIFR expression	48
ii. Aim 2: Identify FAM3C/LIFR interaction-dependent gene regulation	49
iii. Aim 3: Identify phenotypic effects of LIFR expression	49
Chapter 2: Transcriptional Regulation of LIFR	51
2.1 Introduction and rationale	51
2.2 Results	51
i. Loss of PCBP1 expression upregulates LIFR	51
ii. FAM3C participates in regulation of LIFR expression	55
iii. FAM3C regulates LIFR expression through STAT3	62
2.3 Summary	70
Chapter 3: Analysis of the FAM3C/LIFR Transcriptomic Signature	71
3.1 Introduction and rationale	71
3.2 Results	72
i. Transcriptomic analysis reveals a FAM3C/LIFR regulatory signature	72
ii. LIFR and TWIST1 are co-regulated	79
3.3 Summary	82

Chapter 4: The Phenotypic Effects of LIFR Expression and Signaling	84
4.1 Introduction and rationale	84
4.2 Results	85
i. LIFR expression promotes an invasive BCSC phenotype	85
ii. Loss of FAM3C/LIFR attenuates spheroid growth in human mammary carcinoma cells	89
4.3 Summary	91
Chapter 5: Discussion	92
5.1 Interpretation	92
i. Results and conclusions	92
ii. Translational considerations	97
5.2 Additional considerations	104
5.3 Future directions	110
Chapter 6: Materials and Methods	114
References	125
Additional Data Tables (Tables 7-9)	136

List of Tables

Table 1 – List of primary research publications characterizing LIFR in cancer.	20
Table 2 – Initial survival analysis of LIFR expression in patients with breast cancer.	29
Table 3 – Secondary LIFR expression survival analysis.	31
Table 4 – List of proposed methods of STAT3 inhibition.	39
Table 5 – List of breast cancer clinical trials involving STAT3 inhibitors.	42
Table 6 – Survival analysis of pSTAT3 accumulation in patients with breast cancer.	45
Table 7 – List of 490 dysregulated genes from superimposition of three RNA-seq datasets.	135
Table 8 – List of 58 dysregulated transcription factor genes.	143
Table 9 – Nucleotide sequences.	144

List of Figures

Figure 1 – PCBP1 regulates the translation of FAM3C (ILEI) protein.	4
Figure 2 – Proposed schematic of FAM3C/LIFR-induced BCSC phenotype.	22
Figure 3 – FAM3C protein expression has both positive and negative correlations with the survival of patients with mammary carcinoma.	26
Figure 4 – High LIFR mRNA expression correlates with decreased survival in discreet breast cancer patient subsets.	33
Figure 5 – Summary of the mechanism(s) of STAT3 in cancer.	38
Figure 6 – Overarching hypothesis and specific aims.	50
Figure 7 – LIFR is upregulated following loss of PCBP1 expression.	52
Figure 8 – The LIFR Regulatory region is highly conserved .	54
Figure 9 – Activation of a LIFR transcription reporter is increased following loss of PCBP1 expression.	56
Figure 10 – FAM3C participates in regulation of LIFR expression.	57
Figure 11 – FAM3C overexpression drives LIFR expression.	59
Figure 12 – Endogenous LIFR expression levels in human mammary epithelium.	60
Figure 13 – FAM3C expression participates in regulation of LIFR expression in human breast cancer.	61
Figure 14 – FAM3C KO attenuates LIFR/STAT3 transcription reporters.	63
Figure 15 – Application of pharmacological inhibition of STAT3 in shPCBP1 cells.	64
Figure 16 – Validation of pharmacological inhibition of STAT3 in shPCBP1 cells.	65
Figure 17 – LIFR overexpression causes an increase in LIFR transcription reporter signal.	67
Figure 18 – Confirmation of LIFR overexpression.	68
Figure 19 – STAT3 interacts with DNA at the LIFR promoter region.	69
Figure 20 – Evaluation of RNA-Seq data integrity.	73
Figure 21 – Transcriptomic analysis reveals a FAM3C/LIFR regulatory signature.	75
Figure 22 – Validation of TWIST1 expression and regulation by STAT3.	77
Figure 23 – Gene ontology (GO) analysis.	78
Figure 24 – LIFR and TWIST1 are coregulated.	80
Figure 25 – TWIST1 binds to the LIFR promoter.	81
Figure 26 – Knockdown of PCBP1 and overexpression of LIFR alters morphology.	86
Figure 27 – LIFR expression promotes an invasive phenotype.	87
Figure 28 – LIFR expression promotes migration and BCSC phenotype.	88
Figure 29 – Loss of FAM3C/LIFR attenuates spheroid growth in human mammary carcinoma cells.	90
Figure 30 – Summary of conclusions.	96
Figure 31 – Low PCBP1 expression correlates with high FAM3C and STAT3 expression in a subset of human mammary carcinoma patients.	98
Figure 32 – pSTAT3 accumulation correlates with pTWIST1 accumulation in human mammary carcinoma.	100
Figure 33 – High TWIST1 expression correlates with reduced survival in human mammary carcinoma.	103

Abbreviations Key

AKT	Protein kinase B
ANOVA	Analysis of variance
BCSC	Breast cancer stem cell
bp	Base-pair
C185	Cysteine 185
ChIP	Chromatin immunoprecipitation
chr	Chromosome
CIE	Cis-inducible element
CLC	Cardiotrophin-like cytokine
CNTF	Ciliary neurotrophic factor
CRC	Colorectal cancer
CT	Control, also Cycle threshold
CT-1	Cardiotrophin 1
DEG	Differentially expressed gene
DKO	Double knockout
DMEM	Dulbecco's modification of Eagle's medium
DMSO	Dimethyl sulfoxide
ECM	Extracellular matrix
ECR	Evolutionarily conserved region
EDTA	Ethylenediaminetetraacetic acid
eEF1A1	Eukaryotic elongation factor 1A1
EGFR	Epidermal growth factor receptor
ELDA	Extreme limiting dilution analysis
EMT	Epithelial-mesenchymal transition
EPD	Eukaryotic Promoter Database
ERK	Extracellular signal-related kinase
EV	Empty vector
FAM3C	Family with sequence similarity 3, member C
FBS	Fetal bovine serum
FDA	Food and Drug Administration
FDR	False discovery rate
GO	Gene ontology
HCC	Hepatocellular carcinoma
HDACi	Histone deacetylase inhibitor
HeLa	Henrietta Lacks
hESC	Human embryonic stem cell
hnRNP	heterogenous ribonucleoprotein
IFN	Interferon
IL-6	Interleukin 6
IL-6ST	Interleukin 6 signal transducer
ILEI	Interleukin-like EMT inducer
IND	Investigational new drug
JAK	Janus activated kinase
KD	Knockdown
KO	Knockout
LATS	Large tumor suppressor kinase
LIF	Leukemia inhibitory factor
LIFR	Leukemia inhibitory factor receptor
MAPK	Mitogen activated protein kinase

MDA	The University of Texas MD Anderson Cancer Center
mESC	Murine embryonic stem cell
MET	Mesenchymal-epithelial transition
MMP	Matrix metalloprotease
mRNA	Messenger ribonucleic acid
MST	Mammalian STE20-line kinase
NCBI	National Center for Biotechnology Information
NLS	Nuclear localization sequence
NMuMG	Normal murine mammary gland
NSCLC	Non-small cell lung cancer
OE	Overexpressed; overexpression
ORF	Open reading frame
OSCC	Oral squamous cell carcinoma
OSM	Oncostatin M
PCBP1	poly(rC) binding protein 1
PCR	Polymerase chain reaction
PDGFR	Platelet-derived growth factor receptor
PI3K	Phosphoinositide 3-kinase
PIAS	Protein inhibitor of activated STATs
pSTAT3	Phosphorylated STAT3 (at Y705)
qPCR	Quantitative polymerase chain reaction
RIP-ChIP	RNA-binding protein immunoprecipitation microarray
RNA-Seq	Ribonucleic acid sequencing
RTK	Receptor tyrosine kinase
S43A	Serine 43 to Alanine substitution
S727	Serine 727
SEM	Standard error of the mean
sgRNA	Single-guide ribonuclein acid
SH2	Src-homology 2
SHP2	Src homology region 2 domain-containing phosphatase-2
shRNA	Small hairpin RNA
shSCR	Small hairpin "scrambled"
SOCS	Suppressor of cytokine signaling
ssDNA	single-stranded DNA
STAT	Signal transducer and activator of transcription
STWS	Stüve-Wiedeman syndrome
SWH	Salvador-Warts-HIPPO (aka "HIPPO")
TF	Trascription factor
TGF β	Transforming growth factor beta
TICs	Tumor-initiating cells
TNBC	Triple-negative breast cancer
TSS	Transcription start site
UCSC	University of Santa Cruz
uPAR	urokinase-type plasminogen activator receptor
UTR	Untranslated region
VEGF	Vascular endothelial growth factor
Y705	Tyrosine 705
YAP	Yes-associated protein

Abstract

The poly(rC) binding protein 1 gene (PCBP1) encodes the heterogeneous nuclear ribonucleoprotein E1 (hnRNPE1), a nucleic acid-binding protein that plays a tumor-suppressive role in mammary epithelial cells by regulating phenotypic plasticity and cell fate. Following the loss of PCBP1 function, the FAM3C gene (encoding the Interleukin-like EMT inducer, or “ILEI” protein) and the leukemia inhibitory factor receptor (LIFR) gene are upregulated. Interaction between FAM3C and LIFR in the extracellular space induces phosphorylation of signal transducer and activator of transcription 3 (pSTAT3). Overexpression and/or hyperactivity of STAT3 has been detected in 40% of breast cancer cases and is associated with a poor prognosis. Herein, we characterize a “feed-forward” mechanism that regulates the expression of LIFR in response to FAM3C/LIFR/STAT3 signaling in mammary epithelial cells. We show that the loss of PCBP1 expression upregulates LIFR transcription through activity at the LIFR promoter. We also show that LIFR transcription is affected by modulation of FAM3C expression levels. Additionally, our bioinformatic analysis reveals a signature of transcriptional regulation associated with the FAM3C/LIFR interaction and identifies the TWIST1 transcription factor as a downstream effector that participates in the maintenance of LIFR expression. Finally, we characterize the effect of LIFR expression in cell-based experiments using both mouse and human mammary epithelial cells. Our experiments demonstrate the promotion of invasion, migration, and self-renewal of breast cancer stem cells (BCSCs) following increased LIFR expression, which is consistent with previous studies linking LIFR expression to tumor initiation and metastasis in mammary epithelial cells.

Chapter 1: Introduction

1.1 Intracellular function of PCBP1 in mammary epithelium

During mammary gland development, mammary epithelial cells carry out a phenotypic program that facilitates their physiological function and maintains their structural integrity. Epithelial cells must function optimally during the rapid growth phase of puberty and the lactation phase of pregnancy (1). Epithelial cells anchor themselves to a proteinaceous substrate known as the basement membrane and form sheets of tissue through their adhesive partnerships with neighboring epithelial cells (1). The PCBP1 protein (also known as the heterogeneous nuclear ribonucleoprotein E1, or hnRNP E1) carries out multiple intracellular functions in mammary epithelial cells and plays a major role in maintaining the epithelial phenotype (2, 3). PCBP1 is one of approximately 20 proteins belonging to the hnRNP family of nucleic acid-binding proteins and it binds to both DNA and RNA (3, 4). The interaction between PCBP1 and RNA facilitates the formation of functional ribonucleoprotein complexes that regulate RNA processing functions, including splicing, polyadenylation, and protein translation (2). PCBP1 therefore represents an essential component of the intracellular machinery in epithelial cells, and previous work has described its far-reaching influence on key regulatory functions in the nucleus and cytoplasm (2–7).

In the late 20th century, a family of RNA-binding proteins was characterized and defined as capable of binding to and “packaging” heterogeneous nuclear RNA transcripts (hnRNAs), and thus named the hnRNP family of proteins (3, 8). PCBP1 is one of three hnRNPs containing nucleic acid-binding domains known as “KH” domains, which have been shown to bind in a sequence-specific manner to RNA and DNA with high binding affinity for polycytosine tracts (4, 9, 10). Previous studies have identified the accumulation

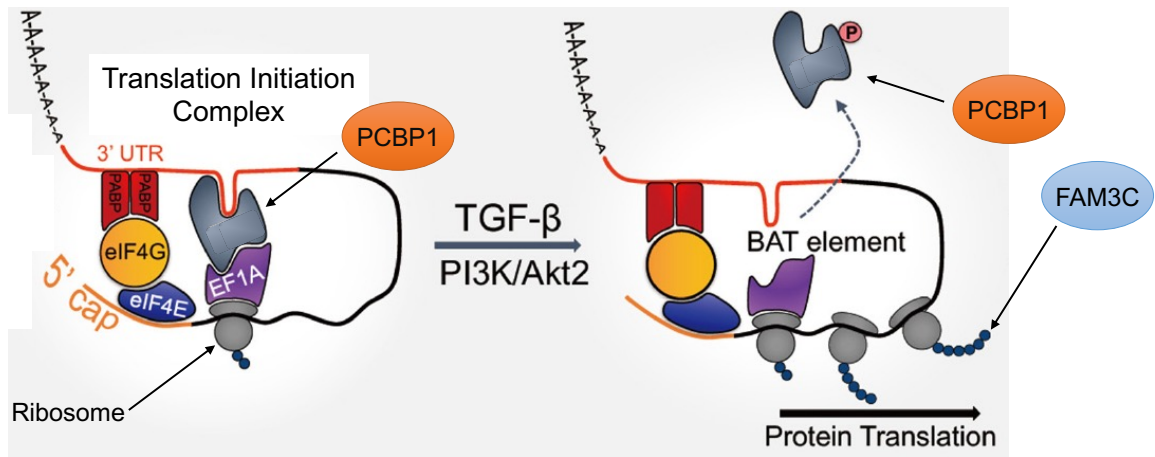
of PCBP1 in both the nucleus and the cytoplasm, and have also identified a nuclear localization sequence (NLS) within the protein structure that is thought to be responsible for regulating the subcellular localization of PCBP1 (3, 10–12).

PCBP1 carries out a specific set of RNA-processing functions that appear to be non-redundant with other KH domain-containing hnRNPs, although some functional overlap has been suggested (13, 14). In the nucleus, PCBP1 interacts with protein components of the spliceosome, thus regulating the alternative splicing of pre-mRNA transcripts. Previous studies have shown that loss of PCBP1 expression and/or function can promote alternatively spliced variants of CD44 and PNUTS transcripts, and cause aberrant changes in the epithelial phenotype (15, 16). PCBP1 also interacts with polycytosine tracts within single-stranded chromosomal DNA (ssDNA) in both telomeric regions and in the promoters of certain genes. Evidence suggests that PCBP1 ameliorates DNA damage-induced intracellular signaling and thus monitors genomic integrity through its complexation with ssDNA and proteins involved in DNA repair (9).

Numerous studies have described the role of PCBP1 as a regulator of mRNA 3' untranslated region (UTR) processing through its interaction with polyadenylation machinery in the nucleus and with nuclease machinery in the cytoplasm (17–19). Evidence suggests that PCBP1 regulates the stability of multiple mRNAs and, thus, the expression of multiple genes through its sequence-specific binding to mRNA 3' UTRs (3). In addition to its regulation of mRNA stability, PCBP1 has also been shown to regulate mRNA translation by binding to sequence-dependent secondary structures in 3' UTRs (7, 20, 21). Using a combination of polysome profiling, immunoprecipitation, and RNA-Binding Protein Immunoprecipitation-Microarray (RIP-ChIP), the Howe laboratory identified 36 mRNAs that were bound by PCBP1 in their 3' UTRs. PCBP1 binding was shown to suppress the protein expression levels of 36 genes by inhibiting the elongation of translation (21). Several of these genes have previously been shown to affect the stability

of the epithelial phenotype, including FAM3C, which underscores its characterization in the current study (7, 21, 22). PCBP1 suppresses the translation of FAM3C and other proteins by forming a ternary complex with the mRNA 3' UTR and eukaryotic elongation factor 1A1 (eEF1A1), (Fig. 1). The formation of the PCBP1-mediated ternary complex prevents the release of eEF1A1 from the ribosome, thus preventing the elongation of translation (22). Although the full scope of PCBP1-dependent intracellular mechanisms remains largely uncharacterized, investigations by the Howe laboratory and others have observed changes in the epithelial phenotype that occur in mammary epithelial cells following loss of PCBP1 expression and/or function. The Howe laboratory and others have also characterized the role of PCBP1 in regulating epithelial-mesenchymal transition (EMT) in epithelial cells in both mice and humans (21, 23, 24).

EMT is a phenomenon that occurs in cells at various stages of growth in developing embryos and mature organisms. The reverse process, known as mesenchymal-epithelial transition (MET), provides a biological “counter-balance” that dynamically guides transient phenotypic gradients in healthy tissues. During pubertal development in mammals, branching morphogenesis of the mammary gland occurs through “programmed” control of EMT/MET. The *plasticity* of cells that is enabled by the control of EMT/MET allows them to become more motile and drive an increase in proliferation as cells build the ductal network of the gland. EMT/MET also plays an important role in phenotypic reprogramming and morphological adaptation by influencing how cells assume specific functional fates; EMT/MET has been shown to be necessary for the differentiation of mammary stem cells into the specific cell types that comprise mature glandular structures (1, 25).



Adapted from Grelet, S. et al. *J Cancer Metastasis Treat* 2019; 5:16

Figure 1 – PCBP1 regulates the translation of FAM3C (ILEI) protein. A diagram extracted from Grelet et al. (2019) illustrating the mechanism of translational suppression of FAM3C by PCBP1. BAT, β -activated translation; UTR, untranslated region.

During embryonic development, wound healing, and carcinogenesis, the extracellular cytokine, transforming growth factor beta (TGF β), initiates intracellular signaling that regulates multiple EMT-related events (26). The Howe laboratory previously determined that TGF β binding to its cognate receptors initiates a cascade of kinase activity that results in phosphorylation of PCBP1 at serine residue 43, which ablates the formation of the ternary complex mentioned above (7). TGF β -induced intracellular signaling and subsequent control of EMT have been extensively characterized for their crucial physiological roles, which include but are not limited to (1) regulation of embryonic morphogenesis during development (aka “Type 1 EMT”), (2) tissue regeneration during wound healing (aka “Type 2 EMT”), and (3) promotion of invasion and metastasis during progression of carcinoma pathology (aka “Type 3 EMT”) (27). Our understanding of how PCBP1 regulates EMT and responds to TGF β in the context of mammary carcinoma remains incomplete and prompts further investigation. Preclinical studies by the Howe laboratory and other investigators clearly demonstrated that PCBP1 plays a role in TGF β -mediated EMT/MET and has a measurable impact on the progression and metastasis of mammary carcinoma (5, 16, 28).

The role of TGF β in the pathology of mammary carcinoma is paradoxical. Healthy epithelial cells exposed to TGF β *in vivo* remain healthy, and their transformation into neoplasia is suppressed in part by TGF β -induced signaling cues. However, it has been suggested that once tumorigenesis occurs, TGF β exposure induces aberrant intracellular events that drive disease progression, including the promotion of EMT in epithelial cells (29). The Howe laboratory has created an experimental context to study the mechanisms of TGF β -dependent pathology in mammary epithelium, using both laboratory mice and cultured epithelial cells. Previous experiments using cultured normal murine mammary gland cells (hereafter “NMuMG cells”) demonstrated that the loss of PCBP1 function is

required for TGF β -mediated EMT to occur. A mutant form of PCBP1 possessing an alanine substitution at position 43 (S43A) was introduced into NMuMG cells followed by exposure to exogenous TGF β . The mutation allowed PCBP1 to maintain its function in the presence of TGF β , and EMT was suppressed (7). Additionally, shRNA-mediated knockdown of PCBP1 was sufficient to induce EMT in NMuMG cells in the absence of TGF β (7). These data established that PCBP1 is both a key responder to TGF β -induced intracellular signaling and a key regulator of EMT.

It was later shown by the Howe laboratory that NMuMG cells with shRNA-mediated knockdown of PCBP1 (hereafter “shPCBP1 cells”) formed tumors when implanted into the mammary fat pads of immunocompromised mice. The tumors progressed and caused pulmonary metastases, suggesting that loss of PCBP1 expression allows NMuMG cells to acquire a phenotype that models the pathology of mammary carcinoma (28). When shPCBP1 cells were implanted into mice following surgical removal of the mammary glands, the implanted cells were able to fully reconstruct the organ (28). These data demonstrate that the phenotype acquired following loss of PCBP1 expression exhibits a gain of differentiation potency, which suggests that PCBP1 regulates the “stemness” of mammary epithelial cells. shPCBP1 cells therefore provide a model by which to study mechanisms that occur in “breast cancer stem cells” (BCSCs), through observation of PCBP1’s influence upon phenotypic plasticity, cellular self-renewal, and tissue growth during tumorigenesis. The use of shPCBP1 cells in the current study also provides utility because of the correlation observed between the BCSC phenotype and increased tumor-initiating capacity and chemoresistance of human cancer cells (30, 31).

Analysis of clinical data from human cancer patient samples revealed that mutations in PCBP1 can result in loss of its expression or function, and in some cases, this loss has been predicted to have a deleterious effect on patient survival. The Genomic

Data Commons Portal maintained by the National Institutes of Health showed that out of 2485 patient tumor samples (all including survival data), 132 (5.3%) had mutations in the PCBP1 gene, with 119 distinct mutations being identified. Of the 132 cases, 60 possessed mutations predicted to cause a consequent loss of PCBP1 protein expression and/or function. However, none of the 60 cases described breast cancer patients (32). Therefore, it is likely that changes in the regulation of PCBP1 expression, which could affect breast cancer pathology, occur through intracellular mechanisms other than those affecting the coding sequence of the gene.

The Howe lab has shown that PCBP1 expression can be regulated through changes in its rate of degradation. The E3 ubiquitin ligase ARIH1 ubiquitinates PCBP1 in NMuMG cells, thereby promoting proteasomal processing (5). ARIH1 knockdown in NMuMG cells stabilizes PCBP1 expression levels and delays EMT following treatment with TGF β (5). Parallel observations were made following ARIH1 knockdown in the lung metastatic derivative (LM2) of the MDA-MB-231 human mammary carcinoma cell line and SUM 159 human mammary carcinoma cell line. Additionally, knockdown of ARIH1 causes a loss of self-renewal capacity in SUM 159 cells, as shown by an *in vitro* spheroid formation (mammosphere) assay (5). In addition to being regulated by changes in proteasomal degradation rates, PCBP1 may also be transcriptionally upregulated in response to hypoxic conditions. However, hypoxia-dependent upregulation of PCBP1 has only been observed in rodent neuronal cells *in vitro* and similar mechanisms in mammary epithelial cells have not been characterized (33, 34). Taken together, these observations suggest that the role of PCBP1 in maintaining the epithelial phenotype is largely determined by its ability to maintain homeostatic functions through the stabilization of PCBP1 protein turnover and post-translational modifications, including phosphorylation and ubiquitination.

The characterization of PCBP1 prior to the current study revealed its multifaceted function and physiological importance in healthy mammary epithelial tissues. In the current study, we sought to further investigate PCBP1-related mechanisms that lead to advanced disease. Specifically, we sought to further our understanding of how changes in the expression of genes regulated by PCBP1 contribute to aberrant phenotypes. Previous study by the Howe laboratory and others have identified the FAM3C gene, which is translationally suppressed by PCBP1, as a contributor to aberrant morphology, motility, and anchorage-independent growth; however, the precise mechanism(s) of its contribution remain unknown (28, 35–37). Logically, the examination of FAM3C expression and related intracellular events presented an opportunity to develop and test hypotheses in the current study.

1.2 The FAM3C gene and the “ILEI” protein

FAM3C is one of four cytokine-like proteins belonging to the “family with sequence similarity 3” (FAM3) family of proteins. The other three family members were found to be similar in size, sequence, and structure, and were therefore grouped together following their initial characterization by Zhu et al. in 2002 (38). Although FAM3 proteins do not share any sequence homology with interleukins, they were originally identified through a search for proteins with structures similar to the four-helix bundle found in many cytokines (38). Later, it was revealed that FAM3 proteins do not form the four-helix bundle found in cytokines and therefore represent a novel class of secreted “cytokine-like” proteins involved in a wide range of physiological functions (39–41). FAM3C and FAM3A are expressed ubiquitously in mammalian tissues, whereas FAM3B is mostly expressed in the pancreas and FAM3D is mostly expressed in the placenta (38). Several studies have described the involvement of FAM3B and FAM3C in the pathology of various cancers, and FAM3C, also known as “The Interleukin-like EMT Inducer” (ILEI), has become the most characterized family member in recent years (42, 43).

The expression and activity of FAM3C have been characterized in several recent studies, indicating that it plays a role in many seemingly unrelated pathologies. Although the mainstay of its characterization is the induction of EMT, several studies have described novel roles for FAM3C. For example, Malik et al. demonstrated that inflammatory stimuli upregulate FAM3C expression, exacerbating the symptoms of psoriasis in transgenic mice (44). Chen et al. demonstrated the participation of FAM3C in the regulation of glucose and lipid metabolism in a mouse model of type I diabetes (45). In the two preceding examples and in the majority of studies, FAM3C has been characterized as an inducer of intracellular signaling cascades; however, a recent study of Alzheimer’s disease demonstrated that FAM3C can act as an extracellular “adapter” molecule that regulates the activity of the γ -

secretase complex (46). In studies describing FAM3C as an inducer of EMT, evidence is not confined to the pathology of cancer. For example, Zhou et al. demonstrated that FAM3C induces intracellular signaling and EMT in a mouse model of chronic kidney disease (47). Bendre et al. demonstrated the involvement of FAM3C in osteogenic differentiation through the regulation of TGF β -1 expression (48). However, the mechanisms by which FAM3C participates in any of these physiological processes have not yet been fully elucidated.

FAM3C has been extensively studied and implicated in the pathology of various cancers including mammary carcinoma, hepatocellular carcinoma (HCC), non-small cell lung cancer (NSCLC), oral squamous cell carcinoma (OSCC), colorectal cancer (CRC), and esophageal cancer (28, 49–53). FAM3C has been shown to predominantly function through extracellular interactions with the cell surface and subsequent activation of various signal transduction cascades. Previous preclinical cancer studies have conclusively shown that changes in FAM3C expression modulate signal transduction pathways including JAK/STAT, PI3K/AKT, and MAPK/ERK (28, 37, 54, 55). The activation of cascades is coupled with the association of EMT events in epithelial cells. However, experimental evidence has not yet identified the precise mechanism of FAM3C-mediated EMT induction.

Recent studies have demonstrated that the biological activity of FAM3C can be regulated during secretory processing and/or extracellular accumulation, suggesting that context-specific cellular activities may influence FAM3C function and possibly the specificity of pathway activation (39, 56, 57). Recent evidence has shown that FAM3C binds to the extracellular matrix (ECM) in a manner dependent on its N-terminal 17-amino acid propeptide sequence. Cleavage of the propeptide by extracellular serine proteases liberates and “activates” FAM3C. This proteolytic processing was shown to be required for increased metastatic potential of EpC40 and 4T1 mouse mammary tumor cells (57).

Experiments have also revealed that the expression of urokinase-type plasminogen activator receptor (uPAR) and its conversion of plasminogen into plasmin serine protease play a role in the regulation of FAM3C secretion (56). Structural analysis has revealed that cysteine residue 185 (C185) is essential for the covalent dimerization of FAM3C (39). A parallel investigation using both mouse and human cell engraftment techniques provided evidence that dimerization is required for FAM3C-induced mammary tumor growth and metastasis in mice (57). Additionally, attempts to manufacture recombinant FAM3C protein have had limited success, as exemplified by reports of inconsistent levels of biological activity rendered by exogenous FAM3C treatments (37, 56). Difficulties in reproducing experimental data owing to the inconsistent potency of exogenous FAM3C have also been reported in the current study. It is possible that the manufacturing method, that is, the choice of *E. coli* versus mammalian expression systems, may play a role in the protein processing that is necessary for FAM3C function. For example, there are differences in the post-translational protein modification capabilities (e.g., glycosylation and ubiquitination) of prokaryotic cells compared with eukaryotic cells. Collectively, this evidence strongly suggests that FAM3C undergoes fine-tuned post-translational regulation in addition to the PCBP1-mediated post-transcriptional regulation described above, and that specific modifications are required for FAM3C to undergo activity-endowing secretion, cleavage, and dimerization in mammalian cells.

Following the identification of the FAM3 family of proteins by Zhu et al. in 2002, a group of researchers led by Dr. Harmut Beug at the Research Institute of Molecular Pathology in Vienna, Austria, began characterization of FAM3C in the context of mammary carcinoma (37). In 2006, Waerner et al. originally referred to FAM3C as the “*Interleukin-like EMT Inducer*” (ILEI), and utilized normal, healthy murine mammary epithelial cells (EpH4 cells) to demonstrate the role of FAM3C in mammary carcinoma pathology (37). Waerner et al. produced EpH4 derivative cell lines by overexpressing FAM3C, and

observed that FAM3C induced EMT. By engrafting Eph4-derived FAM3C-overexpressing cells into immunocompromised mice, Waerner et al. demonstrated that (1) FAM3C expression is required for EMT, tumor formation, and metastasis and (2) FAM3C expression alone is sufficient to cause these outcomes to occur (37). Additional Eph4 derivative cell lines were used to demonstrate that FAM3C knockdown is sufficient to reverse EMT and induce MET, and that FAM3C is required for TGF β -mediated EMT. In 2014, Csiszar et al. continued FAM3C characterization and described the first experiments using human mammary carcinoma cell lines (56). Using both metastatic and non-metastatic human mammary carcinoma cell lines, Csiszar et al. showed that high FAM3C expression levels correlated with increased metastatic potential. Using human tumor tissue sample arrays, it was shown that changes in the subcellular localization of FAM3C indicated that an increased secretory rate was correlated with increased severity of prognosis (56). The findings of Waerner, Csiszar, et al. increased our understanding of the EMT “frontier” of mammary carcinoma pathology and delineated the importance of further investigation into the mechanisms associated with FAM3C expression and function.

Dr. Agnes Csiszar continued to study FAM3C by leading a team of researchers at the Medical University of Vienna, Austria. In 2017, Kral et al. used immunocompromised mice to describe the first orthotopic xenografts of human mammary carcinoma cells with modulation of FAM3C expression (57). Using the highly metastatic LM2 derivative of the MDA-MB-231 mammary carcinoma cell line, Kral et al. showed that tumor growth was severely attenuated by loss of FAM3C expression. However, growth was rescued by re-expression of wild-type human FAM3C, but not by mutant FAM3C, which lacked the capability to form homodimers (57). Kral et al. also demonstrated that FAM3C monomers and homodimers both possess biological functions that can affect the mammary epithelial

phenotype. However, their evidence strongly suggests that the activity of the FAM3C homodimer is more potent and consequently required for disease progression *in vivo* (57).

Near the end of the 20th century, collaboration between Dr. Harmut Beug and the Swiss Institute for Experimental Cancer Research produced a tumorigenic EpH4 derivative cell line known as EpRAS (58). During the first two decades of the 21st century, teams led by Harmut Beug and Agnes Csiszar utilized the EpRAS mouse model to characterize FAM3C in parallel with the EpH4 and human cell experiments described above (37, 56, 57). EpRAS cells were originally used to demonstrate that TGF β -mediated EMT during mammary carcinoma progression *in vivo* requires an aberrant MAPK signaling pathway (58, 59). EpRAS cells were derived from the EpH4 cell line by introducing stable overexpression of a mutated hyperactive RAS GTPase, known as HRAS. HRAS possesses a substitution of glycine with serine at position 12 (G12S), and this mutation was previously identified to be associated with an increased risk of breast cancer (58, 60). EpRAS cells show a dramatically increased proliferation rate and form tumors when orthotopically injected into immunocompromised mice, and demonstrate metastatic potential following tail vein injection (37). EpRAS cells specifically propagate the MAPK/ERK transduction pathway and require MAPK/ERK activity for EMT and metastasis (61). HRAS-associated pathology is detected more frequently in African Americans, young women, and hormone receptor-negative tumors (60). However, HRAS mutations in human breast cancer cases are considered rare, which limits the EpRAS model when attempting to translate experimental observations into clinical relevance (58, 62).

In 2017, work in the Howe laboratory by Howley, et al. reported the creation of a mouse model of mammary carcinoma metastasis for observing the context of TGF β -mediated EMT following loss of PCBP1 expression (hereafter “the Progression Series Model”) (63). Although mutations in PCBP1 in human breast cancer are also rare, the

Progression Series Model exemplifies TGF β -mediated EMT because exposure to TGF β causes loss of PCBP1 function and does not require mutations. NMuMG cells with loss of PCBP1 function (shPCBP1 cells) are tumorigenic, have metastatic potential, and behave similarly to EpRAS cells *in vivo* following engraftment into mice (59). shPCBP1 cells also display increased FAM3C expression and do not require the introduction of exogenous expression vectors such as those described in Waerner et al. (37). In the years that followed, the Howe laboratory continued experiments characterizing FAM3C using the Progression Series Model, prompting the hypotheses that will be described in the current study.

In 2019, the Howe laboratory reported additional evidence of FAM3C participation in mammary carcinoma disease progression *in vitro* and *in vivo*, using the Progression Series Model. The Howe laboratory identified that FAM3C is required for TGF β -mediated EMT in shPCBP1 cells, which recapitulated the previous work by Beug et al. in the EpRAS model (28). To identify the potential mechanisms of FAM3C-mediated EMT, Woosley et al. performed a yeast two-hybrid assay. The yeast two-hybrid assay was constructed using the FAM3C coding sequence as a “bait” protein, and a human mammary carcinoma cell (HeLa cell) cDNA library as “prey” proteins. The data produced by the yeast two-hybrid assay identified potential FAM3C binding partners, and additional experiments revealed an extracellular interaction between FAM3C and leukemia inhibitory factor receptor (LIFR) (28). Woosley et al. showed that the extracellular interaction between FAM3C and LIFR is required to induce the phosphorylation of STAT3 at tyrosine 705 (pSTAT3). They further showed that the loss of FAM3C/LIFR-induced pSTAT3 attenuated cellular self-renewal *in vitro*, suggesting that FAM3C participates in the activation of a signaling pathway that promotes the BCSC phenotype (28). The evidence presented by Woosley et al. is the first

example of an extracellular interaction responsible for driving FAM3C-mediated intracellular signal transduction that directly affects the epithelial phenotype.

By engrafting shPCBP1 cells into the mammary fat pads of immunocompromised mice, Woosley et al. demonstrated that FAM3C knockdown reduced the tumor burden and produced fewer pulmonary metastases (28). Extreme limiting dilution analysis (ELDA) showed that attenuation of the tumor burden following FAM3C knockdown resulted from a decrease in the number of tumor initiating cells (TICs) in the engrafted cell population (28). The results of the ELDA assay further suggested that FAM3C expression promotes “stemness” in tumorigenic mouse mammary epithelial cells. Woosley et al. also showed by immunoblot analysis that high levels of FAM3C expression in human mammary carcinoma cell lines correlates with increased metastatic potential (28). Additionally, immunohistochemical analysis of an array of samples from breast cancer patients with metastatic tumors showed increased FAM3C expression in tumors and lymph nodes, relative to FAM3C expression levels in normal tissue samples from healthy patients (28). Data generated from human tumor sample-based experiments by Woosley et al. and previously by Csiszar et al. demonstrated that FAM3C is a clinically relevant contributor to mammary carcinoma pathology (28, 56). Woosley et al. provided the first direct evidence of an extracellular interaction-dependent mechanism downstream of FAM3C secretion that regulates epithelial phenotype *in vitro* and disease progression *in vivo*. Therefore, the current study sought to develop experimental strategies that might reveal additional mechanistic evidence downstream of FAM3C/LIFR interaction.

1.3 An introduction to LIFR and its role in mammary carcinoma

The leukemia inhibitory factor receptor (LIFR) was identified as a signal-transducing receptor for leukemia inhibitory factor (LIF), a cytokine that was named after it was found to suppress proliferation and induce differentiation of a myeloid leukemia cell line (64). LIFR was later found to bind to four additional cytokines, all of which belong to the interleukin-6 (IL-6) family of cytokines (65). It was also found that each cytokine binds to LIFR with the cooperation of one or more co-receptors, creating cytokine-dependent extracellular complexes that ultimately determine the specific nature of the subsequent intracellular signal transduction (65). Identification of the co-receptors that participate in IL-6 family cytokine-dependent signal transduction therefore established the IL-6 family of cytokine receptors, which was subdivided into two groups: the “signaling receptors,” and the “binding receptors.” LIFR belongs to the signaling receptor group and forms a dimeric complex with another signaling receptor known as the IL-6 signal transducer (IL-6ST), also known as GP130, in response to either LIF or oncostatin M (OSM) cytokines (65). Additionally, LIFR can form trimeric and/or hexameric complexes with IL-6ST and additional receptors from the binding receptor group in response to ciliary neurotrophic factor (CNTF), cardiotrophin-1 (CT-1), and cardiotrophin-like cytokine (CLC) (65). However, evidence suggests that signal transduction may also be possible through a homodimeric LIFR complex in response to LIF (66).

Following the extracellular interaction between LIFR and cytokines, complexation of ligands, receptors, and co-receptors facilitates intracellular proximity-dependent recruitment and activation of Janus-activated kinases (JAKs), either JAK1 or JAK2, followed by phosphorylation of four specific tyrosine residues on the receptor intracellular domains (67, 68). The phosphorylated tyrosine residues of LIFR act as docking sites for the SRC Homology 2 (SH2) domains of the STAT3 protein. Docking of STAT3 to the receptor via SH2 binding facilitates its proximity to activated JAKs, which allows STAT3 to

be phosphorylated (pSTAT3), specifically at tyrosine residue 705 (Y705). pSTAT3 can then homodimerize and translocate to the nucleus, where it acts directly as a transcription factor by binding to the regulatory regions of its target genes (67, 69). JAKs activated by LIFR can propagate signals through two pathways in addition to STAT3. Phosphorylation of the p85 protein by JAK1 following LIFR activation results in the activation of phosphoinositide-3 kinase (PI3K), which phosphorylates and activates members of the protein kinase B (AKT) family of protein kinases (67). JAK1 phosphorylation of the LIFR intracellular domain also recruits Src homology region 2 domain-containing phosphatase-2 (SHP2), which initiates a cascade involving the RAS-RAF-MEK-ERK family of mitogen-activated protein kinases (MAPK) (67). Recent evidence also suggests that LIFR activation can result in the phosphorylation of large tumor suppressor kinases (LATS1 and LATS2) and/or mammalian STE20-like kinases (MST1 and MST2), which results in cytosolic sequestration and deactivation of the transcription factor known as yes-associated protein (YAP). YAP is a component of the Salvador-Warts-HIPPO (SWH, aka "HIPPO") signaling pathway; however, the mechanism by which LIFR activates the HIPPO pathway has not yet been fully elucidated (67, 70). Following the activation of LIFR, the signaling pathway(s) that become activated can be dependent on the cytokine(s) involved, the expression level of the receptor(s) involved, availability of signaling pathway components, and activity levels of inhibitory mechanisms. These variables are regulated in concert by cells that receive signals and cells that produce cytokines. The role of LIFR signaling in maintaining homeostasis and related pathologies is therefore dependent on tissue type, specific pathology, and regulation of additional context-dependent intracellular mechanisms (71).

Extensive characterization of the signaling pathways activated by LIFR has revealed that they are associated with cellular proliferation, survival, and self-renewal (67, 68). For example, LIF-induced STAT3 activation is sufficient to maintain mouse embryonic

stem cell (mESC) pluripotency *in vitro* (64, 68). Additionally, constitutively active STAT3 is sufficient for mESC maintenance in the absence of LIF, underscoring the importance of the STAT3 pathway in embryonic development and cellular self-renewal (72). However, it was later shown that human embryonic stem cells (hESCs) require additional factors, and that neither exogenous LIF nor constitutively active STAT3 is sufficient to maintain hESC pluripotency (73). Further *in vivo* studies of LIF/LIFR/STAT3 revealed that STAT3 knockout (KO) mouse embryos failed to implant and develop, whereas JAK1 KO and LIFR KO mice died soon after birth due to various defects (74). However, LIF KO mice survive to adulthood, with females becoming sterile because of the requirement for maternal LIF for blastocyst implantation. The survival of LIF KO mice suggests that redundancies exist in the LIFR-induced signaling responses to the remaining cytokines in the IL-6 family (74).

Activation of the PI3K/AKT pathway, either through LIFR signaling or in the absence of cytokines, can maintain pluripotency in both mouse and primate ESCs (75). In contrast to the STAT3 and AKT pathways, MAPK *inhibition* is necessary to enhance the self-renewal properties of mESCs (76). Cells can inhibit MAPK through the expression of the STAT3 target gene known as suppressor of cytokine signaling 3 (SOCS3), which competitively binds to the phosphorylated tyrosine residues of LIFR/IL-6ST, thereby preventing the binding of SHP2 (68). Therefore, it appears that LIFR-induced increases in self-renewal caused by activated STAT3 and AKT supersede the differentiation programs promoted by activated MAPK in ESCs. However, the dichotomy of downstream effects rendered by LIFR highlights its ability to control an intricate network of intracellular mechanisms that regulate the precise timing of signals that influence the developing embryo. In humans, autosomal recessive inheritance of a mutation in the LIFR gene can cause a genetic disease known as Stüve-Wiedemann syndrome (STWS), which results from the loss of LIFR expression and subsequent loss of the STAT3 signaling response

from the IL-6 family of cytokines during development. STWS causes developmental disorders in bone tissue, and usually results in perinatal death (77).

Although LIFR is expressed throughout the inner cell mass of the developing embryo, its expression pattern in somatic cells is confined to specific organs and tissues. In contrast, IL-6ST is expressed ubiquitously in adult somatic cells (65, 66). LIFR has been characterized for its role in the development of specific tissues, including skeletal muscle, central nervous system, and urinary tract (78–81). In addition to its characterization during development, LIFR has been well characterized for its role in the pathology of various human cancers and other human diseases affecting skeletal muscle, cardiac muscle, and kidneys (47, 71, 78, 82). However, in somatic cells, LIFR-induced signaling not only affects self-renewal but also drives tissue- and context-dependent phenotypic effects. This suggests that the LIFR gene is *pleiotropic* in adult organisms and offers a potential explanation for its paradoxical role in the pathology of various cancers (71).

Recent preclinical experimental evidence has attempted to establish the role of LIFR in human cancer progression. Forty examples of primary research publications examining various types of cancer were extracted from a recent review by Halder et al. (Table 1). The majority of articles (27 of 40) found LIFR to be a promoter of cancer progression. Additionally, a subset of articles characterizing pathways that promote cellular self-renewal (JAK/STAT3 and PI3K/AKT) mostly found LIFR to be a promoter of disease progression (20 out of 27). However, articles characterizing breast cancer mostly showed that LIFR is a suppressor of disease progression (5 out of 8), but of those eight articles, five characterized JAK/STAT3 and P13K/AKT, and three of those five concluded that LIFR is a disease promoter. This highly conflicting body of evidence clearly illustrates that additional studies are required to fully understand how LIFR expression in tumors participates in the ensuing pathology.

Table 1 – List of primary research publications characterizing LIFR in cancer. Publications were extracted from a recent review by Halder et al. (2022), grouped by cancer type, and sorted by year of publication. The “Role” column describes the conclusions of the authors regarding the role of LIFR as either a suppressor or promoter of cancer progression in preclinical studies. Breast cancer articles show two additional columns indicating whether the investigation included LIFR knockout/knockdown (KO) and/or overexpression (OE) experiments. *Indicates that the article also characterized the PI3K/AKT pathway; **Indicates that the article also characterized the HIPPO and WNT pathways; **Bold** indicates the article published by the Howe laboratory (Woosley, A., 2019) that preceded the current study. PMID, Pubmed ID.

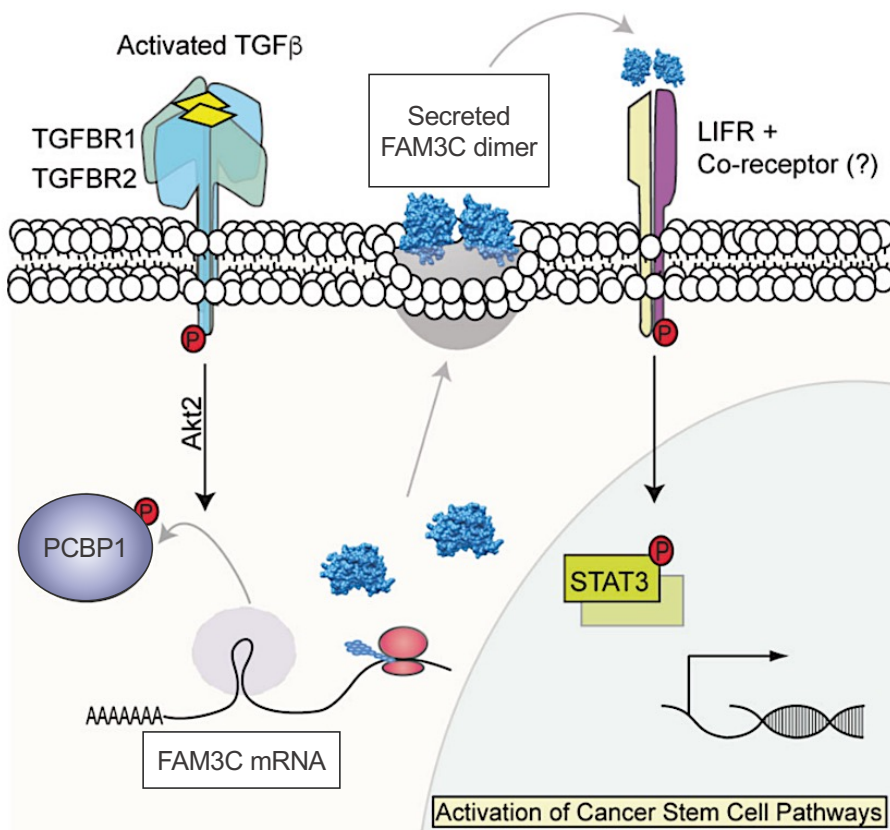
KO	OE	Cancer Type	Pathway	Role	Author	Year	Journal	PMID
YES	YES	Breast	HIPPO	Suppressor	Chen, D.	2012	Nat. Med.	23001183
YES	YES	Breast	Not shown	Suppressor	Iorns, E.	2012	Breast Cancer Res. Treat.	22535017
		Breast	PI3K/AKT	Promoter	Li, X.	2014	Oncotarget	24553191
YES	YES	Breast	HIPPO	Suppressor	Nandy, S.B.	2015	Oncotarget	25962054
YES		Breast	JAK-STAT3	Suppressor	Johnson, R.W.	2016	Nat. Cell. Biol.	27642788
		Breast	JAK-STAT3	Promoter	Zeng, H.	2016	Cancer Cell	27622335
YES	YES	Breast	JAK-STAT3	Promoter	Woosley, A.	2019	Oncogene	30692635
		Breast	JAK-STAT3	Suppressor	Clements, M.E.	2021	Oncogene	34247191
		Pancreas	Not shown	Suppressor	Ma, D.	2016	Oncol. Rep.	27375070
		Pancreas	JAK-STAT3*	Promoter	Bressy, C.	2018	Cancer Res.	29269518
		Pancreas	HIPPO	Promoter	Wang, M.T.	2019	Nat. Commun.	31296870
		Pancreas	JAK-STAT3**	Promoter	Shi, Y.	2019	Nature	30996350
		Pancreas	JAK-STAT3	Suppressor	Liu, S.	2021	Mol. Cancer Res.	33931487
		Gastric	PI3K/AKT	Suppressor	Zhang, F.	2018	J. Exp. Clin. Cancer Res.	30012200
		Gastric	JAK-STAT3	Suppressor	Xu, G.	2019	J. Cell. Physiol.	30565675
		Gastric	HIPPO	Suppressor	Seeneevassen, L.	2020	Cancers (Basel)	32707998
		Gastric	HIPPO	Promoter	Bian, S.B.	2021	Ann. N.Y. Acad. Sci.	32827446
		Prostate	JAK-STAT3	Promoter	Won, H.	2017	J. Leukoc. Biol.	28533357
		Prostate	PI3K/AKT	Promoter	Shao, J.	2019	Cancer Lett.	30851421
		Prostate	JAK-STAT3	Promoter	Liu, Y.N.	2019	Clin. Cancer Res.	30962287
		Prostate	JAK-STAT3	Promoter	Lin, S.R.	2020	Oncogene	32963351
		Melanoma	BMP	Promoter	Kuphal, S.	2013	Exp. Mol. Path.	23831429
		Melanoma	JAK-STAT3	Promoter	Guo, H.	2015	Oncotarget	26329521
		Melanoma	JAK-STAT3	Suppressor	Humbert, L.	2015	BMC Cancer	25885043
		Nasopharyngeal	PI3K/AKT	Promoter	Liu, S.C.	2013	J. Clin. Invest.	24270418
		Nasopharyngeal	HIPPO	Promoter	Liu, S.C.	2018	Nat. Commun.	30504771
		Osteosarcoma	JAK-STAT3	Promoter	Liu, B.	2015	APMIS	26271643
		Osteosarcoma	JAK-STAT3	Promoter	Lu, B.	2020	Mol. Cancer Res.	31615908
		Endometrial	JAK-STAT3*	Promoter	Tang, W.	2021	Cell Death Dis.	34400617
		Colorectal	JAK-STAT3	Promoter	Yu, H.	2014	Nat. Commun.	25323535
		Lung	JAK-STAT3	Promoter	Lin, W.H.	2021	Oncogene	33262462
		Liver	PI3K/AKT	Suppressor	Luo, Q.	2015	Carcinogenesis	26249360
		Chordoma	Not shown	Promoter	Gulluoglu, S.	2017	Oncol. Res.	28247842
		Medulloblastoma	PI3K/AKT	Promoter	Salm, F.	2015	PLoS One	25915540
		Glioblastoma	Not shown	Promoter	Edwards, L.A.	2017	Sci. Rep.	28246407
		Oral Squamous	Not shown	Promoter	Ohata, Y.	2018	PLoS One	29444110
		Ovarian	JAK-STAT3	Promoter	McLean, K.	2019	Oncogene	30305729
		Renal	HIPPO	Suppressor	Lei, C.	2018	DNA Cell Biol.	29902078
		Bile duct	PI3K/AKT	Promoter	Morton, S.D.	2015	Oncotarget	26296968
		Uterine	JAK-STAT3	Promoter	Fitzgerald, J.S.	2005	Int. J. Biochem. Cell Biol.	16125646

It is possible that the type of cancer and the tissue from which it originates determine whether LIFR acts as a promoter or suppressor of disease; however, it is also possible that the phenotypic behavior of cultured cells, either *in vitro* or following injection into laboratory mice, is limited in its ability to produce consistent results and in its ability to provide an adequate parallel to the behavior of human disease. Therefore, novel investigations, such as those illustrated in the current study, are challenged to provide interpretations that demonstrate consideration of the contextual features of their experimental designs, and are prompted to provide a level of scientific rigor that is consistent with the efforts made during the preceding peer review.

In 2019, the Howe laboratory published experiments by Woosley et al. following their discovery of an extracellular binding interaction between FAM3C and LIFR (28). Woosley et al. utilized the Progression Series Model of mammary carcinoma mentioned in the preceding section, which was created using normal murine mammary gland (NMuMG) cells with shRNA-mediated knockdown of PCBP1 (shPCBP1 cells). Woosley et al. demonstrated that knockdown of either FAM3C or LIFR caused a loss of self-renewal capacity in shPCBP1 cells *in vitro*, and that treatment with exogenous FAM3C could rescue this loss, but only when shPCBP1 cells expressed LIFR (28). It was further shown that the maintenance of self-renewal was directly dependent on the phosphorylation of STAT3 at tyrosine 705 (pSTAT3) and that pSTAT3 activation occurred exclusively through LIFR and only in the presence of FAM3C (28). When shPCBP1 cells with knockdown of either FAM3C or LIFR were injected into the fat pads of immunocompromised mice, both the tumor burden and pulmonary metastases were attenuated relative to cells expressing both proteins (28). Extreme limiting dilution analysis (ELDA) determined that the number of tumor-initiating cells present in the fat pad injections was significantly decreased following knockdown of FAM3C or LIFR, which suggests that the loss of self-renewal capacity following loss of FAM3C/LIFR interaction played a role in slowing the growth and

spread of tumors in mice (28). The authors concluded that the interaction between FAM3C and LIFR is responsible for inducing a STAT3-mediated “breast cancer stem cell” (BCSC) self-renewal phenotype in shPCBP1 cells. They also concluded that the Progression Series Model provides a method for further examination of TGF β -induced EMT in the context of mammary carcinoma dissemination and outgrowth at secondary tumor sites. An illustration of the hypothesized FAM3C/LIFR-induced signaling pathway and phenotype is shown in Figure 2 (28).

Woosley et al. demonstrated the first example of an extracellular ligand capable of propagating signals through LIFR that does not belong to the IL-6 family of cytokines, and demonstrated how LIFR signaling affects breast cancer pathology *in vivo* following EMT. This work was further substantiated in a subsequent study by Zhou et al., through examination of FAM3C/LIFR-mediated EMT during renal interstitial fibrosis, although it was found that PI3K/AKT pathway activation played a major role as opposed to JAK/STAT3 (47). Clinical strategies for the treatment of mammary carcinoma are currently challenged by two major facets of pathology that result in poor prognosis: dissemination of cancer cells from the primary tumor, and increased chemotherapeutic resistance of those cells. Cancer cells with increased “stemness” and EMT properties have been previously associated with increased metastatic potential and chemoresistance (83, 84). The identification of FAM3C/LIFR/STAT3 as a pathway that can promote metastasis and cellular self-renewal in the Progression Series Model suggests that further investigation may identify a way to target this pathway and decrease disease severity. Therefore, the current study aimed to identify the intracellular mechanisms responsible for regulating the phenotypic effects of FAM3C/LIFR interaction in shPCBP1 cells.



Adapted from Woosley, A. et al. *Oncogene* 2019; 38:3794-3811

Figure 2 – Proposed schematic of FAM3C/LIFR-induced BCSC phenotype. A diagram extracted from Woosley et al. (2019) illustrates the conclusions drawn from previously published experiments in the Howe laboratory. BCSC, breast cancer stem cell.

1.4 Pathological and clinical implications of FAM3C/LIFR/STAT3

Preclinical investigations have extensively characterized the roles of FAM3C, LIFR, and STAT3 expression in the pathology of various cancers (71, 85, 86). However, investigations using cancer patient samples to demonstrate the role of STAT3 are far more extensive than those on FAM3C and LIFR. Although clinical trials are currently active for drugs that inhibit STAT3 in cancer, no clinical trials have been initiated for drugs that directly target FAM3C or LIFR.

i. Clinical characterization of FAM3C

FAM3C has recently shown promise as an emerging cancer biomarker, and FAM3C expression has been shown to be higher in breast cancer, hepatocellular carcinoma (HCC), stomach cancer, oral squamous cell carcinoma (OSCC), and gastric cancer patient samples when compared to FAM3C expression levels in normal tissues (28, 42, 51, 55, 85). Yin et al. showed that FAM3C expression in gastric cancer tumors correlated positively with the depth of invasion, lymph node metastasis, and vimentin expression (a marker of mesenchymal phenotype), and negatively correlated with E-cadherin expression (a marker of epithelial phenotype) (85). Additionally, FAM3C detection in extracellular vesicles was higher in plasma samples from patients with non-small cell lung cancer (NSCLC) than in healthy subjects (87). The establishment of FAM3C as a potential cancer biomarker and the detection of FAM3C in the blood of patients with cancer have led to its inclusion in an active clinical trial that aims to enhance the early diagnosis of HCC through the identification of molecules in patient blood samples (NCT05825196).

Initial evidence suggesting a correlation between increased FAM3C secretion and worsening carcinoma progression was shown by Csiszar et al., based on a study of subcellular FAM3C localization in human breast cancer tumor arrays (56). Recent studies

in the Howe laboratory using human mammary carcinoma patient tumor microarrays revealed that FAM3C expression was increased in lymph nodes from cancer patients relative to the lymph nodes of healthy patients, suggesting that increased FAM3C expression correlates not only with tumor incidence but also with metastatic progression. However, examination of patient survival statistics from databases that provide FAM3C protein expression levels in breast cancer tumor samples showed variable prediction outcomes. For example, a dataset derived from triple-negative breast cancer (TNBC) patient samples showed that high FAM3C expression significantly increased the probability of overall survival (OS) and distant metastasis-free survival (DMFS) compared to low FAM3C expression (Fig. 3). These examples contradict the predictions made by the pre-clinical and clinical analyses cited above and therefore require further analysis to determine whether additional factors influence the significance of the findings. However, a second independent dataset derived from a mixed population of ER+ and ER- patients showed that high FAM3C expression significantly decreased the probability of overall survival versus low FAM3C expression, which aligns with the conclusions reached thus far regarding the role of FAM3C in pathology (Fig. 3).

When interpreting Kaplan-Meier survival plots of FAM3C expression, additional factors may need to be considered. These may include (1) the detection of disseminated cells in the lymph nodes at the time of sample collection, (2) the disease stage and tumor grade at the time of sample collection, and (3) the age of the patients in the datasets. These examples, in addition to other clinical features, may become potentially confounding factors that limit the applicability of these analyses when attempting to predict survival correlation with gene expression. Perhaps the most important consideration is the fact that FAM3C is secreted into the extracellular space, making it impossible to quantify the true value of FAM3C protein expression as “high” or “low,” simply because the

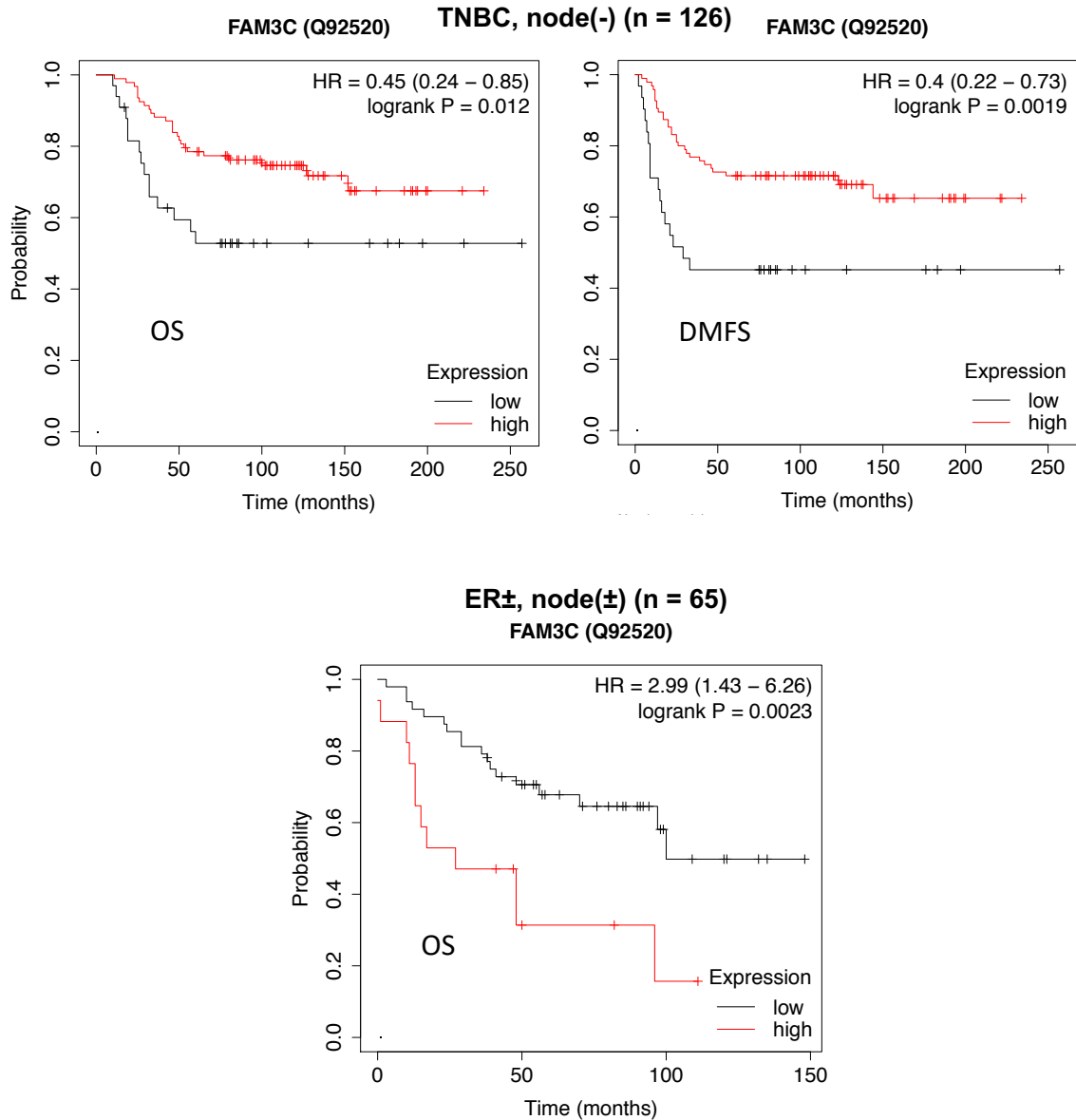


Figure 3 – FAM3C protein expression has both positive and negative correlations with the survival of patients with mammary carcinoma. Kaplan-Meier analysis plots showing the survival rates of mammary carcinoma patients using two independent FAM3C protein expression datasets. Triple-negative breast cancer with lymph node negative status (TNBC, node(-)) samples derived from “KM-plotter (Liu, 2014) show overall survival (OS) and distant metastasis-free survival (DMFS) (top left, top right); Estrogen receptor positive and negative (mixed), lymph node positive and negative (mixed) (ER±, node(±)) samples derived from “KM-plotter (Tang, 2018) show overall survival (OS) (bottom). Additional analyses (not shown) either failed to reach statistical significance or had insufficient sample size. The hazard ratio (HR) represents the cutoff value with the highest hazard rate, where a value of “1” indicates no difference and a value of “2” indicates a 100% difference.

aforementioned sample measurements were taken from the bulk tumor tissue as opposed to being taken from a blood or body fluid sample. Finally, mRNA expression levels were not examined in this analysis, owing to our knowledge of the role of PCBP1 in the suppression of FAM3C mRNA translation. However, it may be possible to expand the number of patients in prospective datasets if the mRNA expression can be accurately included in this type of analysis.

ii. Clinical characterization of LIFR

Characterization of the signaling pathways downstream of LIFR (e.g., JAK/STAT3) has clearly shown an association between high signaling activity and oncogenesis, severity of prognosis, and decreased overall survival of cancer patients (71). The JAK/STAT3 pathway is the predominant pathway associated with LIFR expression and activity and is of paramount interest in the current study. Therefore STAT3-related pathology and clinical research are discussed thoroughly in the following sections, as they apply to mammary carcinomas and other cancers. However, the clinical characterization of LIFR *expression itself* remains paradoxical because evidence suggests that low LIFR expression correlates with an increased severity of prognosis (71). In the preceding section, preclinical investigations of LIFR expression were also described as paradoxical in that they identified LIFR as either a promoter or suppressor of pathology (see Table 1 for a summary). A recent study of serial tissue sections from human patients with mammary carcinoma attempted to describe the pattern of LIFR expression in tumors. In that study, immunohistochemical staining showed that the majority of tumors (67.15%) had lower LIFR expression than healthy tissues, suggesting that the loss of LIFR expression drives disease progression. However, almost one-third of cases (32.85%) showed either no loss or increased LIFR expression (88). A previous study on liver cancer

(HCC) patient tissue samples also showed that LIFR expression is lost in tumors relative to adjacent healthy tissues (89). Interestingly, recent preclinical work in the Howe laboratory by Woosley et al. using the Progression Series Model showed that *ex vivo* cultured cells from mouse tumors and lung metastases showed a loss of LIFR expression relative to engrafted shPCBP1 cells (28). The observation by Woosley et al. was discussed by the authors as a possible model for establishing an experimental context that might reveal the nature of “dynamic” and paradoxical behavior of LIFR expression during the progression of mammary carcinoma pathology (28). Previous work by Okamura et al. suggested that epigenetic mechanisms, including hypermethylation of the LIFR promoter, may be capable of regulating LIFR expression *in vivo*, which might provide an explanation for changes in LIFR levels and in the consequent role of LIFR during disease progression (89).

Analysis of the correlation between LIFR mRNA expression and survival in patients with mammary carcinoma suggests that LIFR plays a complex role in predicting outcomes. Utilizing two separate databases, RNA-seq quantification (n = 2976) and Affymetrix Genechip quantification (n = 1879) were used to analyze patient survival using the Kaplan-Meier model. The initial analysis consisted of 39 comparisons, using all patients or various subsets segregated by specific clinical features. The results indicated that high LIFR expression is predictive of increased overall survival and increased distant metastasis-free survival, with 23 of 39 comparisons (59%) showing a significant association between high LIFR expression and favorable survival (Table 2). None of the comparisons in the initial analysis showed a significant association between high LIFR expression and unfavorable survival, although several comparisons suggested that trends were present (indicated by “*” in Table 2). Of the 39 comparisons made in the initial analysis, 16 (41%) failed to demonstrate statistical significance. Therefore, the initial analysis suggests that

Table 2 – Initial survival analysis of LIFR expression in patients with breast cancer. Outcomes were generated using the Kaplan-Meier analysis engine at www.kmplot.com, based on mRNA abundance of LIFR using either RNA-seq or Affymetrix Gene-chip (probe 205876_at) datasets, and restricted to patient attributes shown in the “cohort” column. “Favorable” indicates that an increased survival rate was shown in the group of patients that was associated with “High LIFR” expression levels when compared to the group of patients with “Low LIFR” expression levels. Only outcomes with P-values <0.05 were considered significant. OS, overall survival; DMFS, distant metastasis-free survival; NS, not significant. “*” symbol indicates an outcome that showed a trend but that did not reach statistical significance, and that was selected for further analysis.

Detection	Survival	Cohort	n	High LIFR	Low LIFR
RNA-seq	OS	All patients	2976	Favorable	Unfavorable
RNA-seq	OS	Node (+)	1067	Favorable	Unfavorable
RNA-seq	OS	Node (-)	1820	Favorable	Unfavorable
RNA-seq	OS	TNBC	126	Favorable	Unfavorable
RNA-seq	OS	ER+, HER2-	2218	Favorable	Unfavorable
RNA-seq	OS	ER+, PR+	2282	Favorable	Unfavorable
RNA-seq	OS	Grade 3 tumors	1074	Favorable	Unfavorable
RNA-seq	OS	Basal subtype	309	NS	NS
RNA-seq	OS	Luminal A subtype	1504	Favorable	Unfavorable
RNA-seq	OS	Luminal B subtype	668	NS	NS
RNA-seq	OS	HER2+ subtype	295	Favorable	Unfavorable
RNA-seq	OS	Endocrine intervention	2302	Favorable	Unfavorable
RNA-seq	OS	Chemo intervention	1195	Favorable	Unfavorable
Gene-chip	OS	All patients	1879	Favorable	Unfavorable
Gene-chip	OS	TNBC	201	Favorable	Unfavorable
Gene-chip	OS	Node (+)	452	NS	NS
Gene-chip	OS	Node (-)	726	NS	NS
Gene-chip	OS	ER+, HER2-	630	NS	NS*
Gene-chip	OS	ER+, PR+	141	NS	NS
Gene-chip	OS	Grade 3 tumors	586	NS	NS
Gene-chip	OS	Basal subtype	431	Favorable	Unfavorable
Gene-chip	OS	Luminal A subtype	596	NS	NS*
Gene-chip	OS	Luminal B subtype	439	NS	NS*
Gene-chip	OS	HER2+ subtype	362	NS	NS
Gene-chip	OS	Endocrine intervention	339	NS	NS*
Gene-chip	OS	Chemo intervention	398	Favorable	Unfavorable
Gene-chip	DMFS	All patients	2765	Favorable	Unfavorable
Gene-chip	DMFS	TNBC	424	Favorable	Unfavorable
Gene-chip	DMFS	Node (+)	889	Favorable	Unfavorable
Gene-chip	DMFS	Node (-)	1309	NS	NS
Gene-chip	DMFS	ER+, HER2-	1002	NS	NS
Gene-chip	DMFS	ER+, PR+	493	Favorable	Unfavorable
Gene-chip	DMFS	Grade 3 tumors	836	NS	NS*
Gene-chip	DMFS	Basal subtype	626	Favorable	Unfavorable
Gene-chip	DMFS	Luminal A subtype	998	NS	NS
Gene-chip	DMFS	Luminal B subtype	673	Favorable	Unfavorable
Gene-chip	DMFS	HER2+ subtype	401	NS	NS
Gene-chip	DMFS	Endocrine intervention	1065	Favorable	Unfavorable
Gene-chip	DMFS	Chemo intervention	968	Favorable	Unfavorable

low expression of LIFR in breast cancer tumors is associated with disease progression, contradicting many previous observations, including those made by the Howe lab in the publication by Woosley et al. (28).

Based on the initial analysis suggesting that high LIFR expression demonstrates an unfavorable trend for certain patient groups, a secondary analysis was conducted utilizing further segregation of the datasets, based on additional clinical features. The results of this analysis revealed that high LIFR expression was significantly associated with decreased overall survival or decreased distant metastasis-free survival in seven comparisons (Table 3). These findings suggest that the predictive value of LIFR expression as a mediator of survival outcomes may depend on the criteria used to segregate patient cohorts, and that confounding factors may influence the results of large datasets. For instance, the observation that all initial comparisons using cohorts of 1350 patients or more were unanimous and significant in their prediction of survival outcome based on LIFR expression may have been influenced by unknown factors capable of skewing the data. This highlights the importance of considering confounding factors and the potential impact of including patients with little or no presence of disease, such as those diagnosed with cancer that later changes to ductal in-situ carcinoma (DCIS), which may increase the survival rate in certain groups. However, preliminary analysis of both RNA-seq and Gene-chip datasets (all patients) was unable to determine whether a single factor (e.g., presence or absence of neoadjuvant chemotherapy or similar intervention) might be indicative of a group of patients that caused the data to be skewed.

It is noteworthy that several of the outcomes shown in the secondary analysis depict a more advanced stage of disease, which is particularly relevant considering that the majority of deaths caused by mammary carcinoma occur in patients diagnosed with metastatic mammary carcinoma (90). Furthermore, the five-year survival rate for patients diagnosed with metastatic mammary carcinoma is less than 25% (91). As such, it is

Table 3 – Secondary LIFR expression survival analysis. Outcomes were generated using the Kaplan-Meier analysis engine at www.kmplot.com, based on mRNA abundance of LIFR using the Affymetrix Gene-chip (probe 205876_at) dataset, and restricted to breast cancer patient attributes shown in the “cohort” column. “Favorable” indicates that an increased survival rate was shown in the group of patients that was associated with “Low LIFR” expression levels when compared to the group of patients with “High LIFR” expression levels. Only outcomes with P-values <0.05 were considered significant. OS, overall survival; DMFS, distant metastasis-free survival; NS, not significant.

Detection	Survival	Cohort	n	High LIFR	Low LIFR
Gene-chip	OS	ER+, HER2- (Grade 3 only)	171	Unfavorable	Favorable
Gene-chip	OS	Luminal A subtype (node- only)	272	Unfavorable	Favorable
Gene-chip	OS	Luminal B subtype (node+ only)	122	Unfavorable	Favorable
Gene-chip	OS	Endocrine intervention (ER+, HER2-, node-)	87	Unfavorable	Favorable
Gene-chip	DMFS	ER+, PR+, HER2- (Grade 3 only)	150	Unfavorable	Favorable
Gene-chip	DMFS	Grade 3 tumors (node- only)	429	Unfavorable	Favorable
Gene-chip	DMFS	Luminal B subtype (node+ only)	260	Unfavorable	Favorable

possible that although the generalized Kaplan-Meier data strongly suggest that high LIFR expression is favorable for patient survival, closer examination of smaller cohorts with specific clinical features, such as molecular subtype, lymph node status, or stage of disease, confined to patients with advanced disease may provide a more informed interpretation. This interpretation may provide a role for LIFR as a prognostic indicator and support the notion that high LIFR expression can be unfavorable, as described in the current study. Examples of Kaplan-Meier plots generated from the secondary analysis are displayed in Figure 4.

It is notable that LIFR protein expression levels were not detectable using either the online “KM-plotter” database (<http://www.kmplot.com>) or the databases catalogued in the National Institutes of Health Proteomic Data Commons (NIH PDC) portal. Based on previous knowledge of LIFR expression and phosphorylation patterns in mammary carcinoma, it was expected that LIFR would be detected in human tumor sample mass spectrometry data available in the “TCGA Breast Cancer Proteome” (PDC000173) and the “TCGA Breast Cancer Phosphoproteome” (PDC000174), which are catalogued in the NIH PDC portal. Interestingly, LIFR detection was reported in proteomic and phosphoproteomic studies catalogued at the NIH PDC, which characterized cancer patient tumor samples from various organs, including the brain, lung, bronchus, ovary, pancreas, kidney, and liver (93). Further analysis of LIFR protein expression data from potential future studies in breast cancer may enable observations of pan-cancer parallels when considering the role of LIFR in clinical settings and may reinforce the trends shown in the survival data mentioned above.

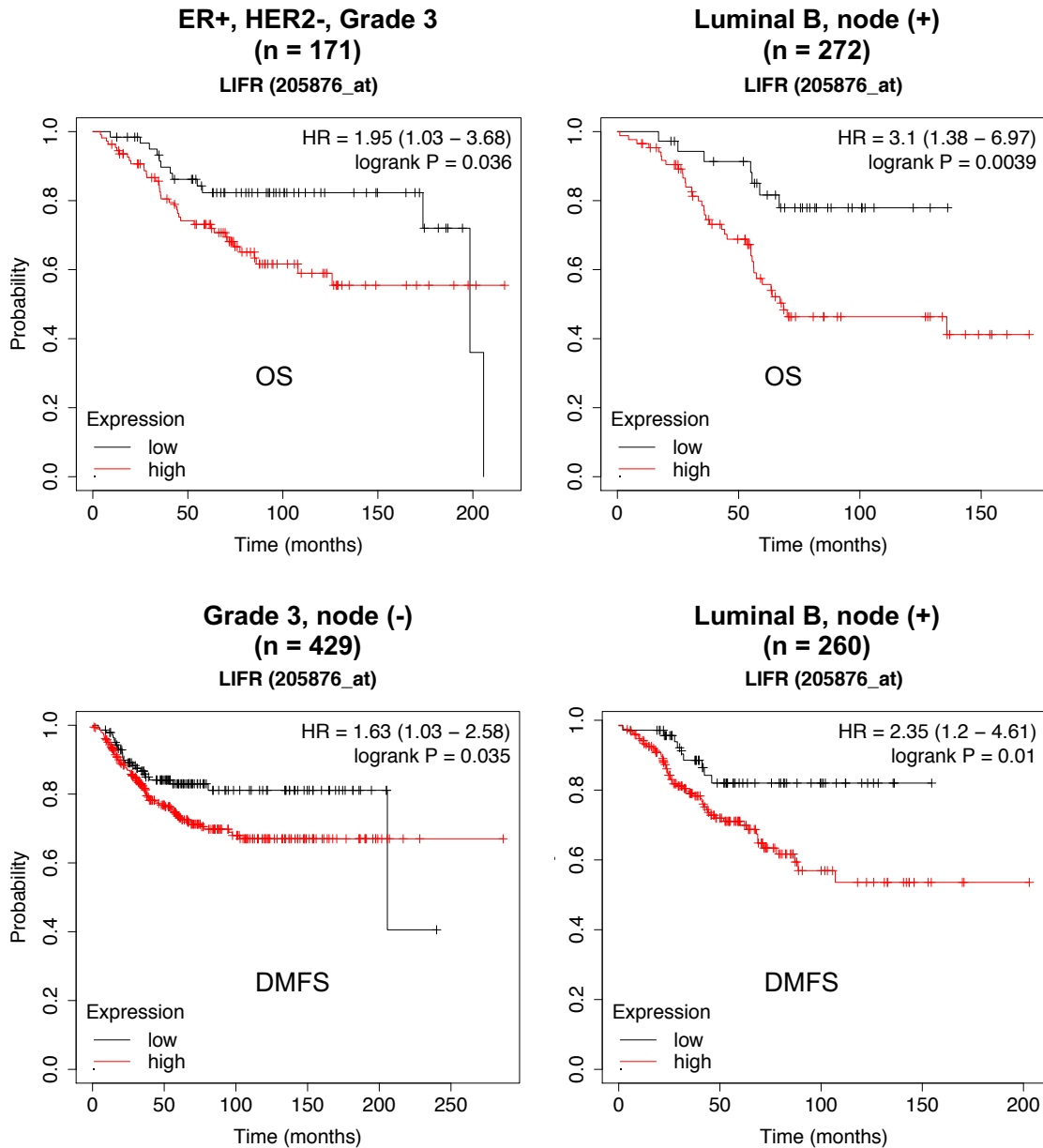


Figure 4 – High LIFR mRNA expression correlates with decreased survival in discreet breast cancer patient subsets. Kaplan-Meier analysis plots showing the survival rates of mammary carcinoma patients using an Affymetrix Gene-chip dataset (205876-at). Plots were selected from the outcomes listed in the secondary analysis shown in “Table 3”. The hazard ratio (HR) represents the cutoff value with the highest hazard rate, where a value of “1” indicates no difference and a value of “2” indicates a 100% difference. OS, overall survival; DMFS, distant metastasis-free survival.

iii. The identification of STAT3 as an oncogene

The signal transducer and activator of transcription (STAT) family of proteins contains seven members (STAT1, STAT2, STAT3, STAT4, STAT5a, STAT5b, and STAT6) (92). STATs were originally characterized in the late 20th century as “acute phase proteins” for their role in responding to the IL-6 family of cytokines during the acute phase of the inflammatory response following injury or infection (93, 94). Characterization of the JAK/STAT pathway revealed that it is also responsive to interferon cytokines (IFNs) and extracellular growth factors (95). In the years that followed, it was found that STATs could be activated not only by the IL-6 family of cytokine receptors, but also by additional receptor tyrosine kinases (RTKs), including epidermal growth factor receptor (EGFR) and platelet-derived growth factor receptor (PDGFR). Additionally, STATs can be activated by members of the G protein-coupled receptor family and non-receptor tyrosine kinases including SRC and ABL (96–98). In the 1990s, STAT proteins were identified as mediators of inflammation-associated pathology related to IL-6-induced signaling (93). By the end of the 20th century, IL-6-induced JAK/STAT signaling had been implicated in multiple inflammation-related disorders, including rheumatoid arthritis, pancreatitis, bacterial and viral meningitis, asthma, and Alzheimer’s disease (93, 99).

During the 1990s, STATs were identified as oncogenic drivers following multiple studies revealing that STAT1, STAT3, STAT5, and STAT6 are family members predominantly implicated in oncogenic transformation downstream of their phosphorylation by an array of tyrosine kinases (100). STAT3 was first characterized by Yu et al. (1995) and Cao et al. (1996) as a constitutively active transcription factor in SRC-transformed murine fibroblasts (101, 102). Additionally, Cao et al. demonstrated that STAT3 phosphorylation occurs due to hyperactive SRC kinase activity (102). Several years later, Bromberg et al. (1999) showed that constitutively active mutant STAT3

expression was sufficient to cause oncogenic transformation of rat fibroblast cells following an *in vitro* soft agar colony-formation assay (103). When STAT3-transformed fibroblasts were injected into immunocompromised mice, tumor growth occurred, whereas mice injected with normal fibroblasts did not form tumors (103). Consistent with *in vitro* studies conducted in the 1990s, elevated activity levels of STAT1, STAT3, and STAT5 proteins were identified in tumor samples from human cancer patients diagnosed with breast cancer, Burkitt's lymphoma, head and neck cancer, and multiple myeloma (96).

The involvement of STAT3 in the pathology of breast cancer was further characterized in 1997 by a group of scientists at the University of Michigan, led by Dr. Stephen Ethier (104). Sartor et al. determined that constitutive STAT3 activity downstream of EGFR activation is a feature common to multiple cell lines derived from patients with human mammary carcinoma (104). A later collaboration between the Ethier laboratory and a group at the Moffit Cancer Center and Research Institute in Tampa, Florida, led by Dr. Richard Jove, produced similar results: Garcia et al. (1997) found that the normal healthy human mammary epithelium does not demonstrate hyperactive EGFR/STAT3, whereas human mammary carcinoma cell lines frequently display constitutively active STAT3. They also found that hyperactive STAT3 in human mammary carcinoma cells could occur downstream of tyrosine kinase activity, independent of EGFR (105). A subsequent study conducted by the Jove laboratory (Garcia et al., 2001) found that selective inhibition of JAK or SRC kinases results in cell cycle arrest, growth inhibition, and increased apoptosis in human mammary carcinoma cell lines with elevated STAT3 activity. Similarly, the expression of a dominant-negative mutant STAT3 resulted in a loss of cell survival (106). Garcia et al. also demonstrated evidence of elevated STAT3 activity in 78% of tumor samples (18 of 23 tumors) from human mammary carcinoma patients, relative to matched samples from adjacent healthy tissue specimens (106). *This study provided the first example of the direct involvement of STAT3 in the pathology of human*

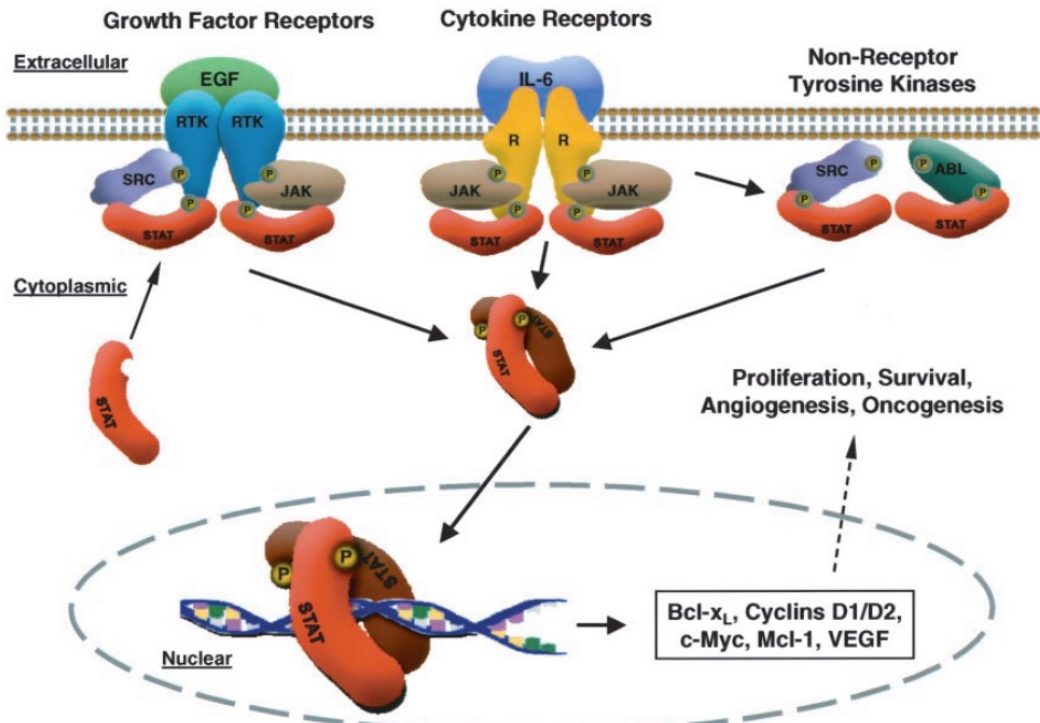
mammary carcinoma. Subsequent studies by other groups have continued to focus on the involvement of STAT3 in pathology, investigating the possibility that dysregulation of gene expression resulting from increased binding of STAT3 to DNA could participate directly in oncogenesis and disease progression.

iv. The development of STAT3 as an anticancer drug target

STAT3 is a transcription factor that can be described as “latent,” in that it accumulates in the cytoplasm but remains largely inactive until signals from multiple converging upstream pathways trigger DNA-binding activity that ultimately affects the phenotype of the cell (98). Prior to the development of STAT3 as an anticancer drug target, the strategy of pharmacologically inhibiting a transcription factor was previously established through the use of glucocorticoids to target glucocorticoid receptor transcription factors for novel anti-inflammatory drugs (98). At the turn of the 21st century, it was asserted that targeting STAT3 was logical and had several advantages. For example, it would be easier to inhibit one overactive transcription factor as opposed to inhibiting multiple overactive tyrosine kinases that could uniquely activate STAT3 with case-dependent outcomes. Additionally, it was hypothesized that all cancer cells possess common dysfunctions, (e.g. overactive tyrosine kinases), which would allow a drug targeting STAT3 to be potentially omnipotent for cancer therapy (98, 107).

Validation of STAT3 as a transcription factor capable of directly upregulating genes involved in the pathology of multiple types of cancer has been demonstrated by experimental investigations conducted at the turn of the 21st century (107). Evidence has demonstrated that STAT3 activates the transcription of genes involved in cell cycle propagation (cyclin D1/D2), promotion of angiogenesis (VEGF), and inhibition of apoptosis (BCL-XL, MCL-1) (107). The first evidence of the effective inhibition of STAT3 *in vivo* was provided by a group of scientists at the Moffitt Cancer Center and Research Institute, led

by Dr. Richard Jove and Dr. Hua Yu. Gene therapy administered by electroinjection of a dominant-negative mutant STAT3 expression vector into mouse melanoma tumors effectively inhibited tumor growth and caused tumor regression (108). Additional investigations have demonstrated that (1) inhibition of STAT3 using antisense oligonucleotides to block STAT3 translation could effectively attenuate the growth of cancer cells *in vitro*, and (2) inhibition of dimerization/activation of STAT3 using phosphopeptides could effectively block STAT3-mediated activation of transcription *in vitro* (107). A summary of the hypothesized mechanism of STAT3-induced pathology in cancer, as outlined by the Jove laboratory, is shown in Figure 5 (107).



Extracted from Buettner, R. et al. *Clinical Cancer Research*, 2002; 8:4

Figure 5 – Summary of the mechanism(s) of STAT3 in cancer. A diagram extracted from Buettner et al. (2002) illustrates the hypothesized mechanism of STAT3 signaling induction and subsequent dysregulation of genes in human cancers.

In accordance with the preceding inhibition studies, multiple prospective molecular methods for the inhibition of STAT3 have been proposed, exemplifying the advent of “rational drug design” for targeting specific intracellular molecular functions. During the decade that followed the initial preclinical investigations of STAT3 inhibitors, multiple synthetic drugs were developed using rational drug design methods. These methods included “in-silico” computer-assisted molecular screens of synthetic compounds that might possess binding affinity for STAT3, based on parallel acquisition of the STAT3 protein structure derived from x-ray crystallography. (109). The proposed molecular methods for the inhibition of STAT3 are summarized in Table 4 (99, 109–114).

Table 4 – List of proposed methods of STAT3 inhibition. Publications describing the proposed methods for STAT3 inhibition at the turn of the 21st century were extracted from a review by Turkson et al. (2000). The “Category” column indicates whether the proposed mechanism and/or synthetic molecule would directly target the STAT3 protein (direct) or whether it would target an upstream mediator of STAT3 activation (indirect). The “Reference” column lists examples of primary research that led to each corresponding proposed mechanism. The complete reference details can be found in the “References” section of this manuscript.

Method Name	Mechanism of Action	Category	Reference
Receptor/ligand antagonists	Synthetic molecule-mediated competitive inhibition of receptor/ligand interactions	Indirect	Catlett-Falcone, R. (1999)
Kinase inhibition	Synthetic molecule-mediated Inhibition of upstream kinases (e.g., JAK2, SRC)	Indirect	Catlett-Falcone, R. (1999)
Physiological protein-mediated inhibition	Modulation of phosphatases or endogenous inhibitors (e.g., SOCS3)	Indirect	Endo, T. (1997); David, M. (1993)
Inhibition of dimerization	Synthetic molecule-mediated competitive inhibition of STAT3 homodimerization	Direct	Becker, S. (1998)
Inhibition of nuclear translocation	Disruption of mechanisms required for STAT3 nuclear translocation	Direct	Sekimoto, T. (1996)
Inhibition of DNA binding	(1) STAT3 "decoy" oligonucleotide-mediated competitive inhibition of DNA binding, (2) expression of dominant-negative STAT3 mutant	Direct	Xiang, X. (1996); Niu, G. (1999)
Inhibition of STAT3 expression	Antisense oligonucleotide-mediated inhibition of STAT3 mRNA translation	Direct	Catlett-Falcone, R. (1999)

v. *Clinical use of STAT3 inhibitor drugs*

Since the turn of the 21st century, preclinical research efforts to identify potent, specific inhibitors of STAT3 have succeeded in accumulating vast amounts of data from experiments in cultured cells and mouse models of cancer (115–117). The cumulative preclinical data resulting from various screening strategies strongly suggest that inhibition of JAKs and small-molecule interference with the SH2-binding domain of STAT3 are the most promising strategies for drug development (115–118). SH2-binding small molecules have the potential to interfere with the phosphorylation, dimerization, and nuclear translocation functions of STAT3, making them capable of inhibiting the key molecular interactions necessary for the nuclear activity of STAT3 (118). In accordance with these data, nine drugs for the direct inhibition of STAT3 for the treatment of various cancers have been approved for investigational new drug (IND) status, and clinical trials involving human patients have been initiated. Several other clinical trials for the treatment of various cancers have been initiated using INDs that target JAKs (115). Additionally, pyrimethamine (Daraprim), a drug previously approved by the Food and Drug Administration (FDA) for the treatment of toxoplasmosis, has shown potential as a STAT3 inhibitor, and clinical trials have been initiated to repurpose it for the treatment of cancer (117). The JAK inhibitor ruxolitinib (Jakafi) has been approved by the FDA for the treatment of myeloproliferative neoplasia, but none of the drugs that directly target STAT3 have gained FDA approval (115). However, BBI608 (napabucasin), a direct STAT3 SH2-targeting inhibitor, has progressed to several completed phase three clinical trials for the treatment of various cancers, and has produced the most promising data thus far (119).

Several clinical trials using four INDs (three STAT3 inhibitors and one JAK inhibitor) have been initiated for the treatment of mammary carcinoma, and there are currently five active trials, although none of the drugs have progressed beyond phase two (115, 117). Bortezomib (Velcade), a drug previously approved by the FDA for the

treatment of multiple myeloma, has shown promise in multiple clinical trials for breast cancer treatment. Preclinical data have suggested that it acts as a STAT3 inhibitor, although the precise mechanism of action remains unknown (120, 121). The newest IND, TTI-101, is the first STAT3 inhibitor to be involved in a clinical trial designed exclusively for the treatment of breast cancer (NCT05384119), and is currently active and recruiting patients. A summary of clinical trials for the treatment of breast cancer using STAT3 inhibitors is presented in Table 5.

Preclinical investigations continue to provide evidence that reinforces the importance of identifying a successful drug for targeting STAT3, including evidence that further suggests the role of STAT3 in regulating pathological features of mammary carcinoma, such as EMT, self-renewal, and invasion. For example, it was shown that regulation of the TWIST1 gene by STAT3 is involved in the migration and invasion of mammary carcinoma cells, and implicates TWIST1 in the prediction of therapy resistance (122). The following sections describe how the current study aimed to further develop the findings of the Howe laboratory, as described by Woosley et al., to gain an understanding of FAM3C/LIFR/STAT3-mediated mechanisms of mammary carcinoma progression.

Table 5 – List of breast cancer clinical trials involving STAT3 inhibitors. Investigational new drugs for JAK/STAT inhibition in patients with breast cancer in the United States. The drugs listed as SH2-binding small molecules inhibit STAT3 through direct interaction. MOA, mechanism of action; Comp., completion; Comb., combination; mol., molecule; BC, breast cancer; Adv., advanced; met., metastatic; TNBC, triple-negative breast cancer; ER, estrogen receptor; HR, hormone receptor.

Drug Name	MOA	Trial Number	Start	Comp.	Condition	Comb. Treatment	Phase	Status
BBI608 (Napabucasin)	SH2-binding small mol.	NCT01775423	3/1/09	8/6/15	All BC	No comb.	1	Complete (Results pending)
OPB-31121	SH2-binding small mol.	NCT00955812	6/1/09	11/1/12	Adv. BC	No comb.	1	Complete (Results published)
OPB-51602	SH2-binding small mol.	NCT01423903	2/1/10	4/1/13	Adv. BC	No comb.	1	Complete (Results published)
BBI608 (Napabucasin)	SH2-binding small mol.	NCT01325441	4/1/11	6/1/21	TNBC	Paclitaxel	2	Complete (Results pending)
Ruxolitinib (Jakafi)	JAK inhibitor	NCT01594216	4/1/12	4/9/16	ER+ BC	Exemestane	2	Complete (Results pending)
Ruxolitinib (Jakafi)	JAK inhibitor	NCT01562873	6/1/12	6/1/16	pSTAT3+ BC	No comb.	2	Terminated (Results available)
Ruxolitinib (Jakafi)	JAK inhibitor	NCT02041429	2/1/14	1/1/21	TNBC	Paclitaxel	2	Complete (Results published)
Ruxolitinib (Jakafi)	JAK inhibitor	NCT02120417	5/1/14	1/1/17	HER2- BC	Capecitabine	2	Terminated (Results available)
Ruxolitinib (Jakafi)	JAK inhibitor	NCT02066532	6/1/14	10/14/20	HER2+ BC	Trastuzumab	2	Complete (Results published)
BBI608 (Napabucasin)	SH2-binding small mol.	NCT02467361	8/1/15	1/29/21	Adv. or met. BC	Ipilimumab Nivolumab Pembrolizumab	1	Complete (Results pending)
Ruxolitinib (Jakafi)	JAK inhibitor	NCT02876302	4/26/17	2/1/24	TNBC	Paclitaxel Doxorubicin Cyclophosphamide	2	Active
C188-9 (TTI-101)	SH2-binding small mol.	NCT03195699	11/15/17	10/1/23	Adv. BC	No comb.	1	Active
Ruxolitinib (Jakafi)	JAK inhibitor	NCT03012230	12/06/17	4/1/24	TNBC	Pembrolizumab	1	Active
Ruxolitinib (Jakafi)	JAK inhibitor	NCT02928978	5/13/18	1/1/25	High risk BC	No comb.	2	Recruiting
C188-9 (TTI-101)	SH2-binding small mol.	NCT05384119	1/9/23	2/1/25	HR+, HER2- met. BC	Palbociclib Aromatase inhibitor	1	Recruiting

vi. *Characterization of STAT3 activation: impact on prognosis*

Early studies characterizing STAT3 activation, specifically pSTAT3 Y705, and STAT3/DNA binding in breast cancer patients has concluded that high pSTAT3 accumulation/DNA binding activity are correlated with a variety of poor clinical outcomes, including survival rates (106, 123, 124). Garcia et al. conducted the first study to link pSTAT3 to mammary carcinoma pathology, using rapid processing of post-surgery human mammary carcinoma tumor samples and non-malignant matched samples to preserve STAT3/DNA binding in nuclear extracts. The study showed that STAT3/DNA binding activity was elevated in tumors, with little to no detection in adjacent normal tissues (106). In a following study by Chen et al., 140 breast cancer patients had their pSTAT3 accumulation levels evaluated by immunohistochemical staining (IHC) following tumor resection, and were followed clinically for 18-79 months (124). Using multivariate analysis, Chen et al. demonstrated a correlation between pSTAT3 accumulation and lymph node metastasis, as well as a decrease in survival for patients with high pSTAT3 accumulation in tumors (124). A recent study by Chen et al. examined 135 mammary carcinoma patients and found that pSTAT3 accumulation correlated with reduced relapse-free survival (RFS) in both TNBC patients and estrogen receptor-negative (ER-) patients, but not in ER+ patients (125). In fact, pSTAT3 accumulation was found to correlate with an increase in RFS in ER+ patients, indicating that pSTAT3-related outcomes and prognostic significance may vary depending on the breast cancer subtype (125).

Additional studies have indicated that pSTAT3 accumulation may have prognostic value as an indicator of *increased* overall survival in breast cancer; however, they also reveal a high degree of variability. In 2003, Dolled-Filhart et al. conducted a multivariate analysis of 346 lymph node-negative breast cancer tumor samples using a tumor microarray technique and found that pSTAT3 correlated with increased overall survival

following five years of clinical follow-up (126). In 2011, Sato et al. analyzed 785 archival breast cancer specimens by microarray, along with normal mammary epithelial specimens, and found that high levels of nuclear pSTAT3 correlated with improved overall survival, although the results did not establish statistical significance by multivariate analysis (127). Sato et al. also showed that nuclear pSTA3 accumulation decreases as disease severity and tumor grade increase when comparing advanced disease to DCIS and normal breast tissues (127). The data describing the efficacy of pSTAT3 as a prognostic indicator do not clearly establish its value in predicting the survival of breast cancer patients, which is perplexing when considering the promising data being collected through the clinical application of investigational new drugs that inhibit STAT3 phosphorylation. Further research is necessary to ascertain how to recognize patients who would gain advantages through characterization of pSTAT3's role in their diseases, perhaps using personalized medicine with individualized combinations of therapeutic interventions.

A formal examination of pSTAT3 protein accumulation in patients with breast cancer was conducted using the Kaplan-Meier survival model, as described in Sections 1.4.i and 1.4.ii. Using a cohort of 843 patients from The Cancer Genome Atlas Reverse Phase Protein Array (TGCA_RPPA) dataset, 27 comparisons were made to attempt to correlate pSTAT3 (Y705) accumulation with overall survival, with various segregations of the cohort that were based on the available pathological feature selections. Of the 27 comparisons, 13 (48%) demonstrated a statistically significant increase in overall survival in patients with high pSTAT3 accumulation compared to those with low pSTAT3 accumulation. Fourteen of the 27 comparisons (52%) were not statistically significant. However, when examining African American patients, a trend was observed that suggested that high pSTAT3 correlated with reduced overall survival. A second comparison was made with African American patients, using only those with negative

lymph node status. In contrast to the other comparisons, the results showed that high pSTAT3 correlated with *reduced* overall survival in this cohort, and when the comparison was repeated with lymph node-positive African American patients, the results failed to reach statistical significance. A detailed presentation of the pSTAT3 Kaplan-Meier analysis is presented in Table 6.

Table 6 – Survival analysis of pSTAT3 accumulation in patients with breast cancer. Outcomes were generated using the Kaplan-Meier analysis engine at www.kmplot.com, based on protein abundance of pSTAT3 (Y705) using “TCGA_RPPA” dataset, and restricted to patient attributes shown in the “cohort” column. “Favorable” indicates that an increased survival rate was shown in the group of patients that was associated with the indicated level of pSTAT3 accumulation compared to the opposite level of accumulation. Only outcomes with P-values <0.05 were considered significant. Analyses were restricted to cohorts of 40 or greater patients. OS, overall survival; NS, not significant. “*” symbol indicates an outcome that showed a trend but that did not reach statistical significance, and that was selected for further analysis.

Detection	Survival	Cohort	n	High pSTAT3	Low pSTAT3
Protein	OS	All patients	873	Favorable	Unfavorable
Protein	OS	Node (+)	452	Favorable	Unfavorable
Protein	OS	Node (-)	407	NS	NS
Protein	OS	TNBC	95	NS	NS
Protein	OS	ER+, HER2-	341	NS	NS
Protein	OS	ER+, PR+	519	NS	NS
Protein	OS	ER-, PR-	182	NS	NS
Protein	OS	HER2+	133	NS	NS
Protein	OS	Stage 3	207	Favorable	Unfavorable
Protein	OS	Stage 2	505	Favorable	Unfavorable
Protein	OS	Stage 1	128	NS	NS
Protein	OS	T = 3 (TNM)	115	NS	NS
Protein	OS	T = 2 (TNM)	525	Favorable	Unfavorable
Protein	OS	T = 1 (TNM)	196	NS	NS
Protein	OS	N = regional (TNM)	287	Favorable	Unfavorable
Protein	OS	N = regional spread (TNM)	103	Favorable	Unfavorable
Protein	OS	M = 0 (TNM)	737	Favorable	Unfavorable
Protein	OS	Radiation intervention	53	NS	NS
Protein	OS	Tamoxifen intervention	203	Favorable	Unfavorable
Protein	OS	Anastrozole intervention	60	Favorable	Unfavorable
Protein	OS	Doxirubicin intervention	307	Favorable	Unfavorable
Protein	OS	Cyclophosphamide intervention	410	Favorable	Unfavorable
Protein	OS	Paclitaxel intervention	188	Favorable	Unfavorable
Protein	OS	Caucasian Americans only	620	NS	NS
Protein	OS	Asian Americans only	58	NS	NS
Protein	OS	African Americans only	134	NS	NS*
Protein	OS	African Americans only, node (-)	69	Unfavorable	Favorable
Protein	OS	African Americans only, node (+)	60	NS	NS

The results of the preceding Kaplan-Meier analysis suggest that high pSTAT3 accumulation levels in patient tumors largely predict favorable survival outcomes, with the exception of a small cohort of patients belonging to a specific ethnic background. However, this conclusion does not align with preclinical and clinical data, which have demonstrated that high pSTAT3 activity is both a driver and a consequence of breast cancer development and progression. The utilization of a large dataset in the Kaplan-Meier analysis makes it difficult to ignore the clearly one-sided results, and further studies are necessary to determine whether correlations between pSTAT3 accumulation and patient survival can be used as a prognostic indicator. The variable results in the collective data suggest that future analyses may benefit from repeated measures using small groups with closely related pathological and/or demographic features, as well as with closely related patterns of neoadjuvant and adjuvant treatment interventions. This may help to delineate the nature of pSTAT3 during prognostic characterization by limiting the confounding variables involved in breast cancer survival rates among patients.

1.5 Central hypothesis and specific aims

The data provided by the Howe laboratory and other groups clearly show that FAM3C/LIFR interaction-induced intracellular signaling through pSTAT3 plays a role in the pathology of mammary carcinoma. Although previous studies have shown that the interaction between FAM3C and LIFR directly affects the behavior of mammary tumor cells *in vivo*, the precise mechanism(s) that regulate cellular phenotype, specifically BCSC self-renewal and metastasis, have not been determined. Additionally, although STAT3 has been clearly identified as a therapeutic target for human mammary carcinoma patients, the contribution of LIFR expression to STAT3-induced pathology remains unclear.

Further characterization of FAM3C/LIFR/STAT3 signaling using the Progression Series Model may reveal intracellular events involving novel therapeutic targets and provide critical information necessary for the improvement of current therapeutic interventions. Additionally, further understanding of the consequences of pSTAT3 activation in mammary epithelial cells may reveal how ensuing changes in gene regulation cause cancer cells to become more aggressive and/or resistant to chemotherapy. It is also possible that an increased understanding of the FAM3C/LIFR interaction can define mechanisms that are directly targetable by small-molecule inhibitors or other pharmacological interventions.

Based on previous studies, several key conclusions have been drawn that provide a rationale for future attempts to fill the gaps in knowledge outlined above: (1) Loss of PCBP1 expression causes EMT and increases tumorigenicity of mammary epithelial cells through upregulation of FAM3C; (2) FAM3C/LIFR interaction is required for pSTAT3 activation in shPCBP1 cells; (3) loss of FAM3C or LIFR expression attenuates tumor growth and metastasis of shPCBP1 cells in mice; (4) loss of FAM3C or LIFR expression and subsequent loss of pSTAT3 attenuates the self-renewal capacity of shPCBP1 cells *in vitro*, and (5) expression of FAM3C and LIFR correlates with the expression of genes

involved in stemness (28). Based on these conclusions, this study proposes an overarching hypothesis:

FAM3C/LIFR-induced intracellular signaling dysregulates genes involved in the promotion of BCSC phenotype and metastasis.

Following the proposed hypothesis, the goals of the current study are to experimentally characterize intracellular events using both the Progression Series Model and human mammary carcinoma cells to (1) identify the mechanisms regulating LIFR expression, (2) identify genes dysregulated by changes in FAM3C/LIFR/STAT3 signaling, and (3) examine how changes in LIFR expression affect the phenotypic features of mammary epithelial cells that contribute to disease progression. Therefore, it was proposed that the preceding goals could be achieved through the following specific aims:

i. Aim 1: Characterize PCBP1-mediated increase in LIFR expression

Previous data published by the Howe laboratory (Woosley et al. 2019) have demonstrated that shPCBP1 cells display increased LIFR expression relative to parental NMuMG cells (28). To identify how LIFR expression is regulated following the loss of PCBP1 expression, the activation of LIFR transcription will be examined through analysis of the LIFR promoter locus using luciferase reporter assays. To identify the transcription factors involved in regulating LIFR expression, protein/DNA binding events at the LIFR promoter locus will be examined using chromatin immunoprecipitation followed by quantitative PCR (ChIP-qPCR). Finally, publicly available datasets that quantify the occupancy of transcription factors at the LIFR regulatory locus will be examined and correlated with the outcomes from the proposed experimental strategy.

ii. Aim 2: Identify FAM3C/LIFR interaction-dependent gene regulation

Previous data published by the Howe laboratory (Woosley et al. 2019) have demonstrated that genes involved in the regulation of self-renewal of epithelial progenitor cells (e.g., BMI1 and NANOG) are upregulated following loss of PCBP1 expression in NMuMG cells, and that expression levels subsequently decrease following knockdown of FAM3C or LIFR (28). To test the hypothesis asserted by the current study, transcriptomic analysis of shPCBP1 cells following KO of either FAM3C or LIFR will be carried out to identify a FAM3C/LIFR-dependent signature of gene regulation. Transcriptomic data will be analyzed to identify candidate genes previously established to be involved in BCSC self-renewal, as well as novel candidate genes. Candidate genes will be validated as (1) dysregulated by FAM3C/LIFR interaction and (2) involved in the phenotypic regulation of shPCBP1 cells. Additional experiments will be conducted to identify the role(s) of candidate genes in key intracellular mechanisms.

iii. Aim 3: Identify phenotypic effects of LIFR expression

Previous data published by the Howe laboratory and others have demonstrated that LIFR expression promotes the progression of mammary carcinoma, both *in vitro* and *in vivo*. However, a clearly defined role of LIFR in mammary carcinoma pathology is yet to be established. To gain an increased understanding of how LIFR expression influences mammary epithelial cells, the current study will aim to examine the modulation of LIFR expression in shPCBP1 cells using *in vitro* cell-based experiments. Analysis of experimental outcomes will provide reinforcement of previously published conclusions, and will establish direction for future *in vivo* studies capable of addressing the paradoxical aspects of previously conducted pan-cancer preclinical studies in mice.

A graphical representation of the specific aims that were used to guide the experimental investigations of the current study is presented below in Figure 6.

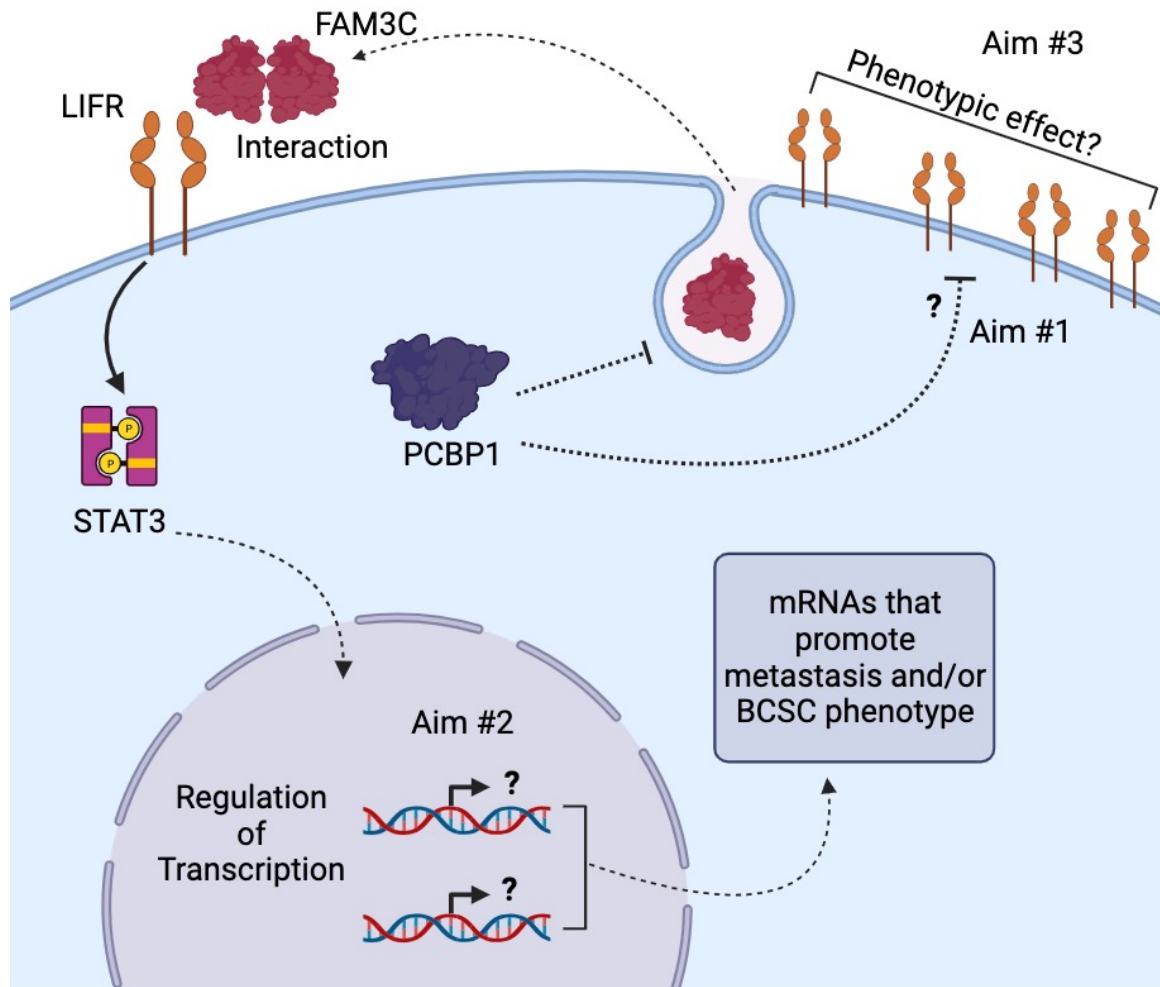


Figure 6 – Overarching hypothesis and specific aims. Illustration depicting the unknown mechanism of LIFR regulation by PCBP1 as described in “Specific Aim 1,” the hypothesized regulation of genes involved in the promotion of metastasis and BCSC self-renewal downstream of FAM3C/LIFR interaction as described in “Specific Aim 2,” and the hypothesized phenotypic effect of increased LIFR expression as described in “Specific Aim 3.” BCSC, breast cancer stem cell.

Chapter 2: Transcriptional Regulation of LIFR

2.1 Introduction and rationale

Previous work by the Howe laboratory determined that NMuMG cells with PCBP1 knockdown (hereafter “shPCBP1 cells”) showed upregulation of LIFR protein by immunoblot assay (28). Woosley et al. noted this observation but did not provide data that would explain how LIFR expression is regulated by PCBP1. Although it is possible that LIFR is regulated in a manner similar to FAM3C, LIFR was not found to possess a nucleotide sequence in its 3' UTR that would facilitate PCBP1 binding and translational suppression. It was therefore hypothesized that unknown mechanisms are responsible for increased LIFR expression following the loss of PCBP1, and that characterization of such mechanisms would provide additional understanding of the role of LIFR in the phenotypic changes observed in shPCBP1 cells. The following sections describe the results obtained from the experiments aimed at identifying the mechanisms responsible for LIFR regulation in shPCBP1 cells.

2.2 Results

i. Loss of PCBP1 expression upregulates LIFR

Following shRNA-mediated knockdown of PCBP1 in NMuMG cells, we observed an increase in LIFR expression and concomitant increase in STAT3 phosphorylation at Y705 (pSTAT3). Immunoblot analysis demonstrated an increase in LIFR protein expression in shPCBP1 cells relative to control cells transduced with “scrambled” non-specific shRNA (hereafter “shSCR cells”) (Fig. 7A). To determine whether LIFR upregulation occurred due to an increase in transcription, LIFR mRNA levels were

measured by quantitative real-time PCR (qPCR). The upregulation of LIFR mRNA was greater than three-fold in shPCBP1 cells relative to control cells (Fig. 7B). To determine whether the increase in LIFR mRNA resulted from an increase in transcription initiation, we performed luciferase-based transcriptional reporter assays. The following section briefly describes the method used to identify and isolate the LIFR promoter nucleotide sequence for luciferase-based transcriptional reporter assays and other experiments performed in the current study.

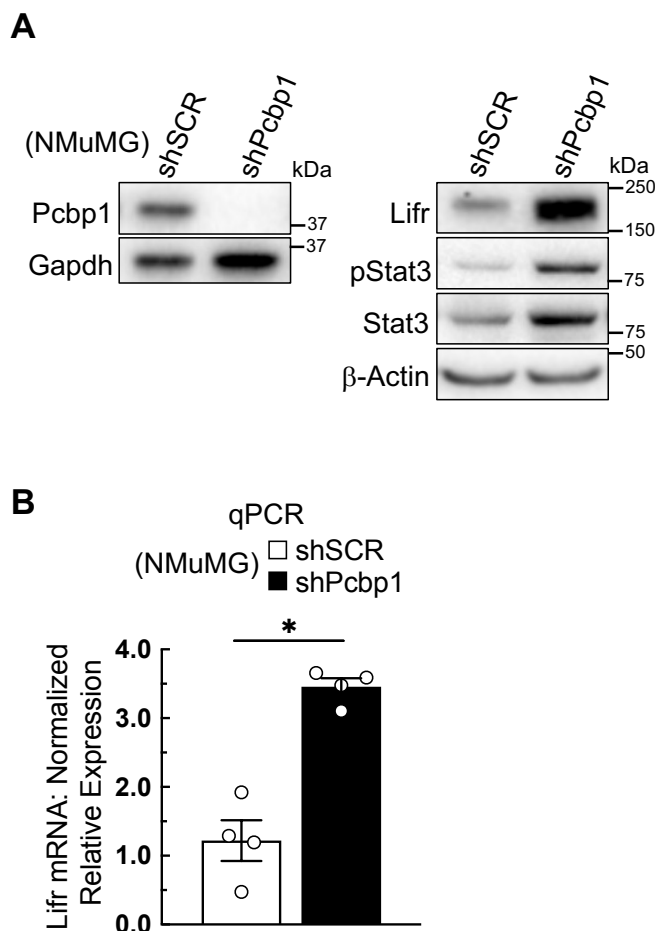


Figure 7 – LIFR is upregulated following loss of PCBP1 expression. (A) Immunoblot analysis of NMuMG cells transduced either with shRNA containing “scrambled” non-targeting control (shSCR) or shRNA targeting PCBP1 (shPcbp1). (B) qPCR analysis of the cells used in panel “A”. All data points represent independent experiments, each performed in triplicate. Error bars represent standard error of the mean, * $P < 0.05$, *** $P < 0.001$ (unpaired Mann-Whitney U test).

The Eukaryotic Promoter Database (EPD, www.epd.expasy.org) was used to identify the nucleotide sequence of the LIFR promoter based on the annotated *Mus musculus* LIFR transcription start site. EPD identified two potential regulatory regions as promoters, denoted “Lifr1” and “Lifr2,” upstream of two independent potential transcription start sites. Lifr1 was found to correspond to transcript variants 2 and 3 (NCBI Refseq NM_001358593.1 and NM_001113386.1, respectively), and Lifr2 corresponded to transcript variant 1 (NCBI Refseq NM_013584.2). Transcript variant identification was based on the GRCm38.p6 genomic sequencing iteration of the C57BL/6J subspecies of *Mus musculus*. It was later determined that Lifr2 was not capable of initiating transcription in NMuMG cells (data not shown); therefore, for the remainder of the current study, only the Lifr1 regulatory region will be used experimentally, and hereafter it will be referred to as “the LIFR promoter region.”

To determine the length of the genomic sequence representing the LIFR promoter to be isolated by PCR, the coordinates of a 2238 base-pair (bp) region of the genomic sequence flanking the LIFR promoter (chr15:7127572 – 7129810) were entered into the ECR Browser online database (www.ecrbrowser.dcode.org). The ECR Browser aligns genomic sequences of interest with “evolutionarily conserved regions” (ECRs) from orthologous genes in various species. Evolutionarily conserved regions represent sequences of high probability of functional necessity for the transcription of genes crucial to cell function and survival, and are therefore considered to be more likely to represent regions of DNA that participate in the regulation of gene expression. Based on the alignments provided by the ECR Browser and comparison with previous methods in the Howe laboratory, a 1421 bp sequence was selected as a representative of the LIFR promoter for PCR-based isolation and recombinant DNA cloning into the pGL3_Basic firefly luciferase reporter vector (Promega). An illustration of the ECR Browser alignments

representing the creation of the LIFR promoter vectors used in the remainder of this study is shown in Figure 8.

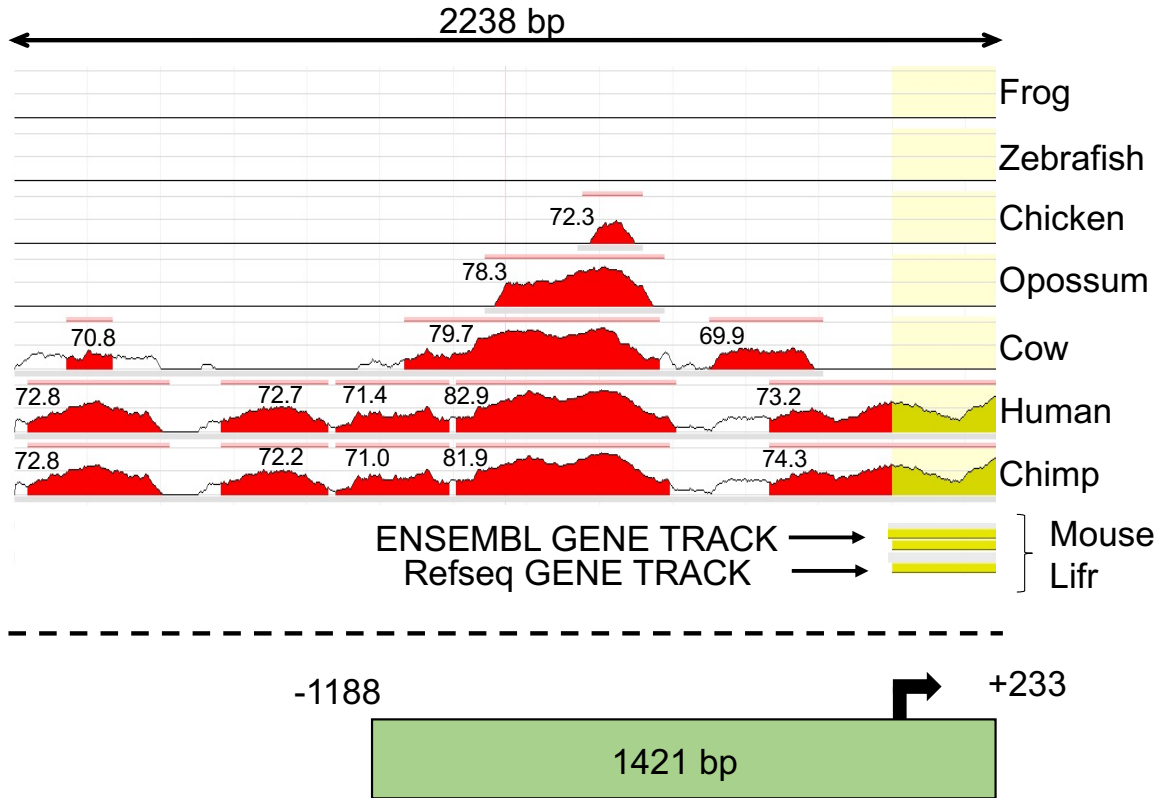


Figure 8 – The LIFR regulatory region is highly conserved. Graphic representation of the 2238 base-pair (bp) DNA sequence adjacent to the *Mus musculus* LIFR transcription start site (TSS), as annotated by the UCSC Genome Browser and the Eukaryotic Promoter Database. The coordinates for the sequence shown (chr15:7127572 – 7129810) were entered into the ECR Browser online tool to display the evolutionarily conserved regions (ECRs) relative to *Mus musculus*, as indicated by the species shown. Red peaks indicate ECRs, and the adjacent numbers indicate the percent identity to the *Mus musculus* nucleotide sequence. Yellow peaks indicate ECRs downstream of the TSS. The graphic below the dotted line indicates the subset of the genomic DNA sequence that was isolated for use in the current study. The isolated sequence includes the most highly conserved regions adjacent to the LIFR TSS, as indicated by ECR browser.

Transfection of the plasmid vector containing the LIFR promoter sequence upstream of the firefly luciferase open reading frame (ORF), followed by a dual-luciferase assay, revealed an increase in the reporter signal in shPCBP1 cells relative to control cells (Fig. 9). A Comparison of LIFR mRNA degradation rates before and after PCBP1 knockdown did not provide any evidence that an increase in mRNA stability contributed to the observed increase in LIFR mRNA (data not shown). These results showed that the loss of PCBP1 expression in NMuMG cells resulted in increased LIFR expression through a mechanism involving increased transcriptional activity at the LIFR promoter.

ii. FAM3C participates in regulation of LIFR expression

Following the conclusion by Woosley et al. that pSTAT3 activation in shPCBP1 cells requires interaction between FAM3C and LIFR, we sought to further characterize FAM3C/LIFR interaction-dependent gene regulation in shPCBP1 cells (28). To perform additional cell-based experiments, FAM3C was knocked out (KO) in shPCBP1 cells using CRISPR-Cas9 (hereafter “FAM3C KO cells”). Total pooled RNA isolates were sequenced (RNA-Seq) and differentially expressed genes (DEGs) were analyzed. Comparisons were made between shPCBP1 cells, multiple FAM3C KO cell line “clones,” and multiple “control” (CT) cell line clones (hereafter “shPCBP1 CT cells”). shPCBP1 CT cells were generated by treating cells with Cas9 in the absence of gene-specific guide RNAs. Interestingly, one of the genes that was found to be differentially expressed following FAM3C KO was LIFR (Fig. 10A). To validate the RNA-Seq results, a subset of cell line clones was selected for further study and qPCR was performed. The qPCR results also demonstrated a loss of LIFR mRNA following FAM3C KO (Fig. 10B). Immunoblot analysis showed that the loss of LIFR mRNA was sufficient to cause a loss of LIFR protein expression (Fig. 10C).

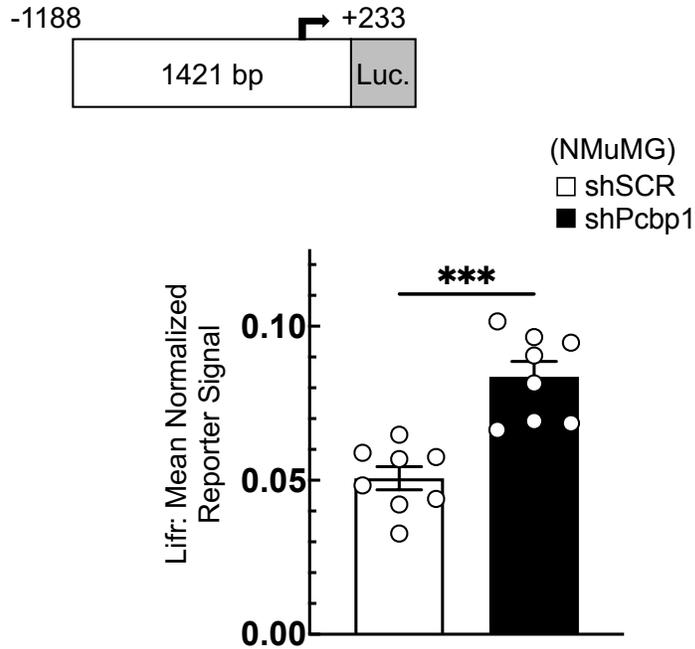


Figure 9 – Activation of a LIFR transcription reporter is increased following loss of PCBP1 expression. Dual luciferase reporter assay using NMuMG cells transduced either with shRNA containing “scrambled” non-targeting control (shSCR) or shRNA targeting PCBP1 (shPcbp1). The luciferase reporter construct contains the indicated region of the mouse LIFR proximal promoter upstream of a firefly luciferase open reading frame. All data points represent independent experiments, each performed in triplicate. Error bars represent standard error of the mean, * $P < 0.05$, *** $P < 0.001$ (unpaired Mann-Whitney U test).

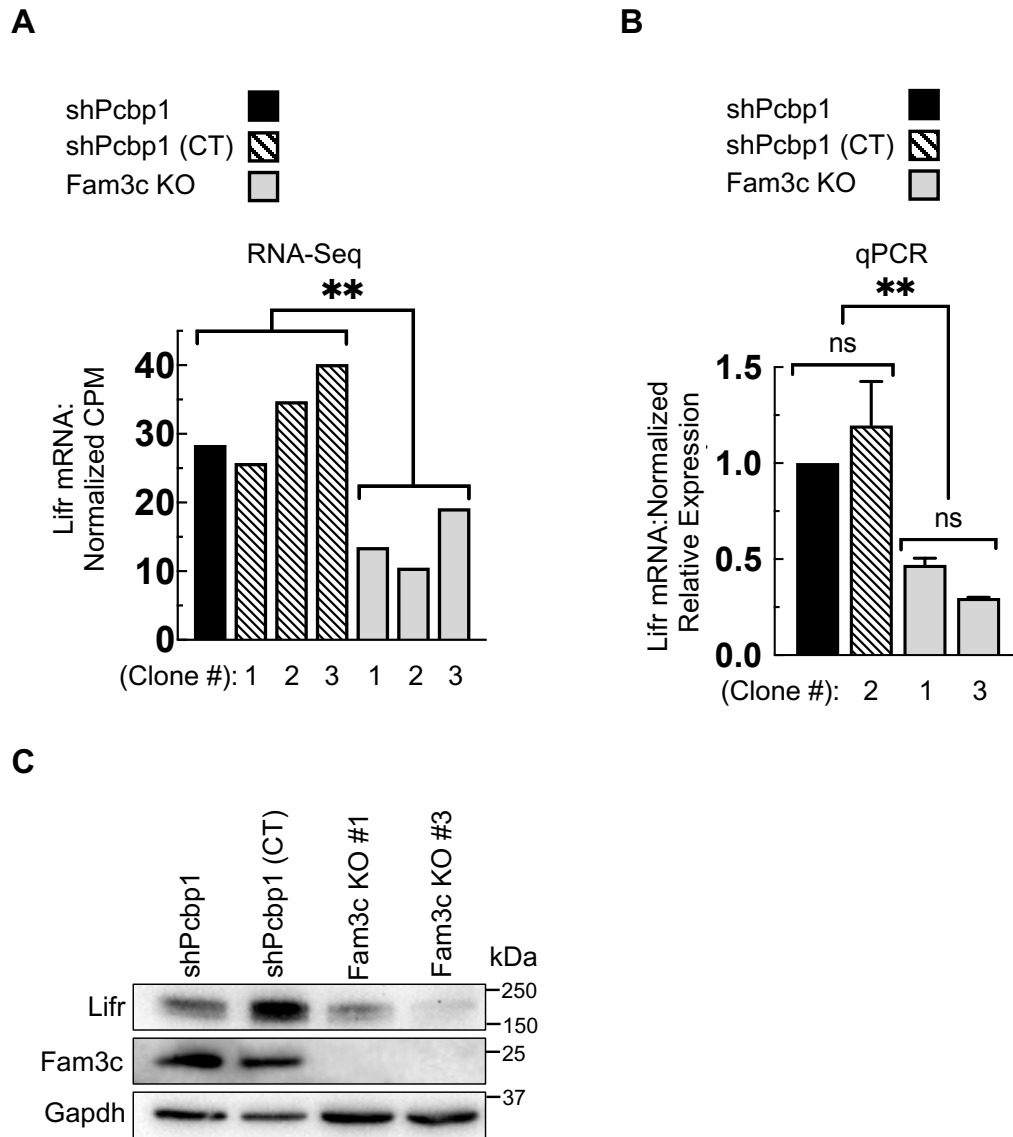


Figure 10 – FAM3C participates in regulation of LIFR expression. (A) RNA-Seq analysis of total RNA isolates from the indicated NMuMG derivative cell lines; “CT” (control) indicates additional shPCBP1 cell lines (“clones”) treated with Cas9 in the absence of gene-specific guide RNAs. The FAM3C KO cell line was derived from parental shPCBP1 cells. Bars represent normalized counts per million paired-end reads from one RNA sample per cell line tested, $**q < 0.01$ (DESeq FDR step-up). (B) qPCR validation of the RNA-Seq data in panel “A”. Error bars represent SEM from three independent experiments, each performed in triplicate, $**P < 0.01$ (one-way ANOVA). (C) Immunoblot analysis of the cells shown in panel “B”. FDR, false discovery rate; SEM, standard error of the mean.

To determine whether the loss of LIFR expression could be restored by re-expressing FAM3C, one FAM3C KO cell line was selected for further study and transduced with either an “empty vector” (EV) control plasmid or a vector containing the mouse FAM3C ORF. Following confirmation of stable overexpression (OE) of FAM3C (hereafter “FAM3C KO OE cells”) (Fig. 11A), qPCR analysis was performed and the results showed an increase in LIFR mRNA levels relative to control cells lacking FAM3C (Fig. 11B). Immunoblot analysis showed that restoration of FAM3C expression was sufficient to measurably increase the abundance of LIFR protein and concomitant levels of pSTAT3 relative to cells lacking FAM3C (Fig. 11C). These data suggested that FAM3C directly participates in the regulation of LIFR in shPCBP1 cells. To determine whether FAM3C expression has a similar effect on LIFR expression in human cells, a panel consisting of normal human mammary epithelial cell lines and human mammary carcinoma cell lines was sampled for comparative analysis of LIFR expression levels by immunoblotting (Fig. 12). Based on these results, two human metastatic mammary carcinoma cell lines (SKBr3 and MDA-MB-231) were selected for further study. Following shRNA knockdown of FAM3C in human cell lines, qPCR analysis revealed a measurable loss of LIFR mRNA levels relative to those in control cells, demonstrating a correlation between LIFR and FAM3C expression in human mammary carcinoma (Fig. 13A). Immunoblot analysis of the same human cell lines showed that the loss of LIFR mRNA was sufficient to cause a measurable attenuation of LIFR protein expression (Fig. 13B).

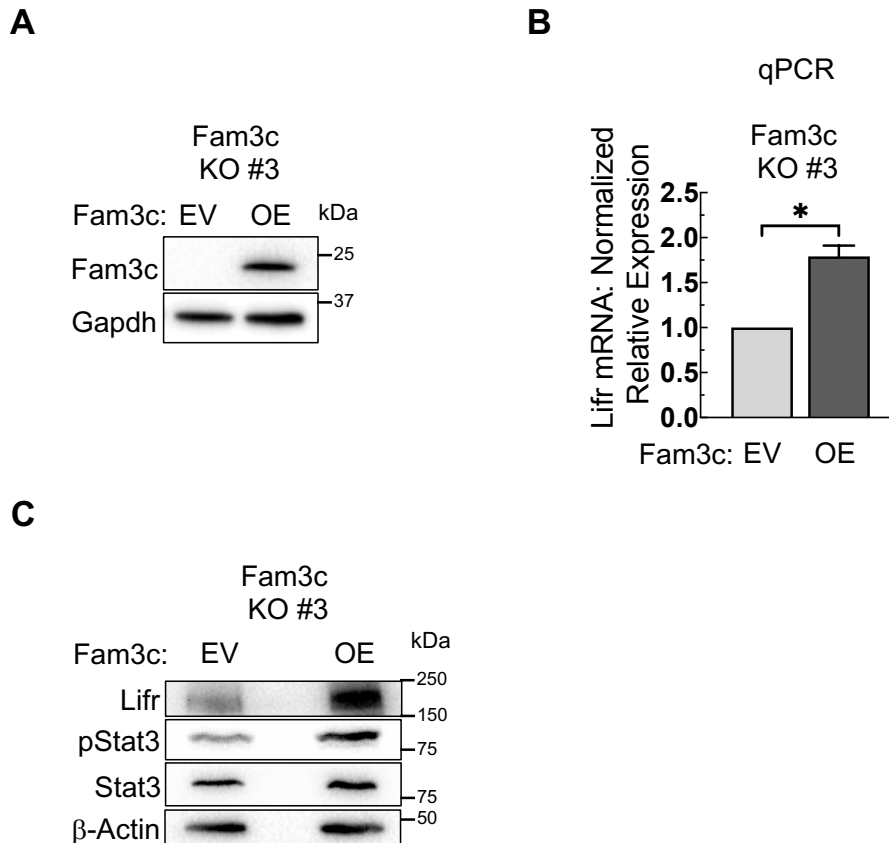


Figure 11 – FAM3C overexpression drives LIFR expression. (A) Immunoblot analysis of FAM3C KO cells derived from parental shPCBP1 cells (clone #3) following transduction with lentivirus containing either empty vector (EV) or a vector for overexpression rescue (OE) of mouse FAM3C protein. (B) qPCR analysis of the cells used in panel “A”. Error bars represent SEM from duplicate independent experiments, each performed in triplicate, * $P < 0.05$ (unpaired Student’s *t*-test). (C) Immunoblot analysis of the cells used in panel “A” using the indicated antibodies.

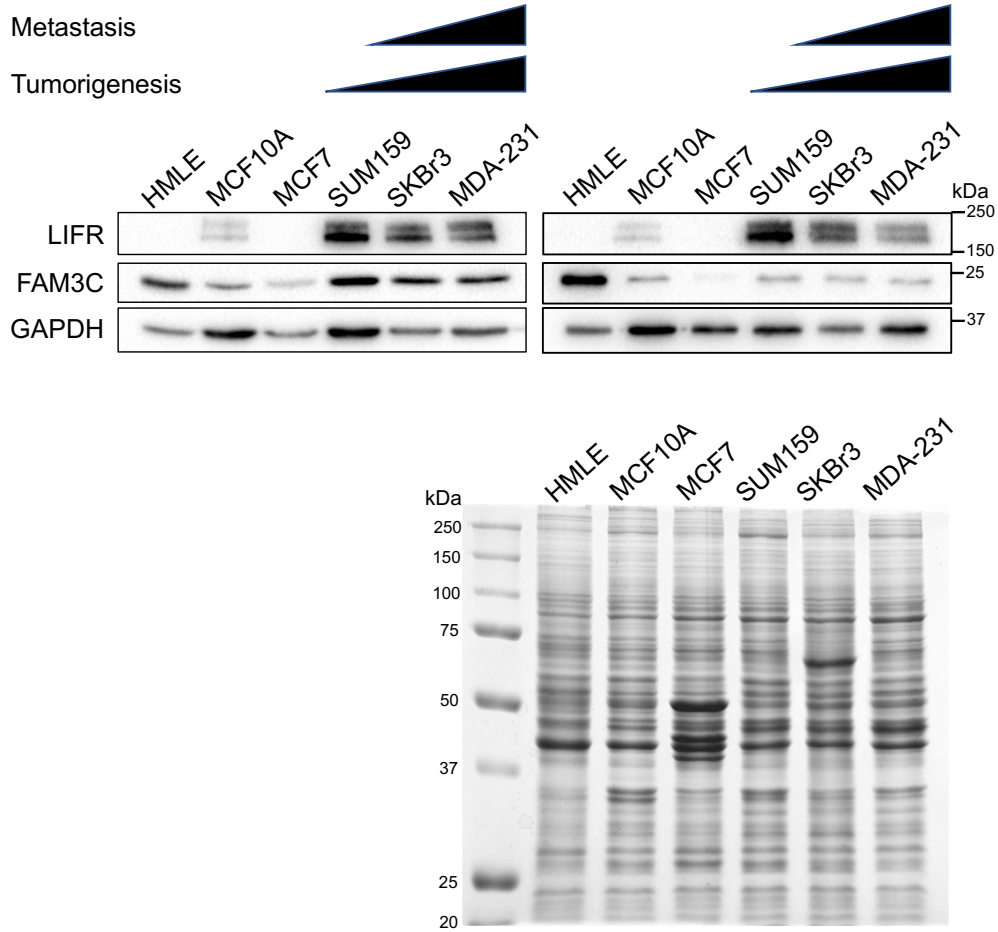


Figure 12 – Endogenous LIFR expression levels in human mammary epithelium. Two independent immunoblot analyses of the indicated healthy human mammary epithelial cell lines (HMLE, MCF10A) and of human mammary carcinoma cell lines (MCF7, SUM159, SKBr3, and MDA-MB-231). Scales indicate the cell lines' relative levels of tumorigenicity and metastasis (top). Coomassie Brilliant Blue staining analysis of the samples shown the top right panel (bottom).

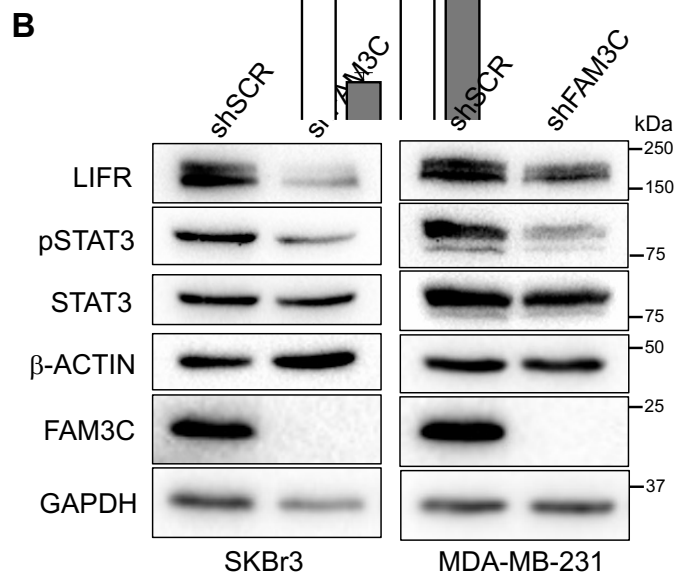
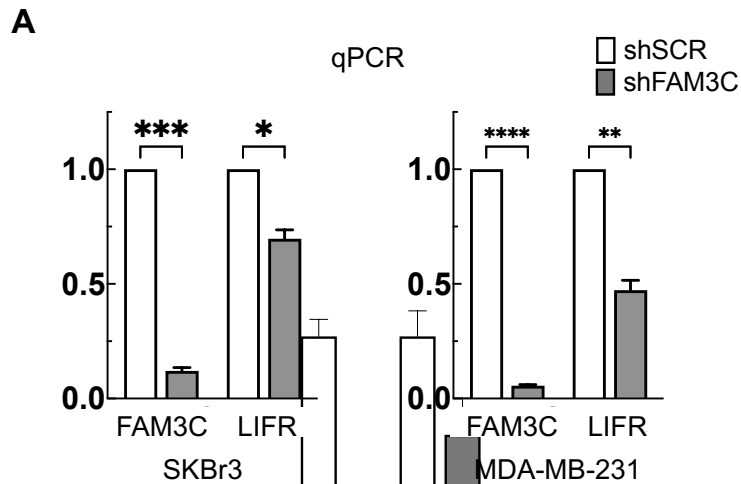


Figure 13 – FAM3C expression participates in regulation of LIFR expression in human breast cancer. (A) qPCR analysis using SKBr3 and MDA-MB-231 human breast cancer cell lines transduced either with “scrambled” non-targeting control shRNA (shSCR) or shRNA targeting FAM3C (shFAM3C). Error bars represent SEM from duplicate independent experiments, each performed in triplicate, * $P < 0.05$, ** $P < 0.01$, *** $P < 0.001$, **** $P < 0.0001$ (unpaired Student’s *t*-tests). (B) Immunoblot analysis using the cells shown in panel “A”. ns, not significant; SEM, standard error of the mean.

iii. FAM3C regulates LIFR expression through STAT3

To determine whether the loss of LIFR mRNA observed in FAM3C KO cells was due to changes in the activation of transcription at the LIFR promoter, dual-luciferase assays were performed to compare shPCBP1 cells and FAM3C KO cells following transfection with the LIFR promoter luciferase vector mentioned in the preceding section. The assay results revealed that loss of FAM3C expression significantly affected the activation of the LIFR reporter (Fig. 14A). To determine whether the loss of pSTAT3 following FAM3C KO could play a role in the loss of LIFR transcriptional activation, a vector containing a STAT3 cis-inducible element (CIE) upstream of a luciferase ORF was transfected into shPCBP1 cells or FAM3C KO cells. Following transfection, dual-luciferase assays were performed, and the results showed a significant loss of the pSTAT3 reporter signal following the loss of FAM3C expression (Fig. 14B). To determine whether pSTAT3 participates in the activation of LIFR transcription, shPCBP1 cells were transfected with the LIFR promoter luciferase vector in the presence of the STAT3 inhibitor STAT3-IN-1. The time of exposure and concentration of the inhibitor were based on previous use of STAT3-IN-1 in human mammary carcinoma cell lines (128). The assay results showed that pharmacological inhibition of STAT3 activation also significantly affected the activation of the LIFR reporter (Fig. 15A). To observe the effect of STAT3 inhibition on LIFR mRNA levels, qPCR was performed after treatment with STAT3-IN-1. The mRNA abundance of LIFR was significantly decreased in cells treated with the inhibitor relative to that in cells treated with vehicle only (Fig. 15B). An immunoblot assay was performed following treatment with STAT3-IN-1, and the results showed that the inhibitor was sufficient to cause a measurable loss of STAT3 phosphorylation (Fig. 16A). The mRNA levels of the STAT3 target genes STAT3 and MYC were also affected (Fig. 16B).

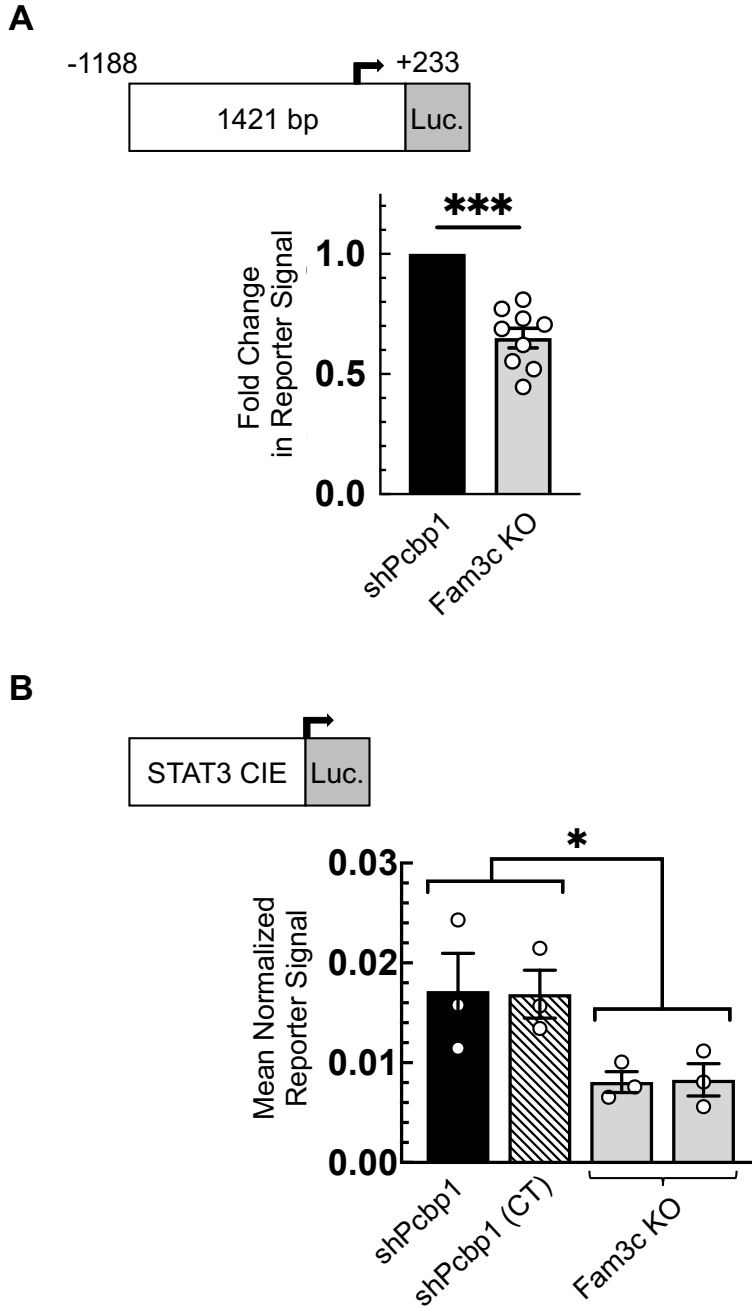


Figure 14 – FAM3C KO attenuates LIFR/STAT3 transcription reporters. (A) Dual-luciferase assay using the indicated region of the mouse LIFR proximal promoter upstream of a firefly luciferase open reading frame (ORF), carried out in the indicated NMuMG-derivative cell lines. FAM3C KO cells were derived from parental shPCBP1 cells. (B) Dual-luciferase reporter assay measuring STAT3 nuclear activity, using a STAT3 cis-inducible element (CIE) upstream of a firefly luciferase ORF, carried out in the indicated NMuMG-derivative cell lines. All data points in panels “A” and “B” represent independent experiments, each performed in triplicate. Error bars represent SEM. * $P < 0.05$, *** $P < 0.001$ (unpaired Student’s *t*-tests). SEM, standard error of the mean.

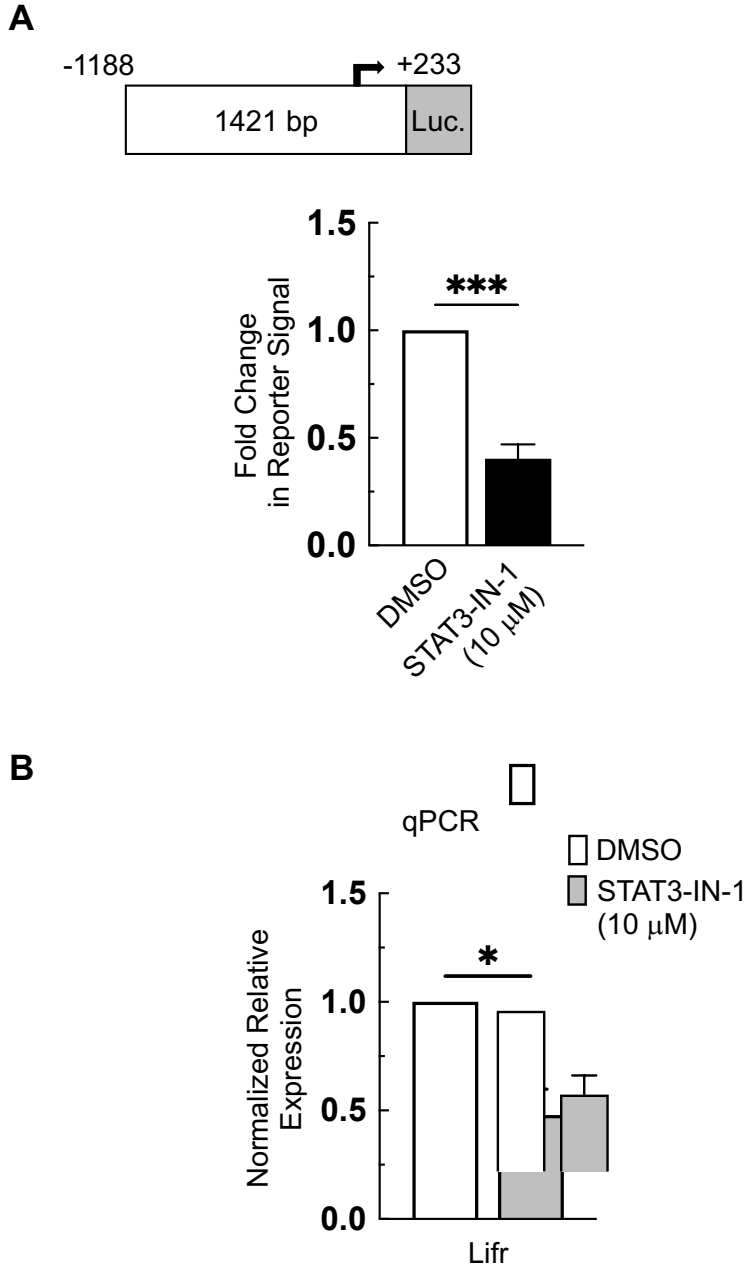


Figure 15 – Application of pharmacological inhibition of STAT3 in shPCBP1 cells. (A) Dual-luciferase assay using the indicated region of the LIFR proximal promoter upstream of a firefly luciferase open reading frame (ORF), carried in shPCBP1 cells treated either with DMSO (vehicle) or 10 μM inhibitor of STAT3 (STAT3-IN-1) for 24 hours. Error bars represent SEM from three independent experiments, each performed in triplicate. (B) qPCR analysis of LIFR transcript abundance in shPCBP1 cells treated either with DMSO or 10 μM STAT3-IN-1 for 48 hours. Error bars represent SEM. *P<0.05, ***P<0.001 (unpaired Student's *t*-tests). SEM, standard error of the mean.

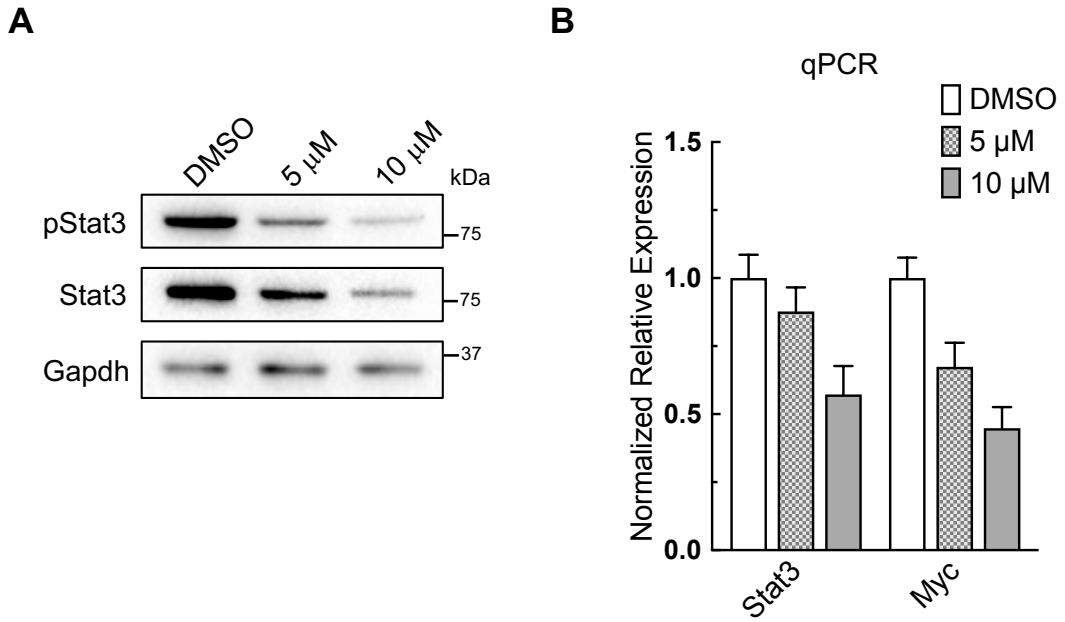


Figure 16 – Validation of pharmacological inhibition of STAT3 in shPCBP1 cells. (A) Immunoblot analysis of shPCBP1 cells treated for 48 hours with DMSO (vehicle) or the indicated concentrations of STAT3-IN-1, using the indicated antibodies. (B) qPCR analysis of the cells/treatments shown in panel “A”. Error bars represent standard error of the mean from triplicate technical replicates.

These results suggested that a feed-forward mechanism of LIFR regulation is present in NMuMG shPCBP1 cells. To determine whether increased LIFR signaling could drive LIFR gene expression, LIFR was knocked out in shPCBP1 cells using CRISPR-Cas9 (hereafter “LIFR KO cells”). A dual-luciferase assay was then performed on shPCBP1 and LIFR KO cells transduced with either EV or a vector containing a viral promoter-driven mouse LIFR ORF. The assay results revealed that LIFR reporter activity was significantly higher in cells overexpressing LIFR (Fig. 17). The relative levels of LIFR expression and pSTAT3 in the cell lines used were confirmed by immunoblotting, which demonstrated a marked increase in basal pSTAT3 levels in the cell lines with LIFR OE (Fig. 18). To determine whether STAT3 binds to DNA at the LIFR promoter locus in live cells during transcription activation, chromatin immunoprecipitation followed by qPCR (ChIP-qPCR) was performed. Briefly, shSCR, shPCBP1, and derivative cell lines were treated with formaldehyde to cross-link proteins with nuclear DNA, and chromatin extracts were immunoprecipitated using a STAT3-specific antibody. DNA isolated from the precipitates was quantified by qPCR using a primer set specific to nucleotides within the LIFR promoter sequence mentioned above. The results clearly demonstrated the binding of STAT3 to the LIFR promoter and a positive correlation between STAT3 binding activity and LIFR expression levels (Fig. 19).

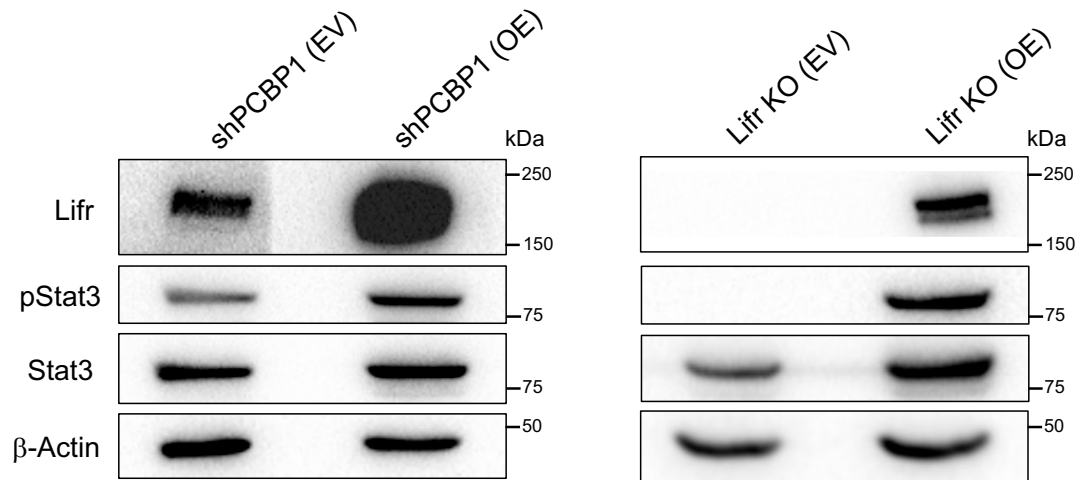


Figure 18 – Confirmation of LIFR overexpression. Immunoblot analysis of shPCBP1 and LIFR KO cells (derived from parental shPCBP1 cells) transduced either with empty vector (EV) or a vector containing the mouse LIFR open reading frame for LIFR overexpression (OE), using the indicated antibodies.

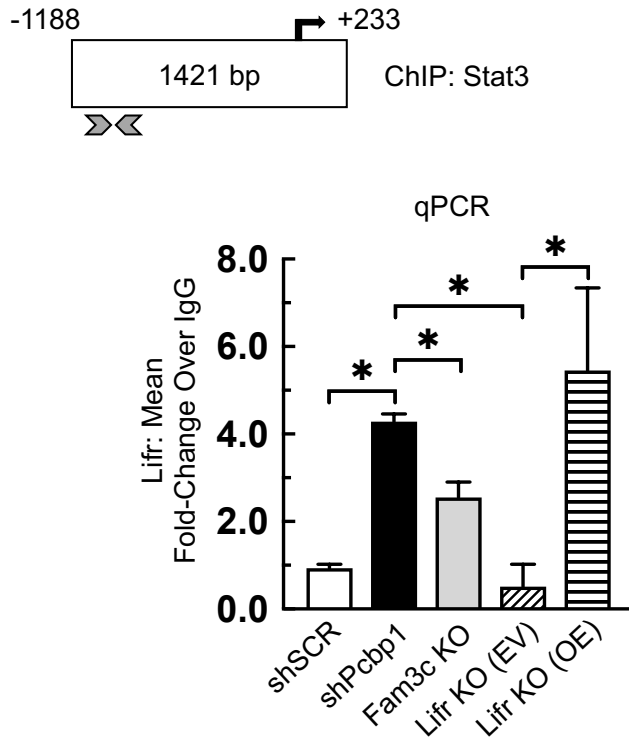


Figure 19 – STAT3 interacts with DNA at the LIFR promoter region. Chromatin immunoprecipitation (ChIP) analysis in the indicated NMuMG derivative cell lines, following live cell cross-linking, incubation of chromatin with a STAT3 antibody, and qPCR analysis of immunoprecipitated DNA. Arrowheads indicate the region of the LIFR proximal promoter targeted by the qPCR primer set. Error bars represent SEM from duplicate independent experiments, each performed in triplicate. * $P < 0.05$, (unpaired Student's *t*-test). SEM, standard error of the mean.

2.3 Summary

The experimental evidence shown in the preceding results section demonstrates that LIFR expression increases in NMuMG cells following the loss of PCBP1 expression, both at the transcript level as measured by qPCR and at the protein level as measured by immunoblot. Experiments using transcription reporters showed that LIFR expression levels increase because of an increase in the initiation of transcription at the LIFR promoter. The results also demonstrated that modulation of FAM3C expression in shPCBP1 cells directly affects the expression of LIFR, and a parallel effect was observed in human mammary carcinoma cells following loss of FAM3C expression. Transcription reporters also demonstrated that FAM3C-dependent STAT3 activation plays a role in regulating the initiation of LIFR transcription in shPCBP1 cells and that overexpression of LIFR in shPCBP1 or LIFR KO cells (derived from parental shPCBP1 cells) was sufficient to drive the initiation of LIFR transcription. Finally, the results demonstrated that the interaction between STAT3 and nuclear DNA at the LIFR promoter locus correlates with LIFR expression levels in shPCBP1 cells, as shown by ChIP-qPCR. Collectively, these results strongly suggest that FAM3C/LIFR interaction participates in the upregulation and maintenance of LIFR expression in shPCBP1 cells through a feed-forward regulatory mechanism.

Chapter 3: Analysis of the FAM3C/LIFR Transcriptomic Signature

3.1 Introduction and rationale

Previously published work by the Howe laboratory identified that STAT3 is phosphorylated at tyrosine residue 705 (pSTAT3) following interaction between FAM3C and LIFR in the extracellular space, and that pSTAT3 accumulation is dependent on the presence of both FAM3C and LIFR in shPCBP1 cells (28). Although the regulation of genes downstream of pSTAT3 has been extensively characterized in various cancers, the regulatory landscape downstream of FAM3C/LIFR interaction in shPCBP1 cells has not been explored (95, 104, 107). It is possible that new analyses could identify novel pSTAT3-regulated genes, in addition to pathways other than JAK/STAT that might be activated downstream of LIFR following FAM3C interaction. Additionally, previous work published by the Howe laboratory demonstrated that the self-renewal capacity of shPCBP1 cells *in vitro* was attenuated following loss of FAM3C/LIFR-dependent pSTAT3. Therefore, it was proposed that analysis of the regulation of gene expression could reveal patterns responsible for the maintenance of self-renewal in the context of mammary carcinoma pathology, and potentially identify novel targets for therapeutic intervention. The following sections describe the results of the experiments aimed at investigating FAM3C/LIFR/STAT3-dependent changes in the regulation of gene expression in shPCBP1 cells.

3.2 Results

i. Transcriptomic analysis reveals a FAM3C/LIFR regulatory signature

Based on our observation that FAM3C and LIFR regulate LIFR expression, and the previously published work that identified FAM3C/LIFR-dependent pSTAT3, we sought to identify additional FAM3C/LIFR-regulated genes. Transcriptomic analysis of shPCBP1, shPCBP1 CT, FAM3C KO, LIFR KO, and double-knockout (DKO) cells (FAM3C KO and LIFR KO in the same cell line) was performed using RNA-Seq. Briefly, the parental shPCBP1 cell line and three additional shPCBP1 control (“CT”) cell lines were compared to three FAM3C KO cell lines, three LIFR KO cell lines, and the DKO cell line. All KO cell lines were derived from the same shPCBP1 parental cell line. As described in the previous section, shPCBP1 CT cells were used as an additional control and were generated by treating cells with Cas9 in the absence of gene-specific guide RNAs. An initial analysis of the combined sequencing datasets from the 11 cell line samples was performed to identify the differentially expressed genes (DEGs). To validate the integrity of the dataset, a stringent threshold was used: DEGs were initially defined as either 1.75-fold upregulated or downregulated by either FAM3C KO or LIFR KO relative to the combined shPCBP1 and shPCBP1 CT sequencing counts, and a q-value of 0.01 was used to prevent false discovery. A total of 372 DEGs were identified, 58 of which were dysregulated by either FAM3C KO or LIFR KO (Fig. 20A). Using Partek Flow software, a heatmap was generated that graphically represented the comparison of the expression levels of the 58 common DEGs identified and showed hierarchical clustering of the DEGs within each sample group. The DKO cell line was used as a reference and was included in the heatmap analysis but was not used to identify DEGs. Heatmap analysis clearly showed that most

of the genes dysregulated by both FAM3C and LIFR were downregulated relative to the control cells, and KO cell lines clustered separately from the control cell lines. (Fig. 20B).

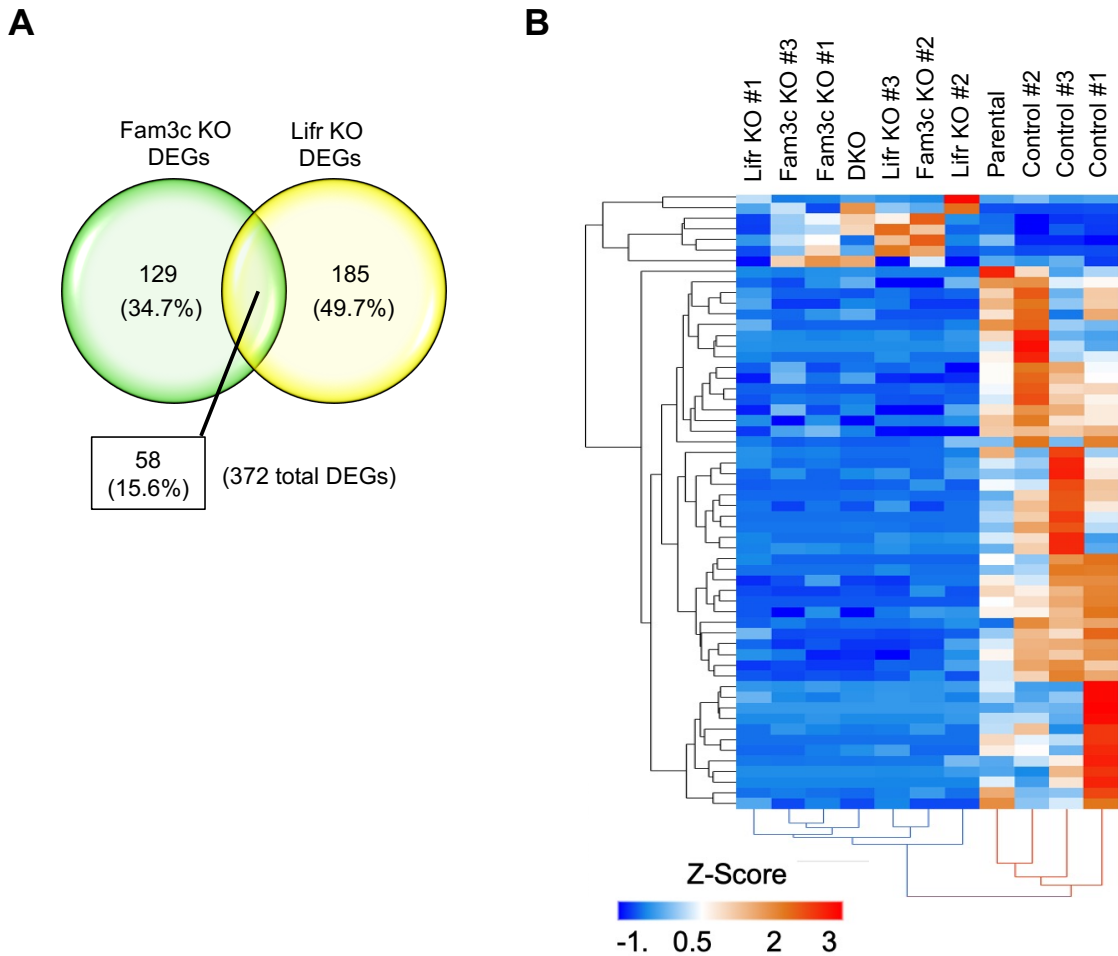


Figure 20 – Evaluation of RNA-Seq data integrity. (A) Venn diagram depicting the overlap of differentially expressed genes (DEGs) from RNA-Seq, comparing counts from FAM3C KO or LIFR KO cell lines (derived from parental shPCBP1 cells) to combined control counts (from parental shPCBP1 and shPCBP1 CT cell lines). (B) Heat map showing hierarchical clustering of the expression levels of the 58 genes identified in panel “A.” Z-scores less than zero indicate downregulated genes, and Z-scores greater than zero indicate upregulated genes.

Based on our observation that LIFR mRNA is upregulated in shPCBP1 cells relative to shSCR NMuMG control cells, we were interested in identifying other genes upregulated at the transcriptional level in shPCBP1 cells. An existing RNA-Seq dataset previously generated by the Howe laboratory was used to create a list of genes that were upregulated by 1.5-fold or greater in shPCBP1 cells relative to shSCR cells. The list of genes was not filtered by the q-value, to ensure that all potential candidates were considered. Similarly, the list of FAM3C KO and LIFR KO DEGs found in the heatmap analysis was recompiled to include all genes either upregulated or downregulated by 1.5-fold or greater, and was not filtered by the q-value. Superimposition of the datasets identified a set of 490 DEGs that were (1) upregulated by the loss of PCBP1 relative to shSCR, and (2) either upregulated or downregulated by FAM3C and LIFR KO relative to shPCBP1 cells (Fig. 21A, Table 7). As expected, LIFR was found in that set of 490 DEGs. Further examination of the 490 DEGs revealed that the majority were dysregulated in the same direction (either upregulated or downregulated together) following FAM3C and LIFR KO. Very few DEGs demonstrated opposite directionality relative to the shPCBP1 cells (Fig. 21B). This suggested that FAM3C/LIFR expression participates in maintaining the increased expression levels of a specific set of genes that are upregulated following the loss of PCBP1.

To examine genes in our superimposed datasets that might be indicative of a FAM3C/LIFR transcriptional cascade, 59 transcription factors (TFs) were identified within the set of 490 DEGs using the FANTOM5 database (Table 8). Using the JASPAR/TRANSFAC database, 15 of the 59 TF DEGs were identified as potential STAT3 target genes. Furthermore, the JASPAR database identified six of the 15 STAT3 target genes as potentially capable of binding to the LIFR promoter sequence used in the preceding sections. From the list of six STAT3/LIFR-participating TFs, we identified

TWIST1 as a gene of interest because it was previously characterized as being involved in EMT and BCSC self-renewal (Fig. 21C) (129–134).

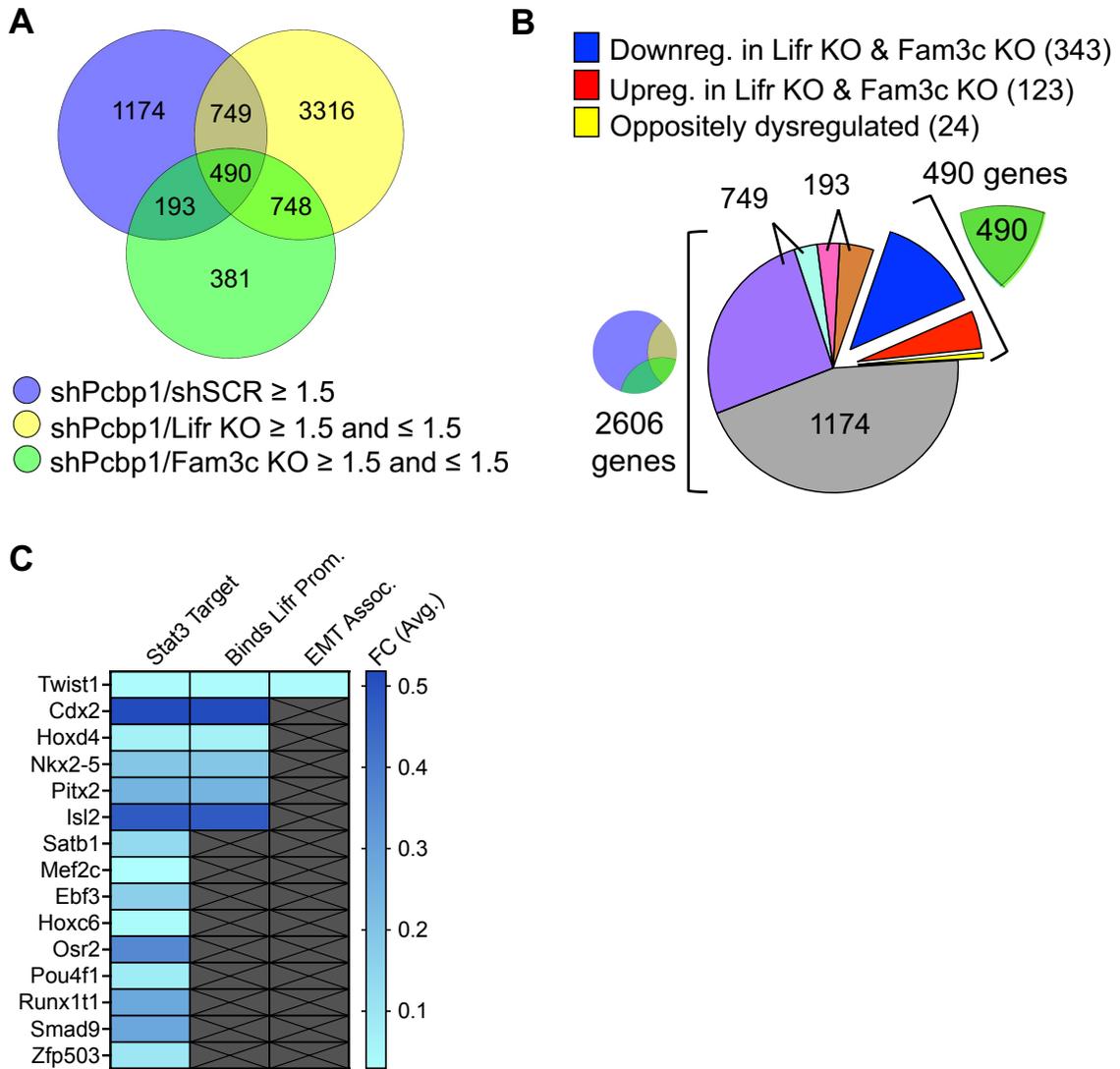


Figure 21 – Transcriptomic analysis reveals a FAM3C/LIFR regulatory signature. (A) Venn diagram depicting the overlap of three independent RNA-Seq dataset analyses using the indicated NMuMG derivative cell lines. The center area (490) indicates the number of differentially expressed protein-coding genes (DEGs) common to all three datasets, that satisfy the indicated fold-change criteria. (B) Exploded pie chart indicating the distribution of DEGs common to the overlap of datasets as indicated in the Venn diagram in panel “A”, with the indicated fractions (purple, brown, dark blue) corresponding to the downregulated DEGs following knockout (KO) of FAM3C and LIFR, relative to shPCBP1. KO cell lines were derived from parental shPCBP1 cells. (C) Heat map indicating the average fold change in FAM3C and LIFR KO cells relative to shPCBP1 cells in the subset of 15 transcription factor (TF) genes that contain STAT3 consensus elements in their respective promoters. Center and right columns indicate if the TF gene also satisfies the indicated condition. Downreg., downregulated; Upreg., upregulated; Prom., promoter; Assoc., associated; SEM, standard error of the mean.

Our RNA-Seq data showed that TWIST1 expression levels increased following the loss of PCBP1 expression but then decreased following KO of either FAM3C or LIFR (Fig. 22A). Changes in TWIST1 expression levels observed in the RNA-Seq data were validated by qPCR and immunoblotting (Figs. 22A, B). Additionally, qPCR in the presence of STAT3-IN-1 demonstrated a loss of TWIST1 mRNA, validating our identification of TWIST1 as a STAT3-regulated gene in shPCBP1 cells (Fig. 22C). To further validate our identification of TWIST1 as a gene regulated by LIFR/STAT3, ChIP was performed using a STAT3 antibody as described in the preceding section, and DNA was measured by qPCR using a primer set specific to the TWIST1 promoter locus. The results demonstrated the binding of STAT3 to the TWIST1 promoter and showed that STAT3 binding activity correlated positively with TWIST1 expression in the NMuMG-derivative cell lines used (Fig. 22D). To investigate the landscape of intracellular signaling pathways and other phenotypic features potentially affected by changes in gene expression downstream of FAM3C/LIFR KO, gene ontology analysis was performed using the DAVID Knowledgebase. The results revealed a significant association between the shPCBP1/FAM3C/LIFR transcriptomic signature and the phenotypic context of mammary carcinoma pathology (Fig. 23). The preceding analysis suggests a transcriptomic pattern downstream of FAM3C/LIFR/STAT3 modulation that is specifically implicated in mammary carcinoma pathology, which is exemplified by changes in the regulation of an established mediator of EMT and cell fate, TWIST1 (130, 134).

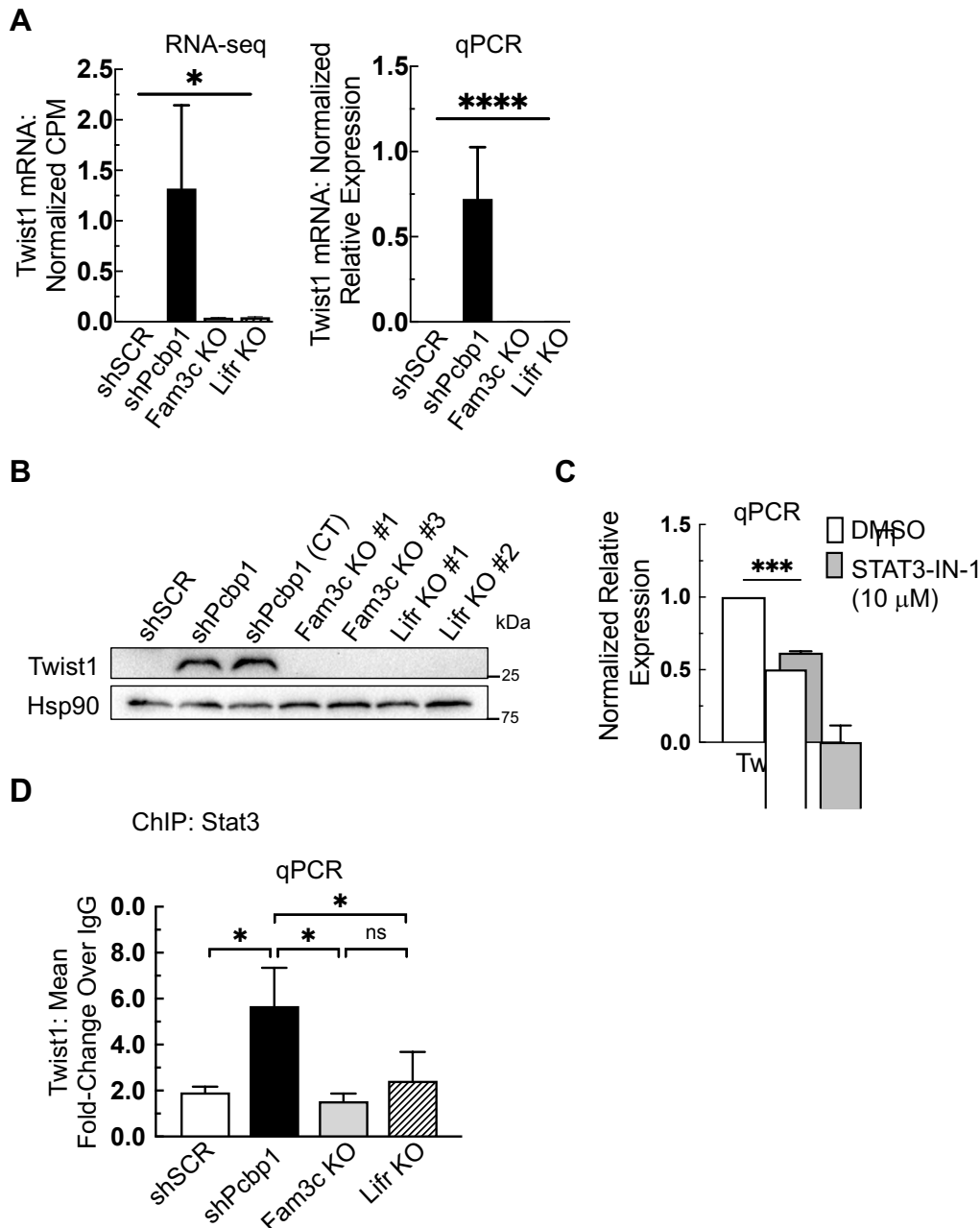


Figure 22 – Validation of TWIST1 expression and regulation by STAT3. (A) Relative expression of the TWIST1 gene from bulk RNA-Seq counts generated from the indicated NMuMG derivative cell lines. Bars indicate average counts per million (CPM) from each sample group. Error bars represent SEM, * $P < 0.05$ (unpaired Student's *t*-tests) (left). Validation of TWIST1 expression by qPCR in a subset of cell lines (right). Error bars represent SEM, **** $P < 0.0001$ (two-way ANOVA). (B) Immunoblot analysis of the cell lines used for qPCR in panel "A". (C) qPCR analysis of shPCBP1 cells treated with 10 μ M inhibitor of STAT3 (STAT3-IN-1) for 48 hours, *** $P < 0.001$ (unpaired Student's *t*-test). (D) Chromatin immunoprecipitation (ChIP) analysis in the indicated NMuMG-derivative cell lines, following live cell cross-linking, incubation of chromatin with a STAT3 antibody, and qPCR analysis of immunoprecipitated DNA, * $P < 0.05$ (one-way ANOVA). Error bars for panels "C" and "D" represent SEM from duplicate independent experiments, each performed in triplicate.

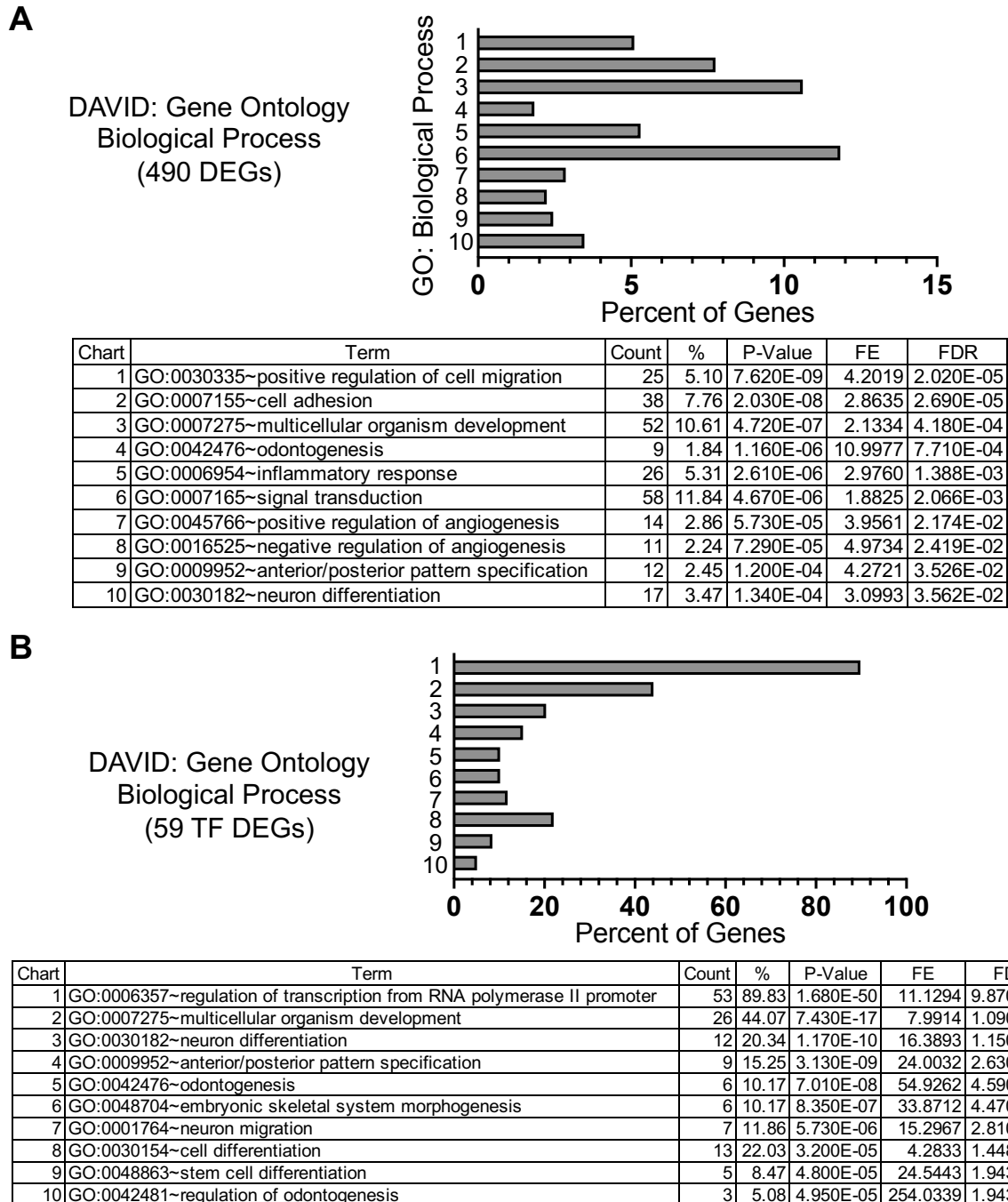


Figure 23 – Gene ontology (GO) analysis. (A) Bar chart indicating the lowest 10 p-values following DAVID GO analysis of the 490 differentially expressed genes (DEGs) from RNA-seq data (top), and descriptions of each chart item (bottom). (B) The same analysis conducted on the subset of 59 transcription factor (TF) genes. FE, fold-enrichment; FDR, false discovery rate (q-value).

ii. LIFR and TWIST1 are co-regulated

To determine whether TWIST1 expression could be driven by LIFR OE, shPCBP1 cells were transduced with either EV or a vector containing the mouse LIFR ORF (LIFR OE), and qPCR was performed. The results showed a significant increase in TWIST1 mRNA abundance in LIFR OE cells relative to control cells (Fig. 24A). Immunoblot analysis of the same cell lines confirmed that the increase in TWIST1 mRNA levels was sufficient to cause a measurable increase in TWIST1 protein levels (Fig. 24B). After observing the prediction from the JASPAR database that TWIST1 could potentially bind to the LIFR promoter, we sought to determine whether TWIST1 OE could drive LIFR expression. FAM3C KO cells (derived from parental shPCBP1 cells as previously) were transduced with either EV or a vector containing a mouse TWIST1 ORF. Immunoblot analysis revealed that the decrease in LIFR protein expression in FAM3C KO cells was partially reversed by TWIST1 OE (Fig. 24C). To determine whether TWIST1 binds to DNA at the LIFR promoter in live cells, ChIP-qPCR was performed using an antibody specific to TWIST1. Using the primer set described in the preceding sections for the detection of LIFR promoter DNA, qPCR results showed that TWIST1 binds to the LIFR promoter in shPCBP1 cells. As expected, binding was not detected in shSCR, FAM3C KO, or LIFR KO cell lines, which do not express measurable levels of TWIST1 (Fig. 25A). These results strongly suggest the presence of a reciprocal regulatory circuit in shPCBP1 cells that maintains LIFR expression through feed-forward regulation of transcription. These results further suggested that shPCBP1 cells achieve increased LIFR expression and signaling through STAT3 and TWIST1 activity (Fig. 25B).

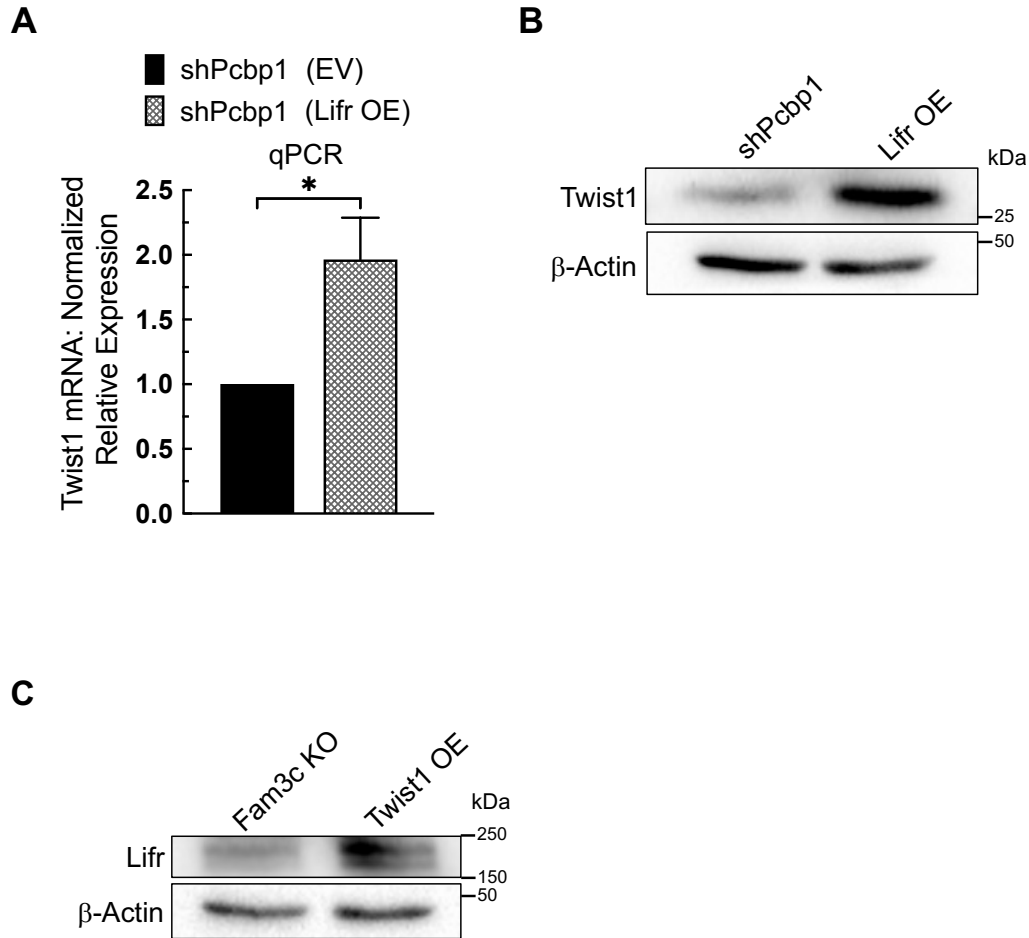


Figure 24 – LIFR and TWIST1 are coregulated. (A) qPCR analysis of shPCBP1 cells transduced with either empty vector (EV) or a vector containing the mouse LIFR open-reading frame (OE). Error bars represent SEM from three independent experiments, each performed in triplicate, * $P < 0.05$ (unpaired Student's *t*-test). (B) Immunoblot analysis of the cells shown in panel "A". (C) Immunoblot analysis of FAM3C KO cells (derived from parental shPCBP1 cells) transduced either with EV or a vector containing the mouse TWIST1 open reading frame.

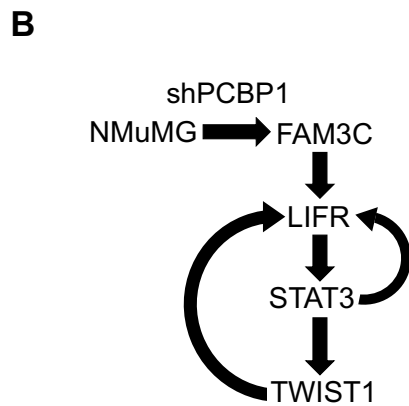
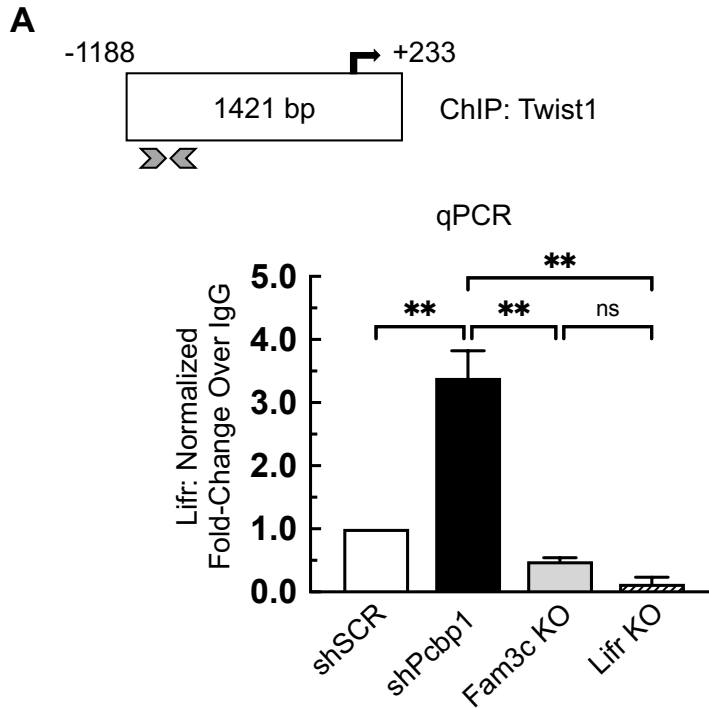


Figure 25 – TWIST1 binds to the LIFR promoter. (A) Chromatin immunoprecipitation (ChIP) analysis in the indicated NMuMG-derivative cell lines, following live cell cross-linking, incubation of chromatin with a TWIST1 antibody, and qPCR analysis of immunoprecipitated DNA. Arrowheads indicate the region of the LIFR proximal promoter targeted by the qPCR primer set. Error bars represent SEM from duplicate independent experiments, each performed in triplicate, ** $P < 0.01$ (one-way ANOVA). (B) Schematic diagram of the hypothesized feed-forward regulatory circuit present in shPCBP1 cells. ns, not significant; SEM, standard error of the mean.

3.3 Summary

The identification by Woosley et al. of (1) a binding partnership between FAM3C and LIFR and (2) the subsequent induction of FAM3C/LIFR-dependent pSTAT3 established the existence of a FAM3C/LIFR signaling axis in shPCBP1 cells (28). The demonstration of pSTAT3-dependent spheroid formation *in vitro* in shPCBP1 cells by Woosley et al. strongly suggests that changes in STAT3-regulated genes downstream of the FAM3C/LIFR interaction might be responsible for the maintenance of self-renewal (28). The current study sought to investigate this possibility through transcriptomic analysis following loss of FAM3C and LIFR expression in shPCBP1 cells. Using CRISPR-Cas9, FAM3C or LIFR was knocked out in shPCBP1 cells, and RNA-seq was used to compare parental (shSCR) NMuMG cells, shPCBP1 cells, and knockout derivatives. The data showed a clear dysregulation signature in a set of genes following loss of FAM3C or LIFR expression and showed that the same set of genes was upregulated in shPCBP1 cells relative to the parental (shSCR) NMuMG cells. Gene ontology (GO) analysis revealed that the dysregulated genes were associated with biological processes involved in EMT (migration and adhesion), stem cell self-renewal (development), angiogenesis, and signal transduction, all of which are relevant in the context of mammary carcinoma pathology. Additionally, GO analysis of a subset of genes that encode transcription factors revealed an association with similar biological processes, indicating that the FAM3C/LIFR interaction is required to maintain the expression of genes involved in regulating the relevant features of shPCBP1 cells. This finding was consistent with the phenotypic data demonstrated by Woosley et al. and additionally demonstrated by previous work published by the Howe laboratory (7, 28).

The transcription factor TWIST1 was identified and validated as a candidate gene suspected to play a direct role in regulating the aforementioned phenotypic features.

TWIST1 has been shown to regulate EMT in various carcinomas and has been shown to regulate the differentiation of embryonic stem cells, making it an interesting candidate for further study (131, 132). However, initial observations following attempts to rescue the phenotype of FAM3C and LIFR KO cells by overexpressing TWIST1 did not indicate that TWIST1 alone was sufficient for rescue (data not shown). TWIST1 overexpression was sufficient to upregulate LIFR in FAM3C KO cells, suggesting that it may act together with STAT3 at the LIFR promoter to regulate the initiation of transcription of the LIFR gene. Although the possibility of an interaction between TWIST1 and STAT3 at the LIFR promoter locus requires additional study, the current study showed by qPCR (using the same set of primers) that TWIST1 and STAT3 both bind to the LIFR promoter, suggesting that TWIST1 binds in proximity to STAT3. Collectively, our transcriptomic analysis provided the basis for the identification of mechanistic evidence contributing to phenotypic changes in NMuMG cells mediated by PCBP1 through its regulation of FAM3C, LIFR, and subsequent cascades.

Chapter 4: The Phenotypic Effects of LIFR Expression and Signaling

4.1 Introduction and rationale

Previous studies by our group have characterized phenotypic changes consistent with EMT in epithelial cells following PCBP1 knockdown (7, 20, 135). Our group and others have further characterized the suppression of invasiveness, stemness, tumorigenesis, and metastasis by PCBP1 in various carcinomas (22, 23, 30, 136, 137). Additionally, numerous recent mammary carcinoma studies have implicated STAT3 signaling as a contributor to invasive potential and metastasis through the exacerbation of EMT (138–140). In previous studies, PCBP1 knockdown measurably altered the expression levels of epithelial and mesenchymal marker genes and dramatically changed the morphological appearance of epithelial cells to resemble that of mesenchymal cells (7, 22). The data displayed in the previous section showed that increased LIFR expression was followed by increased pSTAT3 and increases in STAT3 target genes, including TWIST1. Since TWIST1 has also been extensively implicated in the regulation of EMT in mammary epithelial cells, it was hypothesized that the overexpression of TWIST1 in shPCBP1, FAM3C KO, or LIFR KO cells would cause a measurable increase in EMT, migration, invasion, and spheroid growth *in vitro* (130, 131, 133). However, experiments attempting to quantify increased EMT following overexpression of TWIST1 did not demonstrate any significant changes (data not shown). We hypothesized that increased LIFR expression might be capable of inducing signals in addition to pSTAT3 and in regulating genes in addition to TWIST1, and that unknown LIFR-mediated mechanisms might collectively affect the phenotype of shPCBP1 cells. The following section describes the experimental results that demonstrate phenotypic changes following the modulation of LIFR expression in mammary epithelial cells.

4.2 Results

i. LIFR expression promotes an invasive BCSC phenotype

In the current study, we observed EMT morphology following knockdown of PCBP1 in NMuMG cells and further observed that LIFR OE in shPCBP1 and LIFR KO cells caused an increase in cellular elongation that often accompanies EMT (Fig. 26). To determine whether LIFR expression had a direct effect on the invasiveness of shPCBP1 cells, a 3D invasion assay was performed to compare shPCBP1, LIFR KO (derived from parental shPCBP1 cells as previously), and LIFR KO cells with LIFR OE (LIFR KO OE cells). Invasion was quantified by comparing the relative growth patterns using a software-based method. The results showed that the loss of LIFR dramatically hinders 3D invasion and that its OE restores invasive growth beyond the levels detected in shPCBP1 cells expressing endogenous levels of LIFR (Fig. 27). Similar results were observed when the migration rates of the same cells were measured. LIFR KO significantly attenuated the migration rate, and LIFR OE rescued the loss of migration of LIFR KO cells. However, LIFR OE did not increase the migration rate beyond that achieved by endogenous LIFR expression in shPCBP1 cells (Fig. 28A).

The mammosphere assay quantifies the capacity of mammary epithelial cells to self-renew by measuring the size and frequency of spheroid colony formation. We sought to determine whether the modulation of LIFR expression could affect the self-renewal capacity of shPCBP1 cells. shPCBP1, LIFR KO, and LIFR KO OE cells were compared by mammosphere assay, and the results showed that self-renewal was also dramatically affected by the loss of LIFR expression and that LIFR OE partially rescued this effect (Fig. 28B). When the proliferation rates were compared between the cell lines used in the preceding culture-based experiments, the differences in growth rates were not found to

be significant (data not shown). These results demonstrated that LIFR expression levels can dramatically affect the invasion, migration, and stemness potential of shPCBP1 cells.

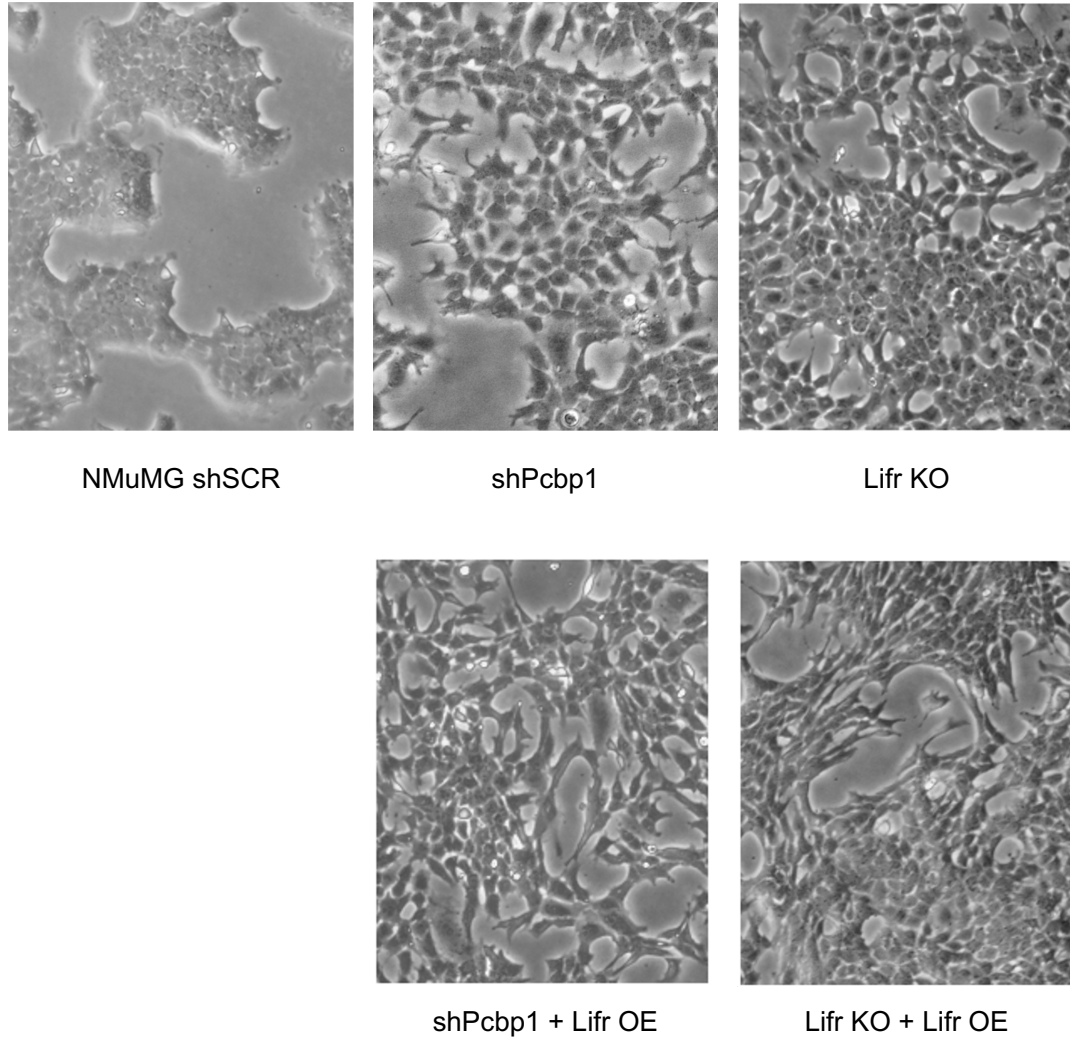


Figure 26 – Knockdown of PCBP1 and overexpression of LIFR alters morphology. Brightfield microscopy at 5X magnification comparing the indicated NMuMG derivative cell lines under standard adherent culture conditions. LIFR KO cells were derived from parental shPCBP1 cells. KO, knockout; OE, overexpression.

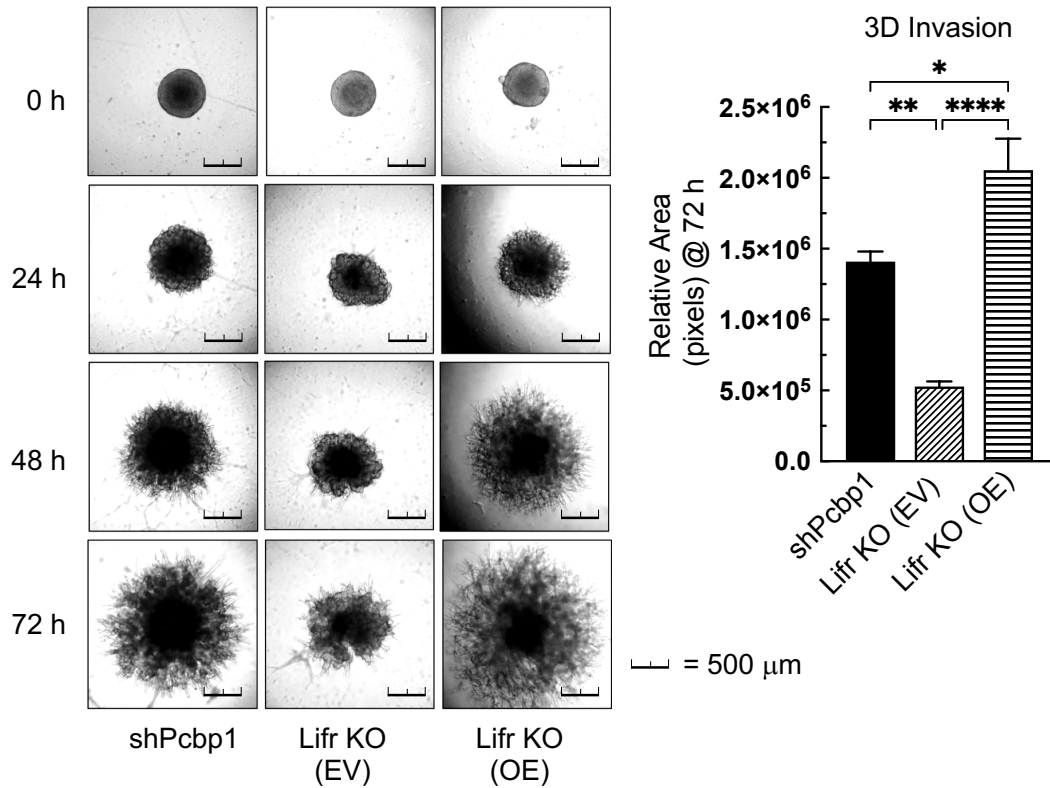


Figure 27 – LIFR expression promotes an invasive phenotype. Representative images of the indicated shPCBP1-derivative cell lines' 3-dimensional growth in Cultrex Basement Membrane Extract at the indicated time points, taken at 5X magnification. LIFR KO cells were derived from parental shPCBP1 cells. 10% fetal bovine serum (FBS) was used as chemoattractant (left), and quantification of the mean total increase in area from zero hours (right). Error bars represent SEM from four independent experiments, ****P<0.0001, **P<0.01, *P<0.05 (one-way ANOVA). EV, empty vector; OE, overexpression; SEM, standard error of the mean.

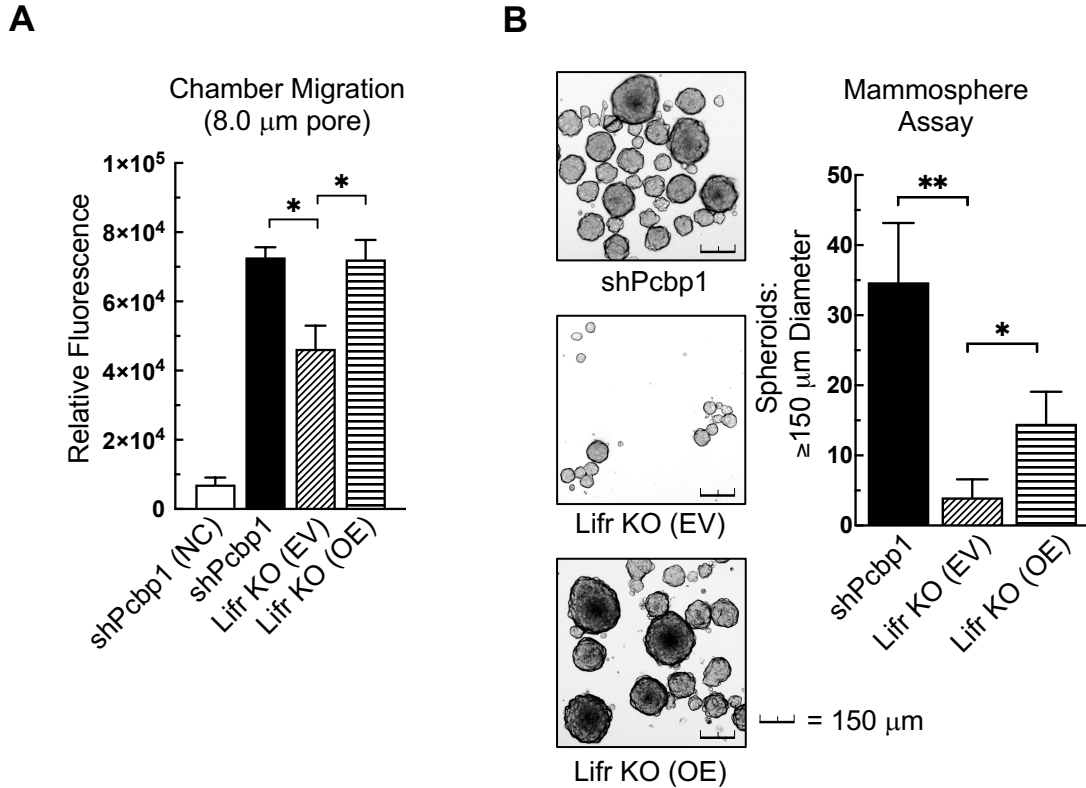


Figure 28 – LIFR expression promotes migration and BCSC phenotype. (A) Quantification of migration through polycarbonate chamber inserts (8.0 μm pore size) over 24-hours following seeding in serum-free medium, in the indicated parental shPCBP1 and KO derivative cell lines. 10% FBS was used as chemoattractant. Calcein AM was used to detect only the cells that successfully migrated through the pore. Error bars represent SEM from three independent experiments, * $P < 0.05$ (unpaired Student's *t*-tests). (B) Representative images of the indicated shPCBP1-derivative cell lines following mammosphere assay culture for 8 days, taken at 5X magnification (left). Comparison of total spheroid counts (right). Error bars represent SEM from five independent experiments, * $P < 0.05$, ** $P < 0.01$ (unpaired Mann-Whitney U-Test). BCSC, breast cancer stem cell; EV, empty vector; OE, overexpression; KO, knockout; NC, no chemoattractant; SEM, standard error of the mean.

ii. Loss of FAM3C/LIFR attenuates spheroid growth in human mammary carcinoma cells

Our group previously observed the attenuation of spheroid growth in shPCBP1 cells following knockdown of either FAM3C or LIFR using a mammosphere assay (28). To determine whether loss of FAM3C/LIFR expression would similarly affect spheroid growth in human cells, SKBr3 cells with shRNA-mediated knockdown of FAM3C (shFAM3C cells) were compared with control cells (HMLE normal human mammary epithelial cells and SKBr3 shSCR cells) using a mammosphere assay. SKBr3 shFAM3C cells showed a measurable reduction in spheroid formation compared to SKBr3 shSCR cells, and, as predicted, normal HMLE cells were not viable under these growth conditions (Fig. 29A, B). Notably, the size of the spheroids in both groups was variable, with large spheroids being present in both groups. To determine whether the proliferative rate of the cells under these conditions was also measurably attenuated by FAM3C knockdown, harvested spheroids were trypsinized, and pooled cells were counted following each experiment. Although shSCR and shFAM3C cells were seeded in equal numbers, shSCR cells showed a greater increase in growth after eight days (Fig. 29C). These results suggest that the loss of FAM3C/LIFR expression attenuates both the self-renewal capacity and viability of human mammary carcinoma cells under non-adherent, serum-free growth conditions *in vitro*.

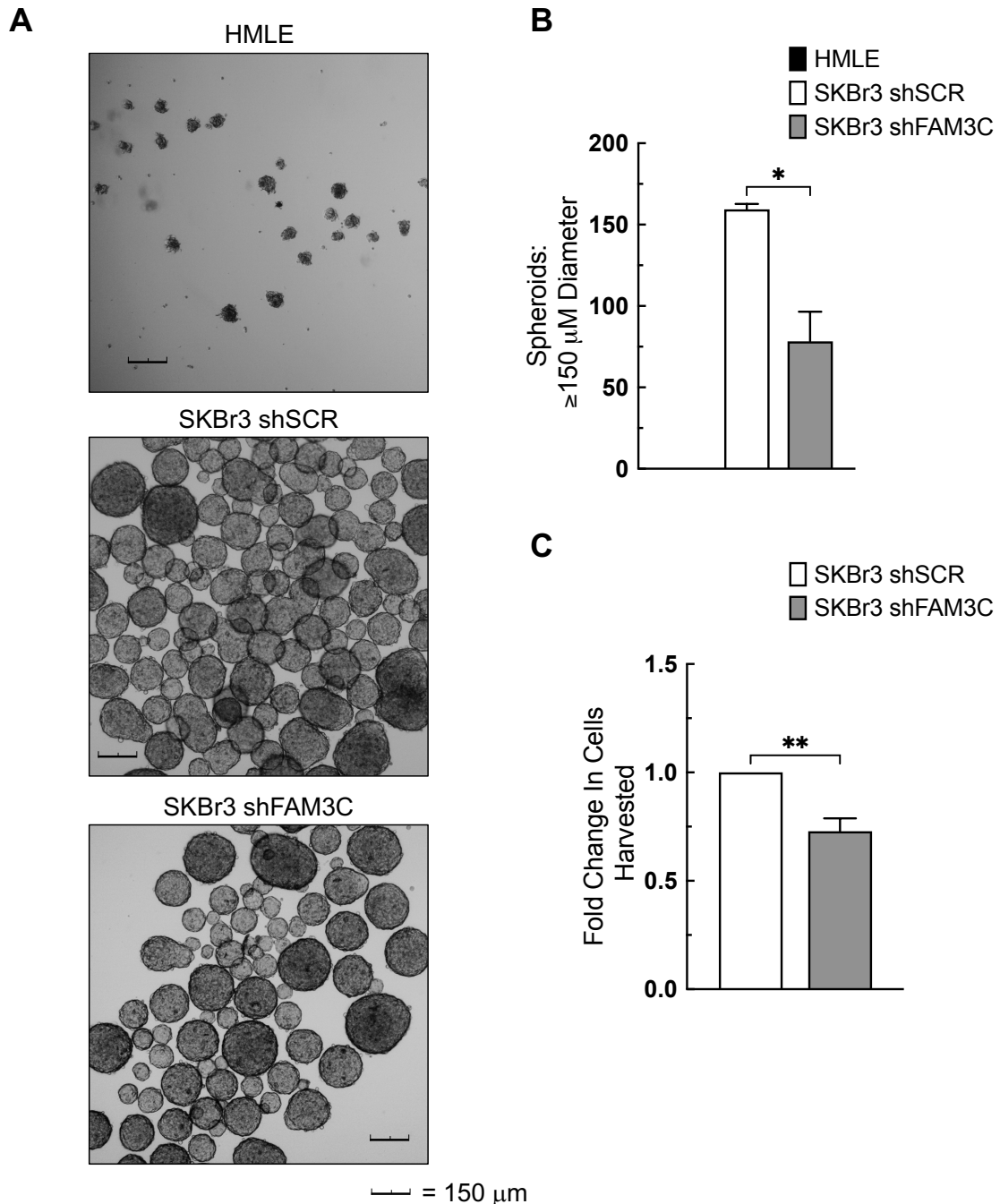


Figure 29 – Loss of FAM3C/LIFR attenuates spheroid growth in human mammary carcinoma cells. (A) Representative images of HMLE cells and SKBr3 cells transduced either with shRNA containing “scrambled” non-targeting control (shSCR) or shRNA targeting FAM3C following mammosphere assay culture for 8 days, taken at 5X magnification. (B) Comparison of total spheroid counts from the cells shown in panel “A”. (C) Comparison of total cell counts from the SKBr3 cells shown in panel “A”, following trypsinization of harvested spheroids. Error bars represent SEM from duplicate independent experiments, * $P < 0.05$, ** $P < 0.01$ (unpaired Student’s *t*-tests). SEM, standard error of the mean.

4.3 Summary

The Howe laboratory previously published data that showed that loss of either FAM3C or LIFR expression in shPCBP1 cells causes attenuation of mammary tumor growth and metastases in mice, and also causes attenuation of spheroid formation *in vitro* (28). Using CRISPR-Cas9, LIFR was knocked out in shPCBP1 cells and phenotypic features were assessed. Although cellular morphology did not change dramatically, rescue of LIFR KO by overexpression (OE) caused cellular elongation in adherent cell cultures, and the same elongation was observed following OE in parental shPCBP1 cells. This suggests that changes in signaling downstream of the high LIFR expression levels achieved by OE in the current study may alter the morphology of epithelial cells. Additionally, LIFR OE measurably altered the phenotypic features of shPCBP1 cells, including increased 3D invasion and increased migration through a porous substrate. Similar to observations in a previous study by Woosley et al., LIFR KO attenuated spheroid formation *in vitro* (28). In the current study, we made additional observations by utilizing LIFR OE, which was able to rescue the KO condition. LIFR is capable of inducing signaling pathways in addition to STAT3, and the involvement of these additional pathways requires further study. However, it is likely that LIFR-induced pSTAT3 participates in regulating the observed phenotypic features, based on similar observations in previous studies (122, 140–142). Finally, we observed that loss of FAM3C expression in human mammary carcinoma cells and the consequent loss of LIFR expression were sufficient to attenuate spheroid formation *in vitro*, which provided a parallel observation to that seen in mouse cells, and expanded upon the findings previously published by Woosley et al. (28).

Chapter 5: Discussion

5.1 Interpretation

i. Results and conclusions

PCBP1 is a multifunctional nucleic acid-binding protein that has been implicated in the pathogenesis of various carcinomas through the suppression of EMT and tumorigenesis (2). Although various PCBP1-dependent mechanisms have been described, those responsible for disease progression in mammary carcinomas remain largely unknown. In the current study, we defined a mechanism of phenotypic change in murine mammary epithelial cells lacking PCBP1 function. Furthermore, we demonstrated a mechanistic explanation for the aberrant expression of the LIFR gene following the loss of PCBP1 expression in mouse mammary epithelial cells and provided parallel observations in human mammary carcinoma cells. We also provided data that describe a signature of gene regulation downstream of the FAM3C/LIFR interaction and identified TWIST1 as a transcription factor that participates in the maintenance of LIFR expression. Finally, we demonstrated that the aberrant expression of LIFR in shPCBP1 cells supports increased invasion, migration, and self-renewal capacity, and that the loss of LIFR expression in SKBr3 human mammary carcinoma cells causes loss of self-renewal capacity.

In the current study, we sought to build upon our previous findings by identifying key intracellular mechanisms and dysregulated genes downstream of FAM3C/LIFR interaction. Our identification of a feed-forward mechanism of LIFR regulation aligns with a previous investigation that demonstrated an increase in LIFR mRNA levels following leukemia inhibitory factor (LIF)-induced pSTAT3 (143). Additionally, examination of a publicly available dataset that determined the genome-wide occupancy of STAT3 using high-throughput sequencing (ChIP-seq) in MDA-MB-231 triple-negative breast cancer

(TNBC) cells revealed an example of STAT3 binding to the 5' region near the promoter of the LIFR gene (144). Additional publicly available CHIP-seq datasets from murine embryonic fibroblasts and oligodendrocyte progenitors revealed that STAT3 binds to the LIFR transcription start site region (145, 146). Furthermore, our identification of LIFR expression/pSTAT3 signaling as promoters of invasion, migration, and self-renewal aligns with previous findings in multiple carcinoma types, including breast cancer (147–153). Finally, the loss of self-renewal and viability in human mammary carcinoma (SKBr3) cells following FAM3C knockdown suggests that FAM3C-mediated maintenance of LIFR expression may be required to maintain the BCSC phenotype in human breast cancer. However, further studies using animal models are required to determine how LIFR expression directly affects the metastatic potential of the invasive mammary carcinoma cell lines used in the current study.

Our transcriptomic analysis examined the overlap of DEGs that were upregulated by the loss of PCBP1 and dysregulated (either up- or down-regulated) by the loss of FAM3C and LIFR expression. Seventy percent of the DEGs identified were downregulated by FAM3C and LIFR KO, which allowed us to assert that the upregulation of FAM3C and LIFR following the loss of PCBP1 provides an interaction that allows cells to maintain the expression of a specific set of genes. A preliminary analysis of the DEGs using gene ontology (GO) revealed associations with biological processes implicated in mammary carcinoma pathology, which were hypothesized to be regulated by the FAM3C/LIFR interaction. These processes included cell migration, adhesion, differentiation, and development. Interestingly, GO analysis also identified angiogenesis and inflammatory responses as processes associated with DEGs in our dataset. STAT3 has previously been shown to regulate genes involved in both angiogenesis and inflammatory responses; therefore, it is possible that these associations are directly affected by the loss of FAM3C/LIFR/STAT3 signaling (93, 94, 107). However, additional studies are required to

identify the relevance of (1) the mechanism(s) involved, and (2) the potential phenotypic contribution(s) in both mouse and human mammary epithelial cells.

Previous studies have identified TWIST1 as a transcription factor that participates in the regulation of the genes responsible for EMT and stem cell self-renewal (129, 131, 132, 154). Zhao et al. demonstrated STAT3-dependent TWIST1 induction and subsequent STAT3/TWIST1-dependent EMT in the lung-metastatic derivative (LM2-4175) MDA-MB-231 human mammary carcinoma cell line (131). Similar evidence was presented by Lin et al. using A549 lung adenocarcinoma cells, and Cho et al. using PC-3 human prostate cancer cells (141). Surprisingly, TWIST1 overexpression did not significantly increase the invasion, migration, or self-renewal of shPCBP1 cells in the current study, nor did it rescue the loss of these properties in LIFR KO cells (data not shown). The direct effect of TWIST1 on EMT, stemness, and migration/invasion in our model requires further investigation. However, we found that TWIST1 participates in the regulation of LIFR. Therefore, it is plausible that TWIST1 influences the phenotype of shPCBP1 cells through the propagation of LIFR-dependent signaling.

In light of the fact that an estimated 90% of breast cancer-related deaths are caused by metastatic disease, it is appropriate to continue research to identify how transformed cells gain the ability to invade adjacent tissues and evade sensitivity to chemotherapy (90). Here, we describe a signaling mechanism in a model system that exemplifies the relevant characteristics of advanced mammary carcinoma pathology and provides evidence of parallel phenomena in human breast cancer cells. We conclude that the loss of PCBP1 expression in NMuMG cells causes upregulation of LIFR and that PCBP1-dependent FAM3C expression is necessary for the maintenance of LIFR expression and signaling. We also conclude that LIFR-induced STAT3 phosphorylation and consequent STAT3 target gene regulation are dependent on the FAM3C/LIFR interaction and that LIFR transcription is regulated by a feed-forward mechanism involving

STAT3 and TWIST1. Finally, we conclude that aberrant expression of LIFR promotes migration, invasion, and self-renewal in NMuMG shPCBP1 cells and that loss of LIFR expression attenuates self-renewal in SKBr3 human mammary carcinoma cells. Although further studies are needed to formulate interventions for the pathology that results from loss of PCBP1 function, we believe that our findings elucidate a key component of the potential role of PCBP1 in the suppression of the metastatic cascade in mammary carcinoma. A graphical representation of the summarized conclusions made by the current study is presented in Figure 30. When considering future directions for continued research related to the current study, relevant questions that were not addressed in the preceding experiments must also be considered. The following section describes the compelling considerations encountered while achieving the objectives outlined in the aforementioned specific aims.

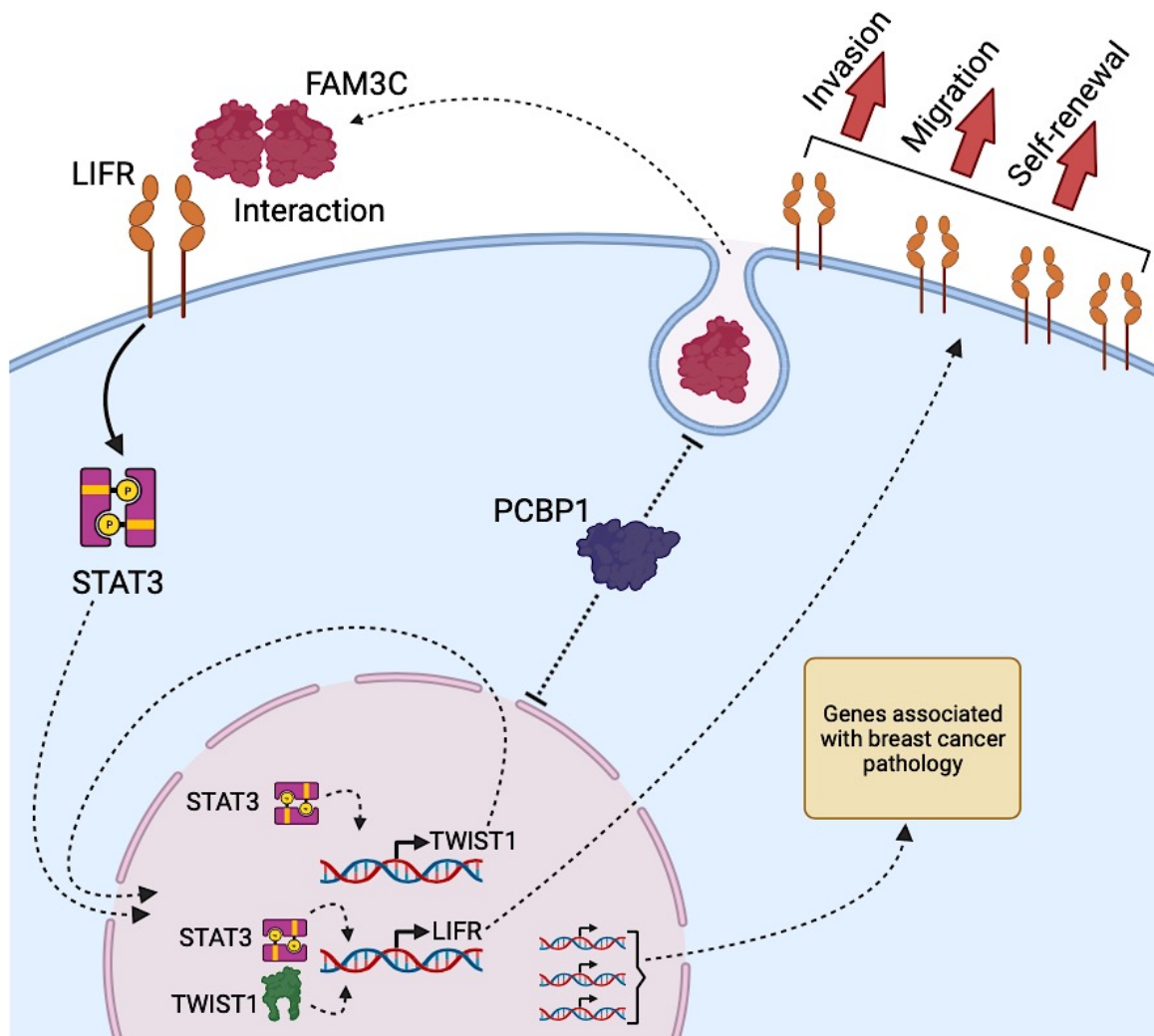


Figure 30 – Summary of conclusions. Illustration depicting the conclusions reached through the experiments conducted in the current study. Experimental designs were based upon the objectives defined in the Specific Aims (illustrated in Figure 6).

ii. Translational considerations

In 2019 Woosley et al. identified that post-transcriptional upregulation of FAM3C occurs following loss of PCBP1 expression in NMuMG cells and results in LIFR-dependent induction of pSTAT3 (28). Although parallel observations were made using human mammary carcinoma cell lines in the current study, these cell lines did not demonstrate a loss of PCBP1 expression (data not shown). To further observe the physiological parallels in breast cancer, proteomic data from breast cancer patient tumor samples were analyzed. Using the National Institutes of Health Proteomic Data Commons (NIH PDC) portal, a dataset was obtained from The Cancer Genome Atlas (TCGA) Breast Cancer Proteome project (155). Protein abundance levels of PCBP1, FAM3C, and STAT3 in 108 tumor samples and 3 healthy control samples were plotted using heatmap analysis, and hierarchical clustering was used to group samples with similar expression patterns. Four discrete clusters containing a total of 20 samples displayed gene expression patterns that (1) differed greatly from the healthy controls and (2) exemplified low PCBP1, high FAM3C, and high STAT3 expression (Fig. 31). Of the 20 samples in the four clusters, 14 clearly showed loss of PCBP1 expression with concomitant increase in FAM3C and STAT3 expression relative to the other samples in the cohort. The cohort of samples was derived from various stages of the disease, ranging from stage 1 to stage 4. All 14 samples that displayed the aforementioned expression pattern were from disease stages 2-3. Additionally, the 14 samples showed some of the highest FAM3C and STAT3 levels in the cohort. These observations suggest that a subset of human patients harbor tumors that maintain intracellular mechanisms parallel to those characterized in the current study. It should be noted that the STAT3 expression in this analysis was not specific to pSTAT3 (Y705), which does not allow confirmation that STAT3 activation and signaling are responsive to FAM3C in these patients. However, it is possible to suggest that STAT3 expression in these samples acts as a surrogate for pSTAT3, as STAT3 has been shown

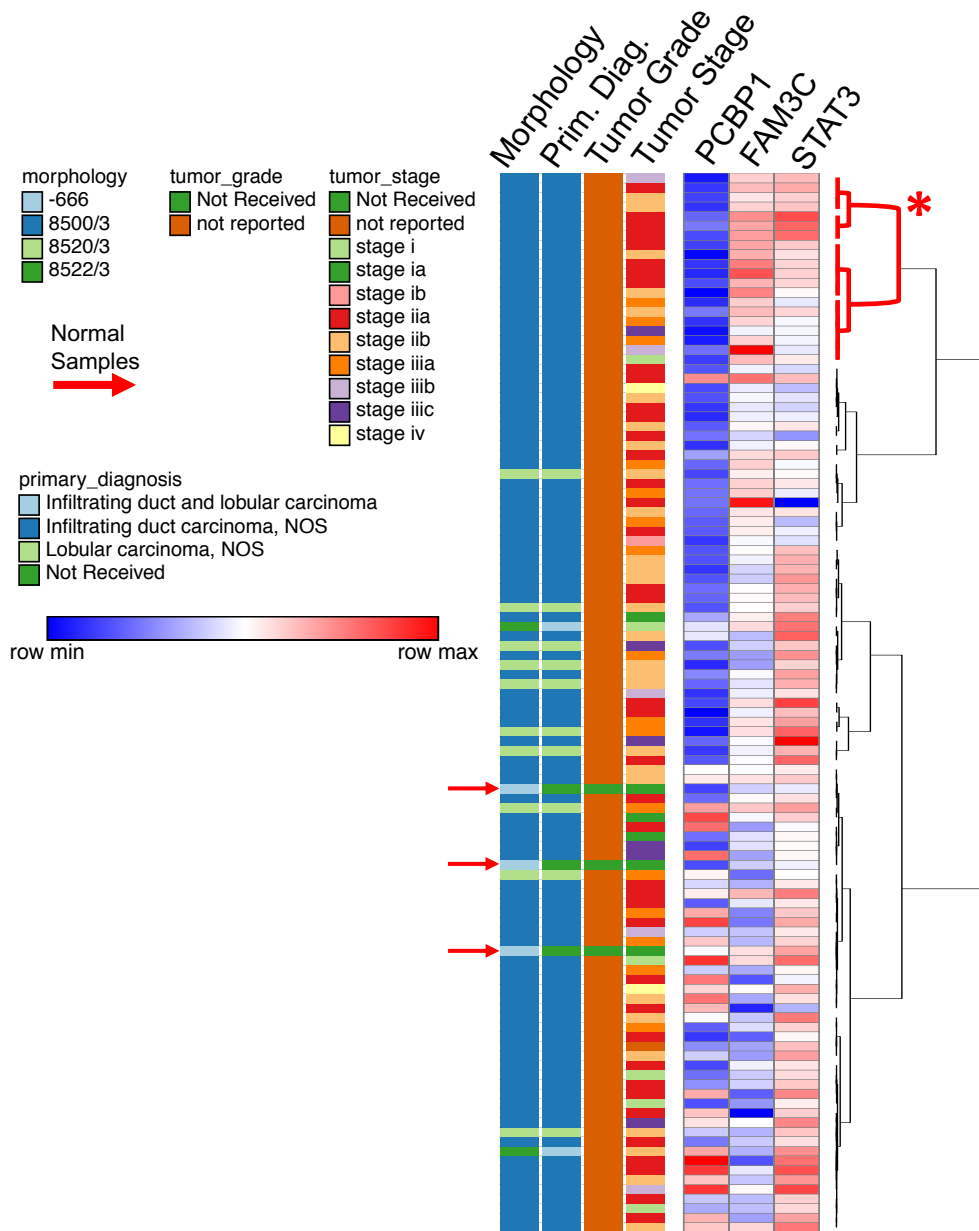


Figure 31 – Low PCBP1 expression correlates with high FAM3C and STAT3 expression in a subset of human mammary carcinoma patients. Heat map analysis derived from “The TCGA Breast Cancer Proteome” dataset, showing the expression levels of PCBP1, FAM3C, and STAT3 108 human mammary carcinoma tumor samples and three normal mammary tissue control samples. Hierarchical clustering analysis (black brackets) indicates similarities found between groups of samples. The top four clusters (red brackets and asterisk) indicate expression levels that align with the current hypothesis.

to be a target gene of active nuclear pSTAT3 in previous genome-wide occupancy studies of the STAT3 promoter (144–146). It should also be noted that a separate dataset containing phosphoproteomic data from the same tumor samples mentioned above was analyzed, and pSTAT3 (Y705) expression was detected. However, FAM3C was not detected in this dataset owing to its lack of post-translational phosphorylation. Interestingly, pPCBP1 (S43) was not detected in the phosphoproteomic dataset, suggesting that the lack of PCBP1 expression in these patients may be responsible for FAM3C upregulation as opposed to the loss of PCBP1 suppression of FAM3C translation that would occur following phosphorylation of PCBP1 at serine 43 by upstream kinases including AKT2.

In the current study, we confirmed that the loss of LIFR expression and signaling resulted in a loss of TWIST1 expression, and that pharmacological inhibition of pSTAT3 caused a loss of TWIST1 expression through decreased transcriptional activity in shPCBP1 cells. To observe parallels in breast cancer, phosphoproteomic data from the TCGA Breast Cancer Proteome were analyzed using the same patient tumor samples shown in the preceding analysis. Heat map analysis showed a clear correlation between high levels of pSTAT3 and high levels of pTWIST1 (Fig. 32). Conversely, low levels of pSTAT3 correlated with low levels of pTWIST1. Additionally, in parallel with our observations in the NMuMG control (shSCR) cells used in the current study, low levels of pSTAT3 accumulated in healthy control samples, along with low pTWIST1 levels. It should be noted that the true accumulation levels of TWIST1 could not be observed in these samples because the analysis was restricted to pTWIST1 (S68). However, a recent study suggested that the phosphorylation of TWIST1 at serine 68 is a beacon of protein stability, owing to an increased proteasomal processing rate of unphosphorylated TWIST1. This study also showed a correlation between pTWIST1 (S68) and total TWIST1 protein in invasive human mammary carcinoma cell lines and concluded that phosphorylation of

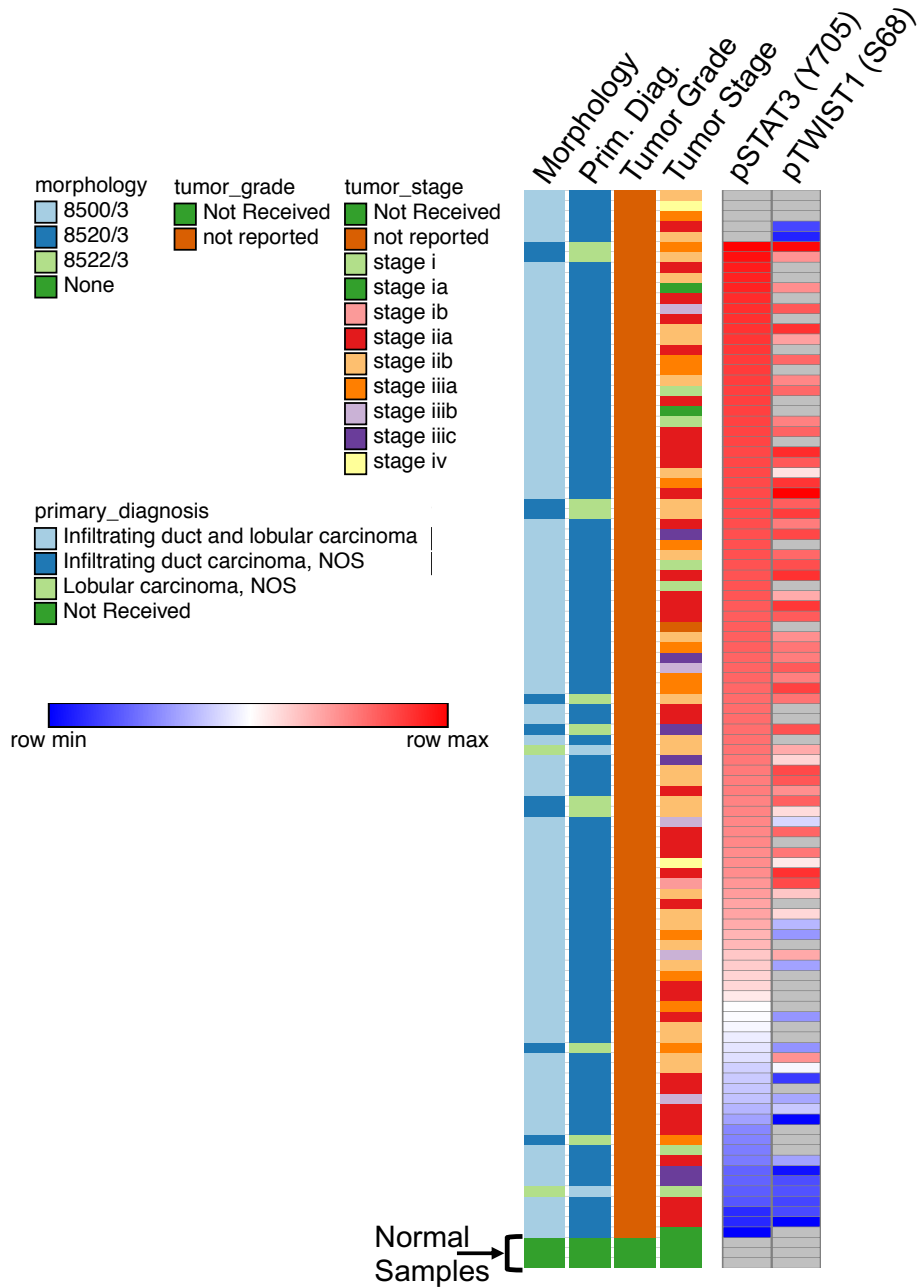


Figure 32 – pSTAT3 accumulation correlates with pTWIST1 accumulation in human mammary carcinoma. Heat map analysis derived from “The TCGA Breast Cancer Phosphoproteome” dataset, showing the expression levels of pSTAT3 (Y705) and pTWIST1 (S68) in 108 human mammary carcinoma tumor samples and three normal mammary tissue control samples.

TWIST1 at serine 68 promotes breast cancer invasion (156). These observations suggest that the intracellular mechanisms characterized downstream of FAM3C/LIFR interaction using mouse cells in the current study can be investigated further in human disease and can potentially reveal properties that are targetable by clinical interventions.

In the current study, we observed that the loss of LIFR expression attenuated the phenotypic properties of shPCBP1 cells, including invasion, migration, and self-renewal. We also observed that recombinant TWIST1 overexpression resulted in increased expression of LIFR in a shPCBP1 cell line derivative that previously lacked TWIST1 (FAM3C KO cells), suggesting that TWIST1 participation in the LIFR-promoted phenotypic properties was plausible. Previous studies have demonstrated TWIST1-dependent EMT downstream of pSTAT3 in metastatic derivatives of human mammary carcinoma cell lines, suggesting that TWIST1 affects breast cancer phenotypes in clinical settings in the context of observations made in mouse cells in the current study (131). Additionally, previous studies have illustrated the applicability of TWIST1 expression levels as a prognostic indicator in breast cancer, and have shown that high TWIST1 expression correlates with poor prognosis, using both tumor microarray immunohistochemistry and PCR from frozen specimens (157, 158).

To examine the possibility that high TWIST1 expression levels correlate with patient survival, Kaplan-Meier analysis was conducted using TWIST1 mRNA levels from Affymetrix Gene-chip analysis in a cohort of breast cancer patients. The results clearly showed a significant decrease in overall survival (OS) and distant metastasis-free survival (DMFS) in large groups of patients with high TWIST1 expression compared to those with low TWIST1 expression (Fig. 33). These data align with the findings of previous clinical studies and suggest a mechanism responsible for the phenotypic changes induced by LIFR expression in the current study. Notably, overexpression of TWIST1 did not yield any significant phenotypic outcomes in the shPCBP1 cell line derivatives in the current study

(data not shown). Additionally, further segregation of the cohort in the Kaplan-Meier analysis described above showed that a significant decrease in OS correlated with high TWIST1 expression in patients with pathologies including TNBC (n=201), ER+, HER2- (n = 630), basal subtype (n = 431), luminal A subtype (n = 596), grade 3 tumors (n = 586), and HER2+ (n = 420) (data not shown). However, when the cohort was adjusted to exclude patients who had not received systemic chemotherapy or endocrine therapy, there was a reverse outcome, and *low* TWIST1 levels correlated with a significant decrease in OS (n = 584). Therefore, TWIST1 expression may fail to provide a universal prognostic indication for all breast cancer pathologies. Further studies are required to delineate the distinct clinical features associated with TWIST1 expression in breast cancer. However, the analyses conducted here provide strong reinforcement for previous preclinical and clinical characterization of TWIST1 as an oncogenic driver and as a protein that plays an important role in the phenotype of mammary epithelial cells.

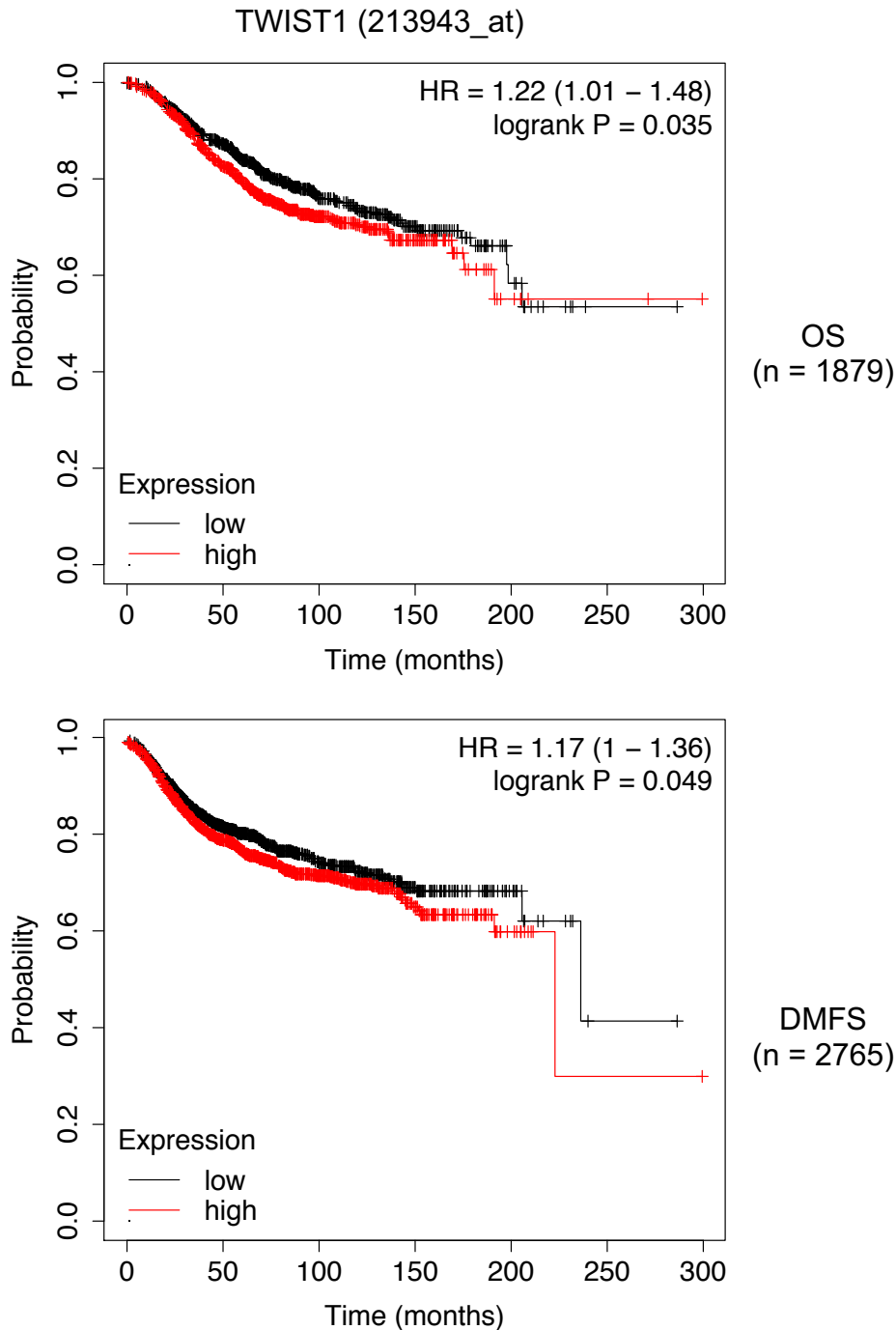


Figure 33 – High TWIST1 expression correlates with reduced survival in human mammary carcinoma. Kaplan-Meier analysis plots showing the overall survival (OS) and distant metastasis-free survival (DMFS) rates of cancer patients and their corresponding mRNA levels of TWIST1, derived from Affymetrix gene chip experimental data. The hazard ratio (HR) represents the cutoff value with the highest hazard rate, where a value of “1” indicates no difference and a value of “2” indicates a 100% difference.

5.2 Additional considerations

Our previous study demonstrated the effect of FAM3C or LIFR knockdown in shPCBP1 cells by revealing that increased self-renewal *in vitro* and decreased tumor burden and metastasis *in vivo* were dependent on FAM3C/LIFR interaction and subsequent pSTAT3 induction (28). Preclinical studies by other groups have likewise demonstrated that LIFR expression promotes breast cancer progression. As described in Chapter 1 (Section 1.3), more than ten examples of preclinical characterization of LIFR/JAK/STAT3 in various cancer types are associated with the conclusion that increased LIFR expression promotes disease progression (71). However, several studies have shown that increased LIFR expression can suppress disease progression through its induction of JAK/STAT3 and other signaling pathways, suggesting that the role of LIFR is “pleiotropic” due to its range of potential downstream regulatory effects. The ability to translate our understanding of LIFR expression into clinical applications is therefore paradoxical and appears to be dependent on the preclinical experimental context and/or tissue of origin.

Considering future directions, it may be most appropriate to revisit contexts that have high potential for clinical translation and improved treatment efficacy. For example, LIFR expression has been considered in the context of therapeutic interventions for breast cancer using histone deacetylase inhibitor (HDACi) drugs. In 2016, Zeng et al. used human mammary carcinoma cell lines and patient-derived xenografts to demonstrate that upregulation of LIFR occurs following histone deacetylase inhibition (HDACi) and subsequently causes increased expression of STAT3-target genes associated with resistance to apoptosis. Zeng et al. concluded that LIFR-induced pSTAT3 promotes disease by decreasing the efficacy of HDACi therapy (159). However, in 2017, Johnson et al. suggested that although LIFR expression increases in human mammary carcinoma cell lines following HDACi treatment, upregulation of STAT3-target genes not only induces

stemness, but also dormancy in cancer cells (160). Although Johnson et al. further characterized the induction of LIFR expression following HDACi treatment in a later study and reached conclusions that were similar to those of Zeng et al., it was demonstrated that LIFR upregulation following HDACi treatment drives cancer cell dormancy, potentially prolonging patient survival (161). The preceding example highlights the need to fully understand the impact of LIFR on disease progression despite the fact that data interpretations from independent inquiries have yielded similar results and conclusions.

Several additional studies by other groups have provided preclinical *in vivo* evidence suggesting that LIFR suppresses disease progression by inducing JAK/STAT3 and other pathways including HIPPO and PI3K/AKT (70, 162). Although examination of the preponderance of pan-cancer preclinical data characterizes LIFR as a promoter of carcinoma pathology (approximately two-thirds of examples), a considerable amount of data has shown that LIFR can act as a suppressor of disease progression, prompting the need to carefully consider each case independently. For example, it is important to note that our experimental context showcased the manipulation of LIFR expression in tumorigenic cells that have previously undergone EMT. The role of EMT in the promotion of disease progression and the degree to which it affects the phenotype of cancer cells can potentially vary and may explain some of the differences in the conclusions drawn by other groups attempting to define the role of LIFR in disease progression. Our previous studies have clearly demonstrated the role of shPCBP1-mediated EMT in the progression of mammary carcinoma *in vivo* and was therefore selected as an appropriate experimental context for further characterization of FAM3C/LIFR/STAT3 participation in the regulation of pathological features. However, it is important to consider that the loss of PCBP1 expression may not cause the same degree of EMT in all epithelial tissues, and therefore may not always create a parallel experimental model for studying the contribution of LIFR expression to carcinoma metastasis and/or disease progression.

In the transcriptomic analysis conducted in the current study, we focused on the genes hypothesized to be regulated downstream of pSTAT3 induction; however, it is important to note that LIFR has been shown to activate signal transduction through several additional pathways, including MAPK, PI3K/AKT/mTOR, and HIPPO-YAP, in a manner that may also be selectively responsive to coupling with other members of the IL-6 family of cytokine receptors (47, 70, 78, 163, 164). Additionally, there are several examples of carcinoma studies that implicate LIFR/STAT3 in regulatory “cross-talk” with additional signaling pathways, including HEDGEHOG and WNT (165–167). Preliminary pathway analysis of our transcriptomic data revealed associations between our set of 490 DEGs and both the HEDGEHOG and WNT pathways (data not shown). However, delineation of the relevant mechanisms related to this study requires further analysis. Additionally, it is not known whether FAM3C interacts with LIFR alone or if other proteins/receptors are recruited and are therefore required to transduce intracellular signals, including pSTAT3. The results demonstrated by Woosley et al. showed an electrophoretic gel shift following extracellular cross-linking of FAM3C to the plasma membrane, and indicated the possibility that other small-to-medium-sized proteins could be present (28). The discovery of additional receptors that interact with FAM3C/LIFR could indicate that other signaling pathways, such as those mentioned above, are induced and/or dependent on FAM3C/LIFR interactions in mammary epithelial cells.

Although the current study illustrated a feed-forward mechanism of regulation of LIFR expression in shPCBP1 cells, it is possible that additional unknown mechanisms participate in the dramatic increase in LIFR expression observed in shPCBP1 cells relative to their parental NMuMG (shSCR) counterpart. The expression of LIFR in shSCR cells was below the level of detection by qPCR, which does not provide a “platform” for FAM3C/LIFR interaction following an increase in FAM3C secretion that would occur following loss of PCBP1 expression or function. Although it is possible that increased

FAM3C secretion alone is sufficient to cause an increase in LIFR expression in cells that express very little basal LIFR protein, it is also possible that additional intracellular mechanisms participate in the regulation of the LIFR gene, and that these mechanisms are responsive to phenotypic changes downstream of the loss of PCBP1 expression or function. For example, Zeng et al. and Johnson et al. showed that treatment with HDACi increased LIFR expression in human mammary carcinoma cells (159, 160). Additionally, Okamura et al. showed that treatment with DNA demethylases rescued the loss of LIFR expression in human hepatocellular carcinoma (HCC) cells (89). These examples suggest that LIFR expression can be altered by the activity of chromatin- and DNA-modifying enzymes that epigenetically regulate gene expression.

The feed-forward mechanism of LIFR regulation illustrated in the current study hypothesized that increased pSTAT3 results in an increase in the nuclear localization of STAT3 dimers that activate the transcription of LIFR and other genes by binding to DNA at gene promoter loci. Following the identification of STAT3 as a “second messenger” transcription factor that plays an important role in shPCBP1 cells, it is important to consider the possibility that additional intracellular mechanisms contribute to the regulation of STAT3 activity downstream of its phosphorylation by FAM3C/LIFR. For example, it has been shown that STAT3 contains a critical serine residue near its C-terminus (S727) that can be phosphorylated in response to treatment with IL-6 family cytokines or EGF. It has also been shown that phosphorylation at both Y705 and S727 is required for the maximal transcriptional activity of STAT3 in human fibrosarcoma-derived epithelial cells (168). However, it was later shown using human cervical cancer (HeLa) cells that S727 and Y705 phosphorylation events are mutually antagonistic and that S727 phosphorylation directly inhibits the DNA-binding activity of STAT3 (169). Additionally, S727 phosphorylation was shown to promote the pluripotency of LIF-induced murine embryonic stem cells (mESCs) in the presence of Y705 phosphorylation, although S727 phosphorylation was found to be

dispensable for induced pluripotency. However, during forced differentiation of cultured mESCs, S727 phosphorylation promotes differentiation and directly inhibits the self-renewal phenotype induced by Y705 phosphorylation (170). Although the role of S727 phosphorylation of STAT3 in shPCBP1 cells in the current study has not been determined, it is possible that factors related to the frequency of S727 phosphorylation could contribute to the transcriptomic landscape of FAM3C/LIFR/STAT3 signaling in our model and in human mammary carcinomas.

In addition to the regulation of phosphorylation events that occur because of the activity of upstream kinases, STAT3 activity is also regulated by a negative feedback loop that involves the suppressor of cytokine signaling 3 (SOCS3) protein (107, 171). SOCS3 has been shown to be a direct transcriptional target of STAT3 and has been shown to inhibit pSTAT3 induction by binding to JAKs and preventing Y705 phosphorylation (107, 171). Examination of the publicly available ChIP-seq datasets mentioned above also revealed that STAT3 occupies the SOCS3 transcription start site region (144–146). In the current study, we hypothesized that changes in pSTAT3 activity downstream of FAM3C/LIFR interaction and/or LIFR overexpression would demonstrate a correlation between pSTAT3 induction and STAT3 target gene mRNA upregulation. We found that STAT3 and MYC genes (both STAT3 target genes) were downregulated upon pharmacological inhibition of STAT3. However, efforts made in the current study to determine whether SOCS3 upregulation responds directly to pSTAT3 induction in mouse or human cells have been inconclusive. Additional examination of the role of SOCS3 and its effect on JAK1/JAK2 activity could provide a better understanding of pSTAT3 induction and feed-forward LIFR regulation in shPCBP1 cells and cells with low expression levels of LIFR.

In the current study, ChIP-qPCR was used to show that both STAT3 and TWIST1 bind to the LIFR promoter locus in proximity to each other; however, the results did not

determine whether STAT3 and TWIST1 interact or whether their regulation of LIFR transcription is interdependent. Additional experiments aimed at revealing STAT3 and TWIST1 binding partnerships at the LIFR promoter could potentially reveal the presence of co-regulating proteins and may also reveal whether their activity and/or expression is dependent on PCBP1 expression levels. For example, the protein inhibitor of activated STATs 3 (PIAS3) has been shown to directly inhibit the transcriptional activation activity of STAT3 in the nucleus by binding to STAT3, thereby preventing STAT3 from binding to DNA (107, 172). Sun et al. showed that PIAS3 expression levels are reduced in human hepatocellular carcinoma (HCC) cells relative to healthy epithelial cells, and that reduced expression of PIAS3 was required to maintain STAT3 activation levels (172). Interestingly, Sun et al. also found that SOCS1 expression levels correlated inversely with STAT3 activation, and that overexpression of SOCS1 ablated the oxidative stress-induced increase in STAT3 phosphorylation (172). This suggests that both PIAS3 and SOCS1, two proteins that were not extensively characterized in the current study, may play a role in the feed-forward mechanism of LIFR regulation. However, preliminary examination of PIAS3 expression levels by RNA-seq did not reveal any changes in mRNA abundance in shPCBP1 cells relative to shSCR cells and did not reveal any changes in mRNA abundance following FAM3C or LIFR KO. Additionally, although a small reduction in SOCS1 mRNA abundance was noted in LIFR KO cells relative to shPCBP1 cells, the expression levels of SOCS1 were very low overall and near the threshold of detection. Therefore, it is necessary to validate the potential downregulation of SOCS1 before suggesting its involvement in the mechanism described in the current study.

Finally, it is important to consider that it has been suggested that STAT3 can heterodimerize with activated STAT1 protein in epithelial cells, and it has been shown that STAT1/STAT3 heterodimers have transcriptional regulation activity in T cells (107, 173). It has also been suggested that small structural differences in STAT family proteins can

alter transcriptional selectivity through changes in DNA-binding affinity (109, 174). Therefore, it is possible that the gene expression patterns maintained by FAM3C/LIFR/STAT3 induction in shPCBP1 cells can be modulated by the activation of STAT1 and/or the upstream factors that may contribute to changes in STAT1 activation. Further analysis of the data generated in the current study will be necessary to determine the effect of pathways upstream of STAT1 and whether changes in FAM3C or LIFR expression have a direct effect on STAT1 participation in the regulation of gene expression. Collectively, the additional considerations discussed above highlight a complex landscape of biological features that function in tandem with the mechanism of LIFR regulation characterized herein. The following section discusses potential opportunities to experimentally examine some of these features, in addition to the proposed extensions of the conclusions reached through the experiments in the current study.

5.3 Future directions

Although the current study is presented as a complete body of work that represents the objectives of the specific aims, there are several areas of continued research that can potentially expand the depth of our conclusions. For example, ongoing analysis of our transcriptomic data may reveal additional DEGs required for invasion and migration that are regulated by LIFR expression and signaling. We identified the matrix metalloprotease 2 (MMP2) gene as a candidate DEG in our dataset, and further characterization of its expression in shPCBP1 cells may enable its connection to FAM3C/LIFR/STAT3 signaling. MMP2 has been shown to be directly regulated by STAT3, and examination of ChIP-seq data from MDA-MB-231 cells showed that STAT3 binds to the 5' region near the MMP2 promoter (142, 144, 175). Additionally, recent studies have characterized the role of MMP2 in invasive breast cancer and metastatic melanoma and demonstrated a correlation

between STAT3 activity and MMP2 expression (142, 176, 177). Coincidentally, Schmidt et al. identified a loss of MMP2 expression following FAM3C knockdown in human breast cancer cells (178). Our transcriptomic data also identified TWIST2 as a dysregulated transcription factor that may be involved in driving phenotypic changes in shPCBP1 cells. Although the expression of TWIST2 was significantly increased in shPCBP1 cells relative to shSCR cells, preliminary experiments failed to reveal how a modest downregulation of TWIST2 following FAM3C or LIFR KO affects the shPCBP1 phenotype (data not shown).

The datasets from our RNA-seq experiments provided the expression levels of approximately 23,000 genes, approximately 14,000 of which had expression levels above our detection threshold. Although our approach to identifying and validating candidate DEGs was successful, it was also restricted to a small number of genes and only included the characterization of one gene, TWIST1. It is possible that collaboration with bioinformaticians who utilize novel software-based analysis methods might reveal biological insights within our RNA-seq data. The current study utilized the Partek Flow web-based client software for data analysis, and because it is equipped with a “point and click” user interface, it does not require advanced knowledge of computer programming or statistical mathematics. However, Partek Flow provides many custom parameters during the data processing steps, and while the selection of custom parameters requires intimate knowledge of the software and the experimental objectives, it does not require computer programming language or statistical modeling. Continued analysis using multiple analytical approaches may reveal phenotypic features of interest that can be investigated experimentally. Most importantly, our analysis did not reveal dysregulation of canonical transcription factors associated with stem cell self-renewal (e.g., SOX2, OCT4, MYC, KLF4, NANOG, and BMI1), and it remains to be seen how FAM3C/LIFR interaction affects self-renewal through the regulation of gene expression, suggesting that novel candidates may need to be identified. Continued analysis of our RNA-seq data, combined

with new sequencing experiments in human cells and customized bioinformatic approaches is therefore a viable proposal for future directions related to the current study.

Following the validation of TWIST1 as a DEG in our RNA-seq dataset that responds to changes in pSTAT3, we attempted to overexpress (OE) TWIST1 to observe its effect on shPCBP1 cells and KO derivatives. Following TWIST1 OE, we did not observe any measurable effects on phenotypic features, including migration, 3D invasion, and self-renewal, as described in Chapter 4 (data not shown). However, we observed an increase in the mRNA and protein expression of LIFR. Because TWIST1 is a transcription factor, it is possible that it participates in the regulation of a subset of DEGs found in our RNA-seq analysis, and it is possible that a subset of DEGs require TWIST1 expression for the initiation of transcription. TWIST1 expression levels were below the threshold of detection in shSCR cells and in FAM3C KO and LIFR KO derivatives of parental shPCBP1 cells; therefore, continued analysis of the RNA-seq data, coupled with validation by qPCR, could reveal a set of genes that are regulated by FAM3C/LIFR interaction, which are dysregulated due to loss of TWIST1 expression. Identification of this hypothesized set of genes may reveal additional proteins that participate in the feed-forward mechanism of LIFR expression, and may also reveal proteins that affect the phenotypic features of shPCBP1 cells and their KO derivatives. Therefore, continued characterization of the gene regulation downstream of TWIST1 expression in shPCBP1 and human cell lines provides a future direction for research in our model of mammary carcinoma.

Although the current study showed by ChIP-qPCR that both STAT3 and TWIST1 bind to the LIFR promoter locus, the nucleotide sequence(s) necessary to facilitate transcription factor binding was not determined. It is possible that continued analysis by transcriptional reporter assays using site-directed mutagenesis could reveal the loci of direct DNA/protein interactions and the binding events that are necessary to regulate the initiation of LIFR transcription. Additionally, it may be possible to isolate chromatin

following the cross-linking of proteins to DNA so that proteomic analysis can be carried out. Proteomic analysis may identify additional binding partners and/or co-regulators at the LIFR locus and may reveal a direct interaction between STAT3 and TWIST1. Further characterization of transcription initiation by factors that are dependent on FAM3C/LIFR interaction, combined with the investigation of epigenetic regulation mechanisms described in the preceding section, may increase our understanding of the dynamics of LIFR regulation in epithelial cells. This proposed future direction is especially interesting when considering the dynamics of LIFR expression observed in shPCBP1 cells compared to shPCBP1 cells cultured *ex vivo* following the extraction of primary tumors and metastases from mice. As mentioned in Chapter 1 (Section 1.4), Woosley et al. found that LIFR expression was below the detection threshold in cells cultured *ex vivo* from primary tumors and lung nodules from mice with mammary fat pad engraftment of shPCBP1 cells (28). This observation was paradoxical because Woosley et al. also found that the loss of LIFR expression in shPCBP1 cells attenuated the growth of tumors and metastases in the same mice (28). In light of the variable conclusions drawn by other groups investigating the role of LIFR in carcinoma progression, it may be useful to observe how multiple factors capable of changing the regulation of LIFR expression participate *in vivo* during the growth and dissemination of tumors. Therefore, continued animal-based experimentation using designs capable of observing LIFR regulation dynamics and/or time-based observations during tumor growth provides a viable future direction beyond the current study.

Chapter 6: Materials and Methods

Cell culture

NMuMG, HEK293T, HMLE, MCF10A, MCF7, SKBr3, and MDA-MB-231 cells (ATCC) were maintained at 37 °C and 5% (v/v) CO₂ in a humidified incubator. MCF7 cells were generously gifted by Dr. Wenjian Gan (MUSC). NMuMG, HEK293T, MCF7, and MDA-MB-231 cells were cultured in DMEM (Corning) 4.5 g/L glucose supplemented with 10% fetal bovine serum (FBS) (Atlanta Biologicals). SKBr3 cells were cultured in McCoy's 5A Modified Medium (Thermo Fisher Scientific) supplemented with 10% FBS. HMLE cells were cultured in DMEM-F12 (Gibco) supplemented with 5% calf serum (VWR), 0.5 µg/ml hydrocortisone, 10 µg/ml insulin, and 20 ng/ml epidermal growth factor (Corning). MCF10A cells were cultured in DMEM F-12 supplemented with 5% horse serum, 20 ng/ml epidermal growth factor, 100 ng/mL cholera toxin (Sigma), 10 µg/mL insulin (Sigma), and 0.5 µg/mL hydrocortisone (Sigma). All cell lines were supplemented with 1% antibiotic/antimycotic (Gibco) and 0.02% prophylactic plasmocin (InvivoGen).

CRISPR-Cas9

Single-guide RNA (sgRNA), tracrRNA, and Cas9 protein (IDT) were assembled into a complex according to the manufacturer's specifications (Lonza) and electroporated into cells using Amaxa Nucleofector II (Lonza). sgRNA pairs were selected for excision of a ~125 bp DNA fragment in the coding sequence of the target gene. The electroporated cells were serially diluted in 96-well culture dishes to isolate KO candidates from discrete colonies. Candidate cell lines were screened by PCR using primers flanking or nested within the excision. Cell lines with positive PCR results were further screened by immunoblotting to confirm KO of the target gene. The sgRNA and PCR primer sequences are listed in Table S3.

Lentiviral transduction

Lentivirus was produced for transduction of either shRNA or protein overexpression vectors using the 2nd generation system. An envelope plasmid (pMD2.G), packaging plasmid (psPAX2), and either an shRNA-containing vector (pLKO.1-puro, Addgene #8453) or mammalian protein expression vector (pLenti-CMVie-IRES-BlastR, Addgene #119863) were transfected into HEK293T cells using Lipofectamine 3000 (Thermo Fisher) in Opti-MEM serum-free medium (Gibco). Virus-containing supernatant media (5 mL) were collected after 36-48 hours, strained through a .45 μm filter, diluted in DMEM by a factor of 5-10, and added to target cells with 8 $\mu\text{g}/\text{mL}$ polybrene. Following incubation for 24-48 hours, 1 $\mu\text{g}/\text{mL}$ puromycin or 10 $\mu\text{g}/\text{mL}$ blasticidin was added to the culture medium to select the target cells. The shRNA sequences for human shSCR and for FAM3C knockdown are listed in Table S3.

Immunoblotting

Whole cell lysates were produced by rinsing cells grown on culture plates twice with PBS, prior to scraping the cells into a small volume of PBS. Cells were pelleted by centrifugation at 300 \times G in microcentrifuge tubes, and an appropriate amount of RIPA lysis buffer (50 mM Tris-Cl, pH 7.6, 1% NP-40, 12 mM sodium deoxycholate, 0.1% sodium dodecyl sulfate (SDS), 165 mM sodium chloride) was added. The cells were kept on ice with occasional mixing for ~45 min and then centrifuged at 16,000 \times G at 4 $^{\circ}\text{C}$ for ten minutes. The supernatants were then transferred into fresh tubes and stored at -20 $^{\circ}\text{C}$. Protein concentrations were measured using a Pierce Micro BCA Protein Assay Kit (Thermo Fisher Scientific). Samples were denatured by adding an appropriate volume of Laemmli sample buffer (62.5 mM Tris-Cl pH 6.8, 1% SDS, 10% glycerol, 50 mM dithiothreitol (DTT), 0.001% bromophenol blue), followed by incubation at 95 $^{\circ}\text{C}$ for 5 min. Denatured samples were resolved by electrophoresis through polyacrylamide gels ranging from 7.5% to 12.5%

and electrotransferred onto polyvinylidene fluoride (PVDF) membranes at a constant current for 16-20 hours. Membranes were incubated in blocking buffer (5% skim milk in Tris-buffered saline with 0.01% Tween-20, TBST) for one hour at room temperature (RT), and then incubated for 2-24 hours at 4 °C in blocking buffer with the addition of a primary antibody to detect the protein of interest. The following primary antibodies were used: LIFR (Santa Cruz #sc-515337), FAM3C (Sigma #AV44904), pSTAT3 (Cell Signaling #9145), STAT3 (Cell Signaling #9139), GAPDH (Santa Cruz #sc-32233), b-Actin (Santa Cruz #sc-47778), TWIST1 (Cell Signaling #90445), and HSP90 (Santa Cruz #sc-13119). After primary antibody incubation, the membranes were rinsed 3 X 10-15 minutes in TBST and then incubated in blocking buffer with the addition of the appropriate secondary antibody for 0.5-1.5 hours at RT. The following horseradish peroxidase (HRP)-conjugated secondary antibodies were used: goat anti-mouse IgG (Thermo Fisher #31430; 1:10,000) and goat anti-rabbit IgG (Thermo Fisher #31460; 1:10,000). After incubation with the secondary antibody, the membranes were washed again as described above. Bands were detected by adding 1-2 mL of HRP substrate (EMD Millipore) directly onto the membrane. Images were acquired using ChemiDoc MP (Bio-Rad) and processed using Image Lab software (Bio-Rad).

Quantitative Real-time PCR

RNA was extracted from cells using TRIzol reagent (Ambion), according to the manufacturer's protocol. RNA concentrations were determined using a Nanodrop 2000 spectrophotometer (Thermo Fisher Scientific). cDNA was synthesized using QScript cDNA Supermix (Quantabio) according to the manufacturer's protocol for a final concentration of 100 ng/mL. PCR reactions were carried out in 10 µL volumes using 2X iTaq Universal SYBR Green Supermix (Bio-Rad), with a final cDNA concentration ranging from 500 pg to 6 ng/mL. Primers were used at a final concentration of 570 nM. A list of the primer sequences used for target genes and for internal control "housekeeping genes"

can be found in Table S3. Nucleic acid standards for the calculation of PCR efficiency were formulated using the purified PCR amplicons. An eight-fold dilution series of four standards ranging from concentrations of approximately 73 to 300 pg/mL was used to calculate a standard curve for each primer set used. The negative controls consisted of cDNA samples prepared without the QScript Supermix. PCR reactions were carried out in triplicate in 384-well opaque, white-skirted plates on a C1000 Touch Thermal Cycler (Bio-Rad) coupled to a CFX384 Real-Time System (Bio-Rad). Data were analyzed using CFX Maestro software (Bio-Rad), and normalized relative expression was calculated using the $\text{Eff}^{-\Delta\Delta\text{CT}}$ method, where $\text{Eff} = 2 \times (\text{PCR efficiency}\% \div 100)$, CT = thermal cycle threshold of detection, $\Delta\text{CT} = (\text{target gene CT} - \text{internal control gene CT})$, and $\Delta\Delta\text{CT} = (\text{experimental sample } \Delta\text{CT} - \text{control sample } \Delta\text{CT})$.

Dual-luciferase assay

A DNA sequence corresponding to the mouse LIFR regulatory region (Table S3) was amplified from genomic DNA extracts and ligated into the pGL3-Basic vector (Promega). Approximately 100 K cells in 12-well culture plates were co-transfected with ~1 mg pGL3 and ~500 ng pNL3.1 (Promega) and allowed to grow for 24 h. The cells were then trypsinized and resuspended in DMEM containing 10% serum, centrifuged at $300 \times G$ and washed 2X with PBS with repeated centrifugation. Cells were then resuspended in 200 μL of PBS and distributed into 96-well opaque white assay plates (triplicate wells at 60 μL). Luminescence was measured using the Nano-Glo Dual-Luciferase Reporter Assay System (Promega) according to the manufacturer's protocol using a Molecular Devices Spectramax iD5 Multi-Mode Microplate Reader. The relative normalized reporter signal was calculated by first subtracting "background signal" firefly luminescence (pGL3) acquired from pGL3-Basic "empty vector" control transfections from each experimental transfection, then dividing the remaining firefly luminescence values by the Nano-Luc

luminescence (pNL3.1) values generated by the same well to determine the normalized reporter signal per well. Finally, the mean normalized reporter signal was determined from triplicate wells and compared between experimental groups. For experiments using the STAT3 CIE reporter, the pGL3 vector was replaced with the pGL4.47 vector (Promega). For experiments using STAT3 inhibition, the cells were seeded in DMEM and allowed to grow overnight. Immediately prior to transfection, the culture medium was replaced with a medium containing STAT3-IN-1 (10 μ M final concentration) or an equal volume of DMSO.

Mammosphere assay

Culture plates containing adherent cells were trypsinized using trypsin-EDTA (Gibco), resuspended in DMEM containing 10% FBS, and centrifuged at 300 \times G. The medium was aspirated, and the cells were resuspended in serum-free DMEM to a concentration of \sim 500 $\times 10^3$ cells per mL. Cells were then counted manually using trypan blue under 10X magnification, using disposable cell counting slides (KOVA Glasstic #87144). Cells were diluted to a concentration of 100 $\times 10^3$ cells per mL and strained through a 40 μ m mesh strainer into 5 mL of mammosphere medium (final concentration 2.0 $\times 10^3$ cells per mL for mouse cells, and 6.7 $\times 10^3$ cells per mL for human cells). The mammosphere medium consisted of DMEM F12 (Gibco) supplemented with recombinant human epidermal growth factor (20 ng/mL), recombinant human basic fibroblast growth factor (20 ng/mL), B-27 supplement (Thermo Fisher #17504044), and 1% antibiotic/antimycotic (Gibco). Strained cells were distributed into six wells of a 24-well ultra-low attachment culture plate (Corning #3473) at a volume of 750 μ L per well (1.5 $\times 10^3$ cells per well for mouse cells, and 5.0 $\times 10^3$ cells per well for human cells). Cells were allowed to grow undisturbed for 8 days, then imaged and counted manually using a 150 μ m cut-off threshold. After 8 days of growth, human mammospheres were collected and pooled in 15 mL conical tubes, and PBS was used to rinse wells to collect spheroids. Trypsin-EDTA (Gibco) was added directly to

spheroid suspensions in 15 mL tubes (final concentration ~0.1%), and incubated at 37 °C for 10 minutes, with occasional inversion of the tube. Tubes were then centrifuged at 300 X G for 5 minutes to pellet cells, followed by resuspension in 500 µL of DMEM and manual counting as described above.

3D Invasion assay

Cells were trypsinized using trypsin-EDTA (Gibco), resuspended in DMEM containing 10% FBS, counted manually as described above, and then diluted to 1.0×10^6 cells/mL concentration in mammosphere medium (see above for recipe). The cells were again diluted to 1.0×10^5 cells/mL in 1 mL of mammosphere medium, and 50 µL (5000 cells) of each cell sample was added (in duplicate) to a 96-well ultra-low binding U-shaped bottom culture plate (Corning #07-202-463). Cells were then centrifuged at $300 \times G$ for 5 min and allowed to grow for 24 h at 37 °C to form spheroids. Following visual confirmation of spheroid formation, culture plates were chilled on ice for 15 minutes, and 37.5 mL of ice cold Cultrex Basement Membrane Extract (R&D Systems #3432-010-01) was added to each well and centrifuged at $300 \times G$ for 5 minutes. Cells were then incubated at 37 °C for 1-2 hours and initial time-point images were taken. DMEM lacking serum (control wells) or containing 10% FBS (chemoattracted wells) was then overlaid (150 µL) onto each well. Spheroids were imaged again at 24-hour intervals thereafter and incubated for 72 additional hours. The relative increase in area was calculated by measuring the pixel area at the 72-hour time point and then subtracting the pixel area from the initial time point. Pixel area was calculated using ImageJ software (version 2.9.0/1.53t) equipped with the lzrs1.zip installation of “Analyze_Spheroid_Cell_Invasion_In_3D_Matrix” tool (Volker Baecker, 2017).

Imaging of mammosphere and 3D-invasion assays

Mammospheres and 3D-invasion spheroids were imaged using a Leica (DMIL LED Fluo) phase-contrast light microscope at 5X magnification, equipped with a USB 2.0 digital camera (Amscope MU 500, 5.1 MP) attached to a PC (Dell Optiplex 380) running a Windows 7 operating system. The mammosphere diameter was measured using Amscope software (version X86 4.11) calibrated with an improved Neubauer hemocytometer grid.

Chromatin immunoprecipitation/DNA isolation

Cells were grown in 150 mm culture plates until 80-90% confluent and were cross-linked, followed by chromatin isolation and analysis using the SimpleChIP[®] Enzymatic Chromatin IP Kit (Cell Signaling, #9003) according to the manufacturer's specifications. 8-10 µg of chromatin was then incubated for 24 h at 4 °C with antibodies against STAT3 (Cell Signaling #9139, 0.275 mg/IP), TWIST1 (Santa Cruz #sc-81417, 3.5 mg/IP), or an equal amount of non-specific mouse IgG (Cell Signaling #5415S). Antibodies were collected using magnetic beads and DNA was purified according to the manufacturer's specifications. qPCR was then carried out as described above using primer sets specific to the genomic region of interest (Table S3). The relative fold-change of DNA abundance over IgG was calculated using the $\text{Eff}^{-\Delta\Delta\text{CT}}$ method, where $\text{Eff} = 2 \times (\text{PCR efficiency}\% \div 100)$, CT = the thermal cycle threshold of detection, $\Delta\text{CT} = (\text{target gene IP CT} - \text{target gene input CT})$, and $\Delta\Delta\text{CT} = (\text{target gene IP } \Delta\text{CT} - \text{IgG IP } \Delta\text{CT})$. 2% of each chromatin sample was set aside to be used as an input sample, and the CT values of input samples were reduced by a value 5.64 ($2^{5.64} = 50$) to adjust for the 1:50 dilution factor relative to the IP sample.

Chamber insert migration assay

Cells were trypsinized using trypsin-EDTA (Gibco), resuspended in phenol red-free DMEM containing 10% FBS, counted, and then diluted in serum-free phenol red-free DMEM at a concentration of 200×10^3 cells/mL. The cell suspension (200 μ L, 4×10^4 cells) was then added to the top chamber of a 12-well polycarbonate membrane-containing insert with an 8.0 μ m pore size (CellTreat #230633). Next, 800 μ L of either serum-free DMEM (control inserts) or DMEM containing 10% FBS was added to the bottom chamber and the cells were incubated at 37 °C for 24-hours. The media were then aspirated from the bottom chambers, 200 μ L of 0.05% trypsin-EDTA containing 2.5 μ g/mL calcein AM (Sigma) was added to the bottom chambers, and inserts were incubated for 30 min at 37 °C to allow migrated cells to detach from the underside of the insert. The plates were gently tapped to aid detachment of the cells, and the inserts were then removed. The 200 μ L volume was then mixed gently, and 180 μ L was added to an opaque white 96-well assay plate (3 \times 60 μ L/well). Fluorescence was measured using a Molecular Devices Spectramax iD5 Multi-Mode Microplate Reader with excitation and emission wavelengths of 488 and 520 nm, respectively. The relative fluorescence was quantified by generating a standard curve using serial dilution of a known quantity of calcein AM-treated cells. Background subtraction was performed by measuring a well containing a 0.05% trypsin-EDTA/calcein AM solution without cells.

RNA-Seq

Cells were seeded on 60 mm culture plates and grown until ~75% confluence, trypsinized, washed twice with PBS, pelleted, and placed on ice. Total RNA was extracted from cells using the simplyRNA Cells kit (cat # AS1390) with Maxwell RSC 16 (Promega) according to the manufacturer's specifications. RNA QC, along with that of the downstream libraries (below), was performed using a 4200 TapeStation (Agilent). One mg of total RNA was

used to construct libraries with the New England Biolabs NEBNext® rRNA Depletion Kit (Cat# E6310X) and Ultra II Directional RNA Library Prep Kit for Illumina (Cat# 7760 L), according to the manufacturer's instructions. Dual-indexed libraries were pooled and sequenced at VANTAGE (Vanderbilt University Medical Center) on an Illumina NovaSeq 6000 (S4 flow cell) to a depth of approximately 50 million paired-end 150 bp reads per library. Files containing paired-end reads (in .fastq.gz format) were uploaded to the Partek Flow web-based software platform (version 10.0.21). Reads were trimmed and aligned to the GRCm38 (mm10) mouse genome assembly using the Bowtie2 applet. Aligned reads were annotated, and differential expression analysis was performed using the DESeq2 applet. Heatmap analysis was performed using the Partek Flow data visualization toolkit. See the "Data Availability" subsection for access to raw and processed data files.

STAT3 Inhibition

Cells were treated with DMEM supplemented with either 5 or 10 μ M STAT3-IN-1 (MedChemExpress) in DMSO, or DMSO only, for 24 or 48 h, as described previously. Cell seeding was adjusted as necessary to compensate for the slightly diminished proliferative rate in the 10 μ M STAT3-IN-1 treatments. Cells were seeded to permit continuous growth over the indicated time periods, without the need for media changes.

Gene ontology analysis

The list of gene IDs (official gene symbols) derived from transcriptomic data (Table S1, S2) was fed directly into the analysis wizard of the DAVID Bioinformatics resource (179, 180). The functional annotation tool and gene ontology were selected. The data returned for biological process annotations were used to generate the graphic visualizations shown in the supplemental data section of this article.

Statistical methods

The experimental results were analyzed using GraphPad Prism (version 9.5.1). Bars in the bar graphs represent the experimental mean, and error bars represent the standard error of the mean, unless otherwise indicated. Independent unpaired Student's *t*-tests were used for individual comparisons, and one-way or two-way ANOVA was used for group comparisons, where applicable. Transcriptomic data analysis for individual genes was performed by DESeq false discovery rate (FDR) step up, which included a post-hoc test (q-value) for multiple comparisons $q < 0.07$ was considered significant. Superimposition of RNA-Seq datasets generated DEG lists based on fold-change and were agnostic to q-values. Individual candidate DEGs expression levels were validated by qPCR analysis where applicable. Post-hoc tests were not performed unless otherwise indicated. All experiments were repeated at least twice, and statistical significance was set at $P < 0.05$. P-values for gene ontology data were generated using methods within the DAVID Bioinformatics Database.

Breast Cancer Patient Survival Analysis

Kaplan-Meier analysis was carried out using the "Kaplan-Meier Plotter" application found at www.kmplot.com. The applet for "breast protein" was selected for FAM3C and pSTAT3 (Y705) analysis, and the applets for "breast cancer," either for "mRNA Gene-chip" or for "mRNA RNA-seq" were chosen for LIFR and TWIST1 analysis. Estrogen receptor (ER) and Progesterone receptor (PR) status were queried using the control for immunohistochemistry (IHC) preferentially, in the applets that offered the IHC option. A minimum cohort of 40 patients was required for each query, and $P < 0.05$ was required for statistical significance. Affymetrix probes were selected based on the largest cohort accessible when more than one probe was listed for the same gene. For protein analysis, dataset selection was based on patient cohort availability for the gene of interest and was confined to the available option.

Breast Cancer Patient Proteomic Analysis

The National Cancer Institute Proteomic Data Commons (NIH PDC) was used to access both the “TCGA Breast Cancer Proteome” (PDC000173) and the “TCGA Breast Cancer Phosphoproteome” (PDC000174). Heatmaps were generated using the Common Data Analysis Pipeline (CDAP), and graphic visualizations were created using the Morpheus matrix visualization software found at <https://software.broadinstitute.org/morpheus/>. Hierarchical clustering was carried out using the default “pair-wise distance” algorithm that prioritized clustering of samples of highest similarity first and lowest similarity last. Heat map color schemes were generated using the minimum and maximum raw expression values for each gene independently. Statistical significance of the observations made between sample groups was not determined, and fold-change in expression values between each group of samples was not determined.

Data Availability

The RNA-Seq data generated in this study are publicly available in the Gene Expression Omnibus (GEO) under GSE234882.

References

1. Biswas, S. K., Banerjee, S., Baker, G. W., Kuo, C. Y., and Chowdhury, I. (2022) The mammary gland: basic structure and molecular signaling during development. *Int. J. Mol. Sci.* 10.3390/ijms23073883
2. Howley, B. V., and Howe, P. H. (2018) TGF-beta signaling in cancer: Post-transcriptional regulation of EMT via hnRNP E1. *Cytokine*. 10.1016/j.cyto.2017.12.032
3. Chaudhury, A., Chander, P., and Howe, P. H. (2010) Heterogeneous nuclear ribonucleoproteins (hnRNPs) in cellular processes: Focus on hnRNP E1's multifunctional regulatory roles. *Rna*. **16**, 1449–1462
4. Geuens, T., Bouhy, D., and Timmerman, V. (2016) The hnRNP family: insights into their role in health and disease. *Hum. Genet.* **135**, 851–867
5. Howley, B. V., Mohanty, B., Dalton, A., Grelet, S., et al. (2022) The ubiquitin E3 ligase ARIH1 regulates hnRNP E1 protein stability, EMT and breast cancer progression. *Oncogene*. **41**, 1679–1690
6. Grelet, S., and Howe, P. (2017) A regulated PNUTS mRNA to lncRNA splice switch mediates EMT and tumour progression. *Nat. Cell Biol.* **19**, 1105–1115
7. Chaudhury, A., Hussey, G. S., Ray, P. S., Jin, G., et al. (2010) TGF-B-mediated phosphorylation of hnRNP E1 induces EMT via transcript-selective translational induction of Dab2 and ILEI. *Nat. Cell Biol.* **12**, 286–293
8. Beyer, A. L., Christensen, M. E., Walker, B. W., and LeSturgeon, W. M. (1977) Identification and characterization of the packaging proteins of core 40S hnRNP particles. *Cell*. **11**, 127–138
9. Mohanty, B. K., Karam, J. A., Howley, B. V., Dalton, A. C., et al. (2021) Heterogeneous nuclear ribonucleoprotein E1 binds polycytosine DNA and monitors genome integrity. 10.26508/lsa.202000995
10. Leffers, H., Dejgaard, K., and Celis, J. E. (1995) Characterisation of two major cellular poly(rC)-binding human proteins, each containing three K-homologous (KH) domains. *Eur. J. Biochem.* **230**, 447–453
11. Gamarnik, A. V., and Andino, R. (1997) Two functional complexes formed by KH domain containing proteins with the 5' noncoding region of poliovirus RNA. *Rna*. **3**, 882–892
12. Chkheidze, A. N., and Liebhaber, S. A. (2003) A novel set of nuclear localization signals determine distributions of the α CP RNA-binding proteins. *Mol. Cell. Biol.* **23**, 8405–8415
13. Ghanem, L. R., Kromer, A., Silverman, I. M., Chatterji, P., et al. (2016) The Poly(C) binding protein Pcbp2 and its retrotransposed derivative Pcbp1 are independently essential to mouse development. *Mol. Cell. Biol.* **36**, 304–319
14. Han, S. P., Tang, Y. H., and Smith, R. (2010) Functional diversity of the hnRNPs: Past, present and perspectives. *Biochem. J.* **430**, 379–392
15. Grelet, S., Link, L. A., Howley, B., Obellianne, C., et al. (2017) A regulated PNUTS mRNA to lncRNA splice switch mediates EMT and tumour progression. *Nat. Cell Biol.* 10.1038/ncb3595
16. Brown, R. L., Reinke, L. M., Damerow, M. S., Perez, D., et al. (2011) CD44 splice isoform switching in human and mouse epithelium is essential for epithelial-mesenchymal transition and breast cancer progression. *J. Clin. Invest.* **121**, 1064–1074
17. Ji, X., Wan, J., Vishnu, M., Xing, Y., and Liebhaber, S. A. (2013) α CP Poly(C) binding proteins act as global regulators of alternative polyadenylation. *Mol. Cell. Biol.* **33**, 2560–2573

18. Thiele, B. J., Doller, A., Kähne, T., Pregla, R., et al. (2004) RNA-binding proteins heterogeneous nuclear ribonucleoprotein A1, E1, and K are involved in post-transcriptional control of collagen I and III synthesis. *Circ. Res.* **95**, 1058–1066
19. Shi, H., Li, H., Yuan, R., Guan, W., et al. (2018) PCBP1 depletion promotes tumorigenesis through attenuation of p27Kip1 mRNA stability and translation. *J. Exp. Clin. Cancer Res.* 10.1186/s13046-018-0840-1
20. Brown, A. S., Mohanty, B. K., and Howe, P. H. (2016) Identification and characterization of an hnRNP E1 translational silencing motif. *Nucleic Acids Res.* **44**, 5892–5907
21. Hussey, G. S., Link, L. A., Brown, A. S., Howley, B. V., et al. (2012) Establishment of a TGF β -induced post-transcriptional EMT gene signature. *PLoS One.* **7**, 1–12
22. Hussey, G. S., Chaudhury, A., Dawson, A. E., Lindner, D. J., et al. (2011) Identification of an mRNP complex regulating tumorigenesis at the translational elongation step. *Mol. Cell.* **41**, 419–431
23. Howley, B. V., Hussey, G. S., Link, L. A., and Howe, P. H. (2016) Translational regulation of inhibin β a by TGF β via the RNA-binding protein hnRNP E1 enhances the invasiveness of epithelial-to-mesenchymal transitioned cells. *Oncogene.* **35**, 1725–1735
24. Liu, Y., Gai, L., Liu, J., Cui, Y., et al. (2015) Expression of poly(C)-binding protein 1 (PCBP1) in NSCLC as a negative regulator of EMT and its clinical value. *Int. J. Clin. Exp. Pathol.* **8**, 7165–7172
25. Dalton, A. C., and Howe, P. H. (2022) *Epithelial to Mesenchymal Transition*, Elsevier, 10.1016/b978-0-12-820472-6.00005-0
26. Moses, H., and Barcellos-Hoff, M. H. (2011) TGF- β Biology in mammary development and breast cancer. *Cold Spring Harb. Perspect. Biol.* **3**, 1–14
27. Kalluri, R., and Weinberg, R. A. (2009) The basics of epithelial-mesenchymal transition. *J. Clin. Invest.* **119**, 1420–1428
28. Woosley, A. N., Dalton, A. C., Hussey, G. S., Howley, B. V., et al. (2019) TGF β promotes breast cancer stem cell self-renewal through an ILEI/LIFR signaling axis. *Oncogene.* **38**, 3794–3811
29. Morrison, C. D., Parvani, J. G., and Schiemann, W. P. (2013) The relevance of the TGF- β Paradox to EMT-MET programs. *Cancer Lett.* **341**, 30–40
30. Chen, Q., Cai, Z. K., Chen, Y. B., Gu, M., et al. (2015) Poly r(C) binding protein-1 is central to maintenance of cancer stem cells in prostate cancer cells. *Cell. Physiol. Biochem.* **35**, 1052–1061
31. Kreso, A., and Dick, J. E. (2014) Evolution of the cancer stem cell model. *Cell Stem Cell.* **14**, 275–291
32. Grossman, R. L., Heath, A. P., Ferretti, V., Varmus, H. E., et al. (2016) Toward a shared vision for cancer genomic data. *N. Engl. J. Med.* **375**, 1109–1112
33. Zhu, Y., Sun, Y., Mao, X. O., Jin, K. L., and Greenberg, D. A. (2002) Expression of poly(C)-binding proteins is differentially regulated by hypoxia and ischemia in cortical neurons. *Neuroscience.* **110**, 191–198
34. Paulding, W. R., and Czyzyk-Krzeska, M. F. (1999) Regulation of tyrosine hydroxylase mRNA stability by protein-binding, pyrimidine-rich sequence in the 3'-untranslated region. *J. Biol. Chem.* **274**, 2532–2538
35. Noguchi, K., Dalton, A. C., Howley, B. V., McCall, B. J., et al. (2017) Interleukin-like EMT inducer regulates partial phenotype switching in MITF-low melanoma cell lines. *PLoS One.* **12**, 1–24

36. Noguchi, K., Dincman, T. A., Dalton, A. C., Howley, B. V., et al. (2018) Interleukin-like EMT inducer (ILEI) promotes melanoma invasiveness and is transcriptionally up-regulated by upstream stimulatory factor-1 (USF-1). *J. Biol. Chem.* **293**, 11401–11414
37. Waerner, T., Alacakaptan, M., Tamir, I., Oberauer, R., et al. (2006) ILEI: A cytokine essential for EMT, tumor formation, and late events in metastasis in epithelial cells. *Cancer Cell.* **10**, 227–239
38. Zhu, Y., Xu, G., Patel, A., McLaughlin, M. M., et al. (2002) Cloning, expression, and initial characterization of a novel cytokine-like gene family. *Genomics.* **80**, 144–150
39. Jansson, A. M., Csiszar, A., Maier, J., Nyström, A. C., et al. (2017) The interleukin-like epithelial-mesenchymal transition inducer ILEI exhibits a non-interleukin-like fold and is active as a domain-swapped dimer. *J. Biol. Chem.* **292**, 15501–15511
40. Yang, J., and Guan, Y. (2013) Family with sequence similarity 3 gene family and nonalcoholic fatty liver disease. *J. Gastroenterol. Hepatol.* **28**, 105–111
41. Johansson, P., Bernström, J., Gorman, T., Öster, L., et al. (2013) FAM3B PANDER and FAM3C ILEI represent a distinct class of signaling molecules with a non-cytokine-like fold. *Structure.* **21**, 306–313
42. Zhu, Y., Pu, Z., Wang, G., Li, Y., et al. (2021) FAM3C: an emerging biomarker and potential therapeutic target for cancer. *Biomark. Med.* **15**, 373–384
43. Song, C., and Duan, C. (2020) Upregulation of FAM3B promotes cisplatin resistance in gastric cancer by inducing epithelial-mesenchymal transition. *Med. Sci. Monit.* **26**, e921002
44. Malik, B., Vokic, I., Mohr, T., Poppelaars, M., et al. (2023) FAM3C / ILEI protein is elevated in psoriatic lesions and triggers psoriasiform hyperproliferation in mice. *EMBO Mol. Med.* 10.15252/emmm.202216758
45. Chen, Z., Wang, J., Yang, W., Chen, J., et al. (2017) FAM3C activates HSF1 to suppress hepatic gluconeogenesis and attenuate hyperglycemia of type 1 diabetic mice. *Oncotarget.* **8**, 106038–106049
46. Hasegawa, H., Liu, L., Tooyama, I., Murayama, S., and Nishimura, M. (2014) The FAM3 superfamily member ILEI ameliorates Alzheimer's disease-like pathology by destabilizing the penultimate amyloid- β precursor. *Nat. Commun.* 10.1038/ncomms4917
47. Zhou, J., Jiang, H., Jiang, H., Fan, Y., et al. (2022) The ILEI/LIFR complex induces EMT via the Akt and ERK pathways in renal interstitial fibrosis. *J. Transl. Med.* **20**, 54
48. Bendre, A., Büki, K. G., and Määttä, J. A. (2017) Fam3c modulates osteogenic differentiation by down-regulating Runx2. *Differentiation.* **93**, 50–57
49. Lahsnig, C., Mikula, M., Petz, M., Zulehner, G., et al. (2009) ILEI requires oncogenic Ras for the epithelial to mesenchymal transition of hepatocytes and liver carcinoma progression. *Oncogene.* **28**, 638–650
50. Song, Q., Sheng, W., Zhang, X., Jiao, S., and Li, F. (2014) ILEI drives epithelial to mesenchymal transition and metastatic progression in the lung cancer cell line A549. *Tumor Biol.* **35**, 1377–1382
51. Wu, C. C., Xiao, Y., Li, H., Mao, L., et al. (2019) Overexpression of FAM3C is associated with poor prognosis in oral squamous cell carcinoma. *Pathol. Res. Pract.* **215**, 772–778
52. Gao, Z. H., Lu, C., Wang, Z. N., Song, Y. X., et al. (2014) ILEI: A novel marker for epithelial-mesenchymal transition and poor prognosis in colorectal cancer. *Histopathology.* **65**, 527–538

53. Jin, L. L., Zhang, S. J., Lu, G. X., Lv, F., et al. (2019) miR-574-3p inhibits proliferation and invasion in esophageal cancer by targeting FAM3C and MAPK1. *Kaohsiung J. Med. Sci.* 10.1002/kjm2.12176
54. Shi, M., Duan, G., Nie, S., Shen, S., and Zou, X. (2018) Elevated FAM3C promotes cell epithelial– mesenchymal transition and cell migration in gastric cancer. *Onco. Targets. Ther.* **11**, 8491–8505
55. Yang, W., Feng, B., Meng, Y., Wang, J., et al. (2019) FAM3C-YY1 axis is essential for TGF β -promoted proliferation and migration of human breast cancer MDA-MB-231 cells via the activation of HSF1. *J. Cell. Mol. Med.* **23**, 3464–3475
56. Csiszar, A., Kutay, B., Wirth, S., Schmidt, U., et al. (2014) Interleukin-like epithelial-to-mesenchymal transition inducer activity is controlled by proteolytic processing and plasminogen-urokinase plasminogen activator receptor system-regulated secretion during breast cancer progression. *Breast Cancer Res.* **16**, 1–18
57. Kral, M., Klimek, C., Kutay, B., Timelthaler, G., et al. (2017) Covalent dimerization of interleukin-like epithelial-to-mesenchymal transition (EMT) inducer (ILEI) facilitates EMT, invasion, and late aspects of metastasis. *FEBS J.* **284**, 3484–3505
58. Oft, M., Peli, J., Rudaz, C., Schwarz, H., et al. (1996) TGF- β 1 and Ha-Ras collaborate in modulating the phenotypic plasticity and invasiveness of epithelial tumor cells. *Genes Dev.* **10**, 2462–2477
59. Oft, M., Heider, K. H., and Beug, H. (1998) TGF β signaling is necessary for carcinoma cell invasiveness and metastasis. *Curr. Biol.* **8**, 1243–1252
60. Garrett, P. A., Hulka, B. S., Kim, Y. L., and Farber, R. A. (1993) HRAS protooncogene polymorphism and breast cancer. *Cancer Epidemiol. Biomarkers Prev.* **2**, 131–138
61. Janda, E., Lehmann, K., Killisch, I., Jechlinger, M., et al. (2002) Ras and TGF β cooperatively regulate epithelial cell plasticity and metastasis: Dissection of Ras signaling pathways. *J. Cell Biol.* **156**, 299–313
62. Kraus, M. H., Yuasa, Y., and Aaronson, S. A. (1984) A position 12-activated H-ras oncogene in all HS578T mammary carcinosarcoma cells but not normal mammary cells of the same patient. *Proc. Natl. Acad. Sci. U. S. A.* **81**, 5384–5388
63. Howley, B. V., Link, L. A., Grelet, S., El-Sabban, M., and Howe, P. H. (2017) A CREB3-regulated ER–Golgi trafficking signature promotes metastatic progression in breast cancer. *Oncogene.* **37**, 1308–1325
64. Williams, R. L., Hilton, D. J., Pease, S., Willson, T. A., et al. (1988) Myeloid leukaemia inhibitory factor maintains the developmental potential of embryonic stem cells. *Nature.* **336**, 684–687
65. Rose-John, S. (2018) Interleukin-6 family cytokines. *Cold Spring Harb. Perspect. Biol.* **10**, 1–28
66. Wang, X. jun, Qiao, Y., Xiao, M. M., Wang, L., et al. (2017) Opposing roles of acetylation and phosphorylation in LIFR-dependent self-renewal growth signaling in mouse embryonic stem cells. *Cell Rep.* **18**, 933–946
67. Hirai, H., Karian, P., and Kikyo, N. (2011) Regulation of embryonic stem cell self-renewal and pluripotency by leukaemia inhibitory factor. *Biochem. J.* **438**, 11–23
68. Nicola, N. A., and Babon, J. J. (2015) Leukemia inhibitory factor (LIF). *Cytokine Growth Factor Rev.* **26**, 533–544
69. Manore, S. G., Doheny, D. L., Wong, G. L., and Lo, H. W. (2022) IL-6/JAK/STAT3 signaling in breast cancer metastasis: biology and treatment. *Front. Oncol.* **12**, 862

70. Chen, D., Sun, Y., Wei, Y., Zhang, P., et al. (2012) LIFR is a breast cancer metastasis suppressor upstream of the Hippo-YAP pathway and a prognostic marker. *Nat. Med.* **18**, 1511–1517
71. Halder, S., Parte, S., Kshirsagar, P., Muniyan, S., et al. (2022) The Pleiotropic role, functions and targeted therapies of LIF/LIFR axis in cancer: Old spectacles with new insights. *Biochim. Biophys. Acta - Rev. Cancer.* **1877**, 188737
72. Matsuda, T., Nakamura, T., Nakao, K., Arai, T., et al. (1999) STAT3 activation is sufficient to maintain an undifferentiated state of mouse embryonic stem cells. *EMBO J.* **18**, 4261–4269
73. Daheron, L., Opits, S., Zaehres, H., Lensch, W., et al. (2004) LIF/STAT3 signaling fails to maintain self-renewal of human embryonic stem cells. *Stem Cells.* **22**, 770–778
74. Onishi, K., and Zandstra, P. W. (2015) LIF signaling in stem cells and development. *Dev.* **142**, 2230–2236
75. Watanabe, N., Nakano, M., Mitsuishi, Y., Hara, N., et al. (2022) Transcriptional downregulation of FAM3C/ILEI in the Alzheimer's brain. *Hum. Mol. Genet.* **31**, 122–132
76. Burdon, T., Stracey, C., Chambers, I., Nichols, J., and Smith, A. (1999) Suppression of SHP-2 and ERK signalling promotes self-renewal of mouse embryonic stem cells. *Dev. Biol.* **210**, 30–43
77. Mikelonis, D., Jorcyk, C. L., Tawara, K., and Oxford, J. T. (2014) Stüve-Wiedemann syndrome: LIFR and associated cytokines in clinical course and etiology. *Orphanet J. Rare Dis.* **9**, 1–11
78. Hunt, L., and White, J. (2016) The role of leukemia inhibitory factor receptor signaling in skeletal muscle growth, injury and disease. *Adv. Exp. Med. Biol.* **900**, 45–59
79. Turnley, A. M., and Bartlett, P. F. (2000) Cytokines that signal through the leukemia inhibitory factor receptor- β complex in the nervous system. *J. Neurochem.* **74**, 889–899
80. Kosfeld, A., Brand, F., Weiss, A.-C., Kreuzer, M., et al. (2017) Mutations in the leukemia inhibitory factor receptor (LIFR) gene and Lifr deficiency cause urinary tract malformations. *Hum. Mol. Genet.* **26**, 1716–1731
81. Christians, A., Weiss, A. C., Martens, H., Klopff, M. G., et al. (2020) Inflammation-like changes in the urothelium of Lifr-deficient mice and LIFR-haploinsufficient humans with urinary tract anomalies. *Hum. Mol. Genet.* **29**, 1192–1204
82. López-Yoldi, M., Moreno-Aliaga, M. J., and Bustos, M. (2015) Cardiotrophin-1: A multifaceted cytokine. *Cytokine Growth Factor Rev.* **26**, 523–532
83. Fischer, K. R., Durrans, A., Lee, S., Sheng, J., et al. (2015) Epithelial-to-mesenchymal transition is not required for lung metastasis but contributes to chemoresistance. *Nature.* **527**, 472–476
84. Mani, S. A., Guo, W., Liao, M. J., Eaton, E. N., et al. (2008) The epithelial-mesenchymal transition generates cells with properties of stem cells. *Cell.* **133**, 704–715
85. Yin, S., Chen, F., Ye, P., and Yang, G. (2018) Overexpression of FAM3C protein as a novel biomarker for epithelial-mesenchymal transition and poor outcome in gastric cancer. *Int. J. Clin. Exp. Pathol.* **11**, 4247
86. Inghirami, G., Chiarle, R., Simmons, W. J., Piva, R., et al. (2005) New and old functions of STAT3: A pivotal target for individualized treatment of cancer. *Cell Cycle.* **4**, 1131–1133

87. Thuya, W. L., Kong, L. R., Syn, N. L., Ding, L. W., et al. (2023) FAM3C in circulating tumor-derived extracellular vesicles promotes non-small cell lung cancer growth in secondary sites. *Theranostics*. **13**, 621–638
88. Real, S. A. S., Parveen, F., Rehman, A. U., Shaik, R., et al. (2019) Mutation, methylation and expression analysis of LIFR gene in Indian breast cancer patients. *Mutat. Res. - Fundam. Mol. Mech. Mutagen.* 10.1016/j.mrfmmm.2019.111677
89. Okamura, Y., Nomoto, S., Kanda, M., Li, Q., et al. (2010) Leukemia inhibitory factor receptor (LIFR) is detected as a novel suppressor gene of hepatocellular carcinoma using double-combination array. *Cancer Lett.* **289**, 170–177
90. Chaffer, C. L., and Weinberg, R. A. (2011) A perspective on cancer cell metastasis. *Science (80-)*. **331**, 1559–1564
91. American Cancer Society (2019) Survival Rates for Breast Cancer. *Am. Cancer Soc.* **10**, 1–5
92. Bromberg, J., and Darnell, J. E. (2000) The role of STATs in transcriptional control and their impact on cellular function. *Oncogene*. **19**, 2468–2473
93. Gadiant, R. A., and Patterson, P. H. (1999) Leukemia inhibitory factor, interleukin 6, and other cytokines using the GP130 transducing receptor: Roles in inflammation and injury. *Stem Cells*. **17**, 127–137
94. Wegenka, U. M., Lütticken, C., Buschmann, J., Yuan, J., et al. (1994) The interleukin-6-activated acute-phase response factor is antigenically and functionally related to members of the signal transducer and activator of transcription (STAT) family. *Mol. Cell. Biol.* **14**, 3186–3196
95. Darnell, J. E., Kerr, I. M., and Stark, G. R. (1994) Jak-STAT pathways and transcriptional activation in response to IFNs and other extracellular signaling proteins. *Science (80-)*. **264**, 1415–1421
96. Bowman, T., Garcia, R., Turkson, J., and Jove, R. (2000) STATs in oncogenesis. *Oncogene*. **19**, 2474–2488
97. Jing, N., and Tweardy, D. J. (2005) Targeting Stat3 in cancer therapy. *Anticancer. Drugs*. **16**, 601–607
98. Darnell, J. E. (2002) Transcription factors as targets for cancer therapy. *Nat. Rev. Cancer*. **2**, 740–749
99. Turkson, J., and Jove, R. (2000) STAT proteins: Novel molecular targets for cancer drug discovery. *Oncogene*. **19**, 6613–6626
100. Garcia, R., and Jove, R. (1998) Activation of STAT transcription factors in oncogenic tyrosine kinase signaling. *J. Biomed. Sci.* **5**, 79–85
101. Yu, C. L., Meyer, D. J., Campbell, G. S., Larner, A. C., et al. (1995) Enhanced DNA-binding activity of a stat3-related protein in cells transformed by the Src oncoprotein. *Science (80-)*. **269**, 81–83
102. Cao, X., Tay, A., Guy, G. R., and Tan, Y. H. (1996) Activation and association of Stat3 with Src in v-Src-transformed cell lines. *Mol. Cell. Biol.* **16**, 1595–1603
103. Bromberg, J. F., Wrzeszczynska, M. H., Devgan, G., Zhao, Y., et al. (1999) Stat3 as an oncogene. *Cell*. **98**, 295–303
104. Sartor, C. I., Dziubinski, M. L., Yu, C. L., Jove, R., and Ethier, S. P. (1997) Role of epidermal growth factor receptor and STAT-3 activation in autonomous proliferation of SUM-102PT human breast cancer cells. *Cancer Res.* **57**, 978–987
105. Garcia, R., Yu, C. L., Hudnall, A., Catlett, R., et al. (1997) Constitutive activation of Stat3 in fibroblasts transformed by diverse oncoproteins and in breast carcinoma cells. *Cell Growth Differ.* **8**, 1267–1276

106. Garcia, R., Bowman, T. L., Niu, G., Yu, H., et al. (2001) Constitutive activation of Stat3 by the Src and JAK tyrosine kinases participates in growth regulation of human breast carcinoma cells. *Oncogene*. **20**, 2499–2513
107. Buettner, R., Mora, L. B., and Jove, R. (2002) Activated STAT signaling in human tumors provides novel molecular targets for therapeutic intervention. *Clin. Cancer Res.* **8**, 945–954
108. Niu, G., Heller, R., Catlett-Falcone, R., Coppola, D., et al. (1999) Gene therapy with dominant-negative Stat3 suppresses growth of the murine melanoma B16 tumor in vivo. *Cancer Res.* **59**, 5059–5063
109. Becker, S., Groner, B., and Müller, C. W. (1998) Three-dimensional structure of the Stat3 β homodimer bound to DNA. *Nature*. **394**, 145–151
110. Catlett-Falcone, R., Landowski, T. H., Oshiro, M. M., Turkson, J., et al. (1999) Constitutive activation of Stat3 signaling confers resistance to apoptosis in human U266 myeloma cells. *Immunity*. **10**, 105–115
111. Endo, T. A., Masuhara, M., Yokouchi, M., Suzuki, R., et al. (1997) A new protein containing an SH2 domain that inhibits JAK kinases. *Nature*. **387**, 921–924
112. David, M., Grimley, P. M., Finbloom, D. S., and Lerner, A. C. (1993) A Nuclear Tyrosine Phosphatase Downregulates Interferon-Induced Gene Expression. *Mol. Cell. Biol.* **13**, 7515–7521
113. Sekimoto, T., Nakajima, K., Tachibana, T., Hirano, T., and Yoneda, Y. (1996) Interferon- γ -dependent nuclear import of Stat1 is mediated by the GTPase activity of Ran/TC4. *J. Biol. Chem.* **271**, 31017–31020
114. Xu, X., Sun, Y. L., and Hoey, T. (1996) Cooperative DNA binding and sequence-selective recognition conferred by the STAT amino-terminal domain. *Science (80-)*. **273**, 794–797
115. Hashimoto, S., Hashimoto, A., Muromoto, R., Kitai, Y., et al. (2022) Central roles of STAT3-mediated signals in onset and development of cancers: tumorigenesis and immunosurveillance. *Cells*. 10.3390/cells11162618
116. Beebe, J. D., Liu, J., and Zhang, J. (2018) Pharmacology & Therapeutics Two decades of research in discovery of anticancer drugs targeting STAT3 , how close are we ? *Pharmacol. Ther.* **191**, 74–91
117. Dong, J., Cheng, X.-D., Zhang, W.-D., and Qin, J.-J. (2021) Recent update on development of small-molecule STAT3 inhibitors for cancer therapy: from phosphorylation inhibition to protein degradation. *J. Med. Chem.* **64**, 8915
118. Walker, S. R., Xiang, M., and Frank, D. A. (2014) Distinct roles of STAT3 and STAT5 in the pathogenesis and targeted therapy of breast cancer. *Mol. Cell. Endocrinol.* **382**, 616–621
119. Hubbard, J. M., and Grothey, A. (2017) Napabucasin: an update on the first-in-class cancer stemness inhibitor. *Drugs*. **77**, 1091–1103
120. Germain, D., and Frank, D. A. (2007) Targeting the cytoplasmic and nuclear functions of signal transducers and activators of transcription 3 for cancer therapy. *Clin. Cancer Res.* **13**, 5665–5669
121. Yang, C. H., Gonzalez-Angulo, A. M., Reuben, J. M., Booser, D. J., et al. (2006) Bortezomib (VELCADE®) in metastatic breast cancer: Pharmacodynamics, biological effects, and prediction of clinical benefits. *Ann. Oncol.* **17**, 813–817
122. Sadrkhanloo, M., Entezari, M., Orouei, S., Ghollasi, M., et al. (2022) STAT3-EMT axis in tumors: Modulation of cancer metastasis, stemness and therapy response. *Pharmacol. Res.* **182**, 106311
123. Sheen-Chen, S. M., Huang, C. C., Tang, R. P., Chou, F. F., and Eng, H. L. (2008) Prognostic value of signal transducers and activators of transcription 3 in breast cancer. *Cancer Epidemiol. Biomarkers Prev.* **17**, 2286–2290

124. Chen, Y., Wang, J., Wang, X., Liu, X., et al. (2013) STAT3, a poor survival predictor, is associated with lymph node metastasis from breast cancer. *J. Breast Cancer*. **16**, 40–49
125. Nakagawa, T., Oda, G., Kawachi, H., Ishikawa, T., et al. (2022) Nuclear Expression of p-STAT3 Is Associated with Poor Prognosis in ER(-) Breast Cancer. *Clin. Pract.* **12**, 157–167
126. Dolled-Filhart, M., Camp, R. L., Kowalski, D. P., Smith, B. L., and Rimm, D. L. (2003) Tissue microarray analysis of signal transducers and activators of transcription 3 (Stat3) and phospho-Stat3 (Tyr705) in node-negative breast cancer shows nuclear localization is associated with a better prognosis. *Clin. Cancer Res.* **9**, 594–600
127. Sato, T., Neilson, L. M., Peck, A. R., Liu, C., et al. (2011) Signal transducer and activator of transcription-3 activation and breast cancer prognosis. *Am J Cancer Res.* **1**, 347–355
128. Li, S., Zhang, W., Yang, Y., Ma, T., et al. (2016) Discovery of oral-available resveratrol-caffeic acid based hybrids inhibiting acetylated and phosphorylated STAT3 protein. *Eur. J. Med. Chem.* **124**, 1006–1018
129. Vesuna, F., Lisok, A., Kimble, B., and Raman, V. (2009) Twist modulates breast cancer stem cells by transcriptional regulation of CD24 expression. *Neoplasia*. **11**, 1318–1328
130. Cakouros, D., Raices, R. M., Gronthos, S., and Glackin, C. A. (2010) Twist-ing cell fate: Mechanistic insights into the role of twist in lineage specification/differentiation and tumorigenesis. *J. Cell. Biochem.* **110**, 1288–1298
131. Zhao, D., Besser, A. H., Wander, S. A., Sun, J., et al. (2015) Cytoplasmic p27 promotes epithelial-mesenchymal transition and tumor metastasis via STAT3-mediated Twist1 upregulation. *Oncogene*. **34**, 5447–5459
132. Grzegorzolka, J., Biala, M., Wojtyra, P., Kobierzycki, C., et al. (2015) Expression of EMT markers SLUG and TWIST in breast cancer. *Anticancer Res.* **35**, 3961–3968
133. Kim, M. S., Lee, H. S., Kim, Y. J., Lee, D. Y., et al. (2019) MEST induces Twist-1-mediated EMT through STAT3 activation in breast cancers. *Cell Death Differ.* **26**, 2594–2606
134. Cheng, G. Z., Zhang, W. Z., Sun, M., Wang, Q., et al. (2008) Twist is transcriptionally induced by activation of STAT3 and mediates STAT3 oncogenic function. *J. Biol. Chem.* **283**, 14665–14673
135. Prunier, C., and Howe, P. H. (2005) Disabled-2 (Dab2) is required for transforming growth factor β -induced epithelial to mesenchymal transition (EMT). *J. Biol. Chem.* **280**, 17540–17548
136. Wang, H., Vardy, L. A., Tan, C. P., Loo, J. M., et al. (2010) PCBP1 suppresses the translation of metastasis-associated PRL-3 phosphatase. *Cancer Cell*. **18**, 52–62
137. Zhang, Z. Z., Shen, Z. Y., Shen, Y. Y., Zhao, E. H., et al. (2015) HOTAIR long noncoding RNA promotes gastric cancer metastasis through suppression of Poly r(C)-binding protein (PCBP) 1. *Mol. Cancer Ther.* **14**, 1162–1170
138. Du, P., Zeng, H., Xiao, Y., Zhao, Y., et al. (2020) Chronic stress promotes EMT-mediated metastasis through activation of STAT3 signaling pathway by miR-337-3p in breast cancer. *Cell Death Dis.* **11**, 1–13
139. Wang, N., Wei, L., Huang, Y., Wu, Y., et al. (2017) MiR520c blocks EMT progression of human breast cancer cells by repressing STAT3. *Oncol. Rep.* **37**, 1537–1544
140. Liu, F., Zhang, H., and Song, H. (2017) Upregulation of MEK5 by Stat3 promotes breast cancer cell invasion and metastasis. *Oncol. Rep.* **37**, 83–90

141. Cho, K. H., Jeong, K. J., Shin, S. C., Kang, J., et al. (2013) STAT3 mediates TGF- β 1-induced TWIST1 expression and prostate cancer invasion. *Cancer Lett.* **336**, 167–173
142. Xie, T. X., Wei, D., Liu, M., Gao, A. C., et al. (2004) Stat3 activation regulates the expression of matrix metalloproteinase-2 and tumor invasion and metastasis. *Oncogene.* **23**, 3550–3560
143. Kamohara, H., Ogawa, M., Ishiko, T., Sakamoto, K., and Baba, H. (2007) Leukemia inhibitory factor functions as a growth factor in pancreas carcinoma cells: Involvement of regulation of LIF and its receptor expression. *Int. J. Oncol.* **30**, 977–983
144. Conway, M. E., McDaniel, J. M., Graham, J. M., Guillen, K. P., et al. (2021) STAT3 and GR cooperate to drive gene expression and growth of basal-like triple-negative breast cancer. *Cancer Res.* **80**, 4355–4370
145. Edgar, R., Domrachev, M., and Lash, A. E. (2002) Gene Expression Omnibus: NCBI gene expression and hybridization array data repository. *Nucleic Acids Res.* **30**, 207–210; PRJNA389388; GEO: GSE99708
146. Barrett, T., Wilhite, S. E., Ledoux, P., Evangelista, C., et al. (2013) NCBI GEO: archive for functional genomics data sets--update. *Nucleic Acids Res.* **41**, PRJNA527977; GEO: GSE128516
147. Li, X., Yang, Q., Yu, H., Wu, L., et al. (2014) LIF promotes tumorigenesis and metastasis of breast cancer through the AKT-mTOR pathway. *Oncotarget.* **5**, 788–801
148. Shi, Y., Gao, W., Lytle, N. K., Huang, P., et al. (2019) Targeting LIF-mediated paracrine interaction for pancreatic cancer therapy and monitoring. *Nature.* **569**, 131–135
149. Lu, B., He, Y., He, J., Wang, L., et al. (2020) Epigenetic profiling identifies LIF as a super-enhancer-controlled regulator of stem cell-like properties in osteosarcoma. *Mol. Cancer Res.* **18**, 57–67
150. Shao, J., Zhu, W., Ding, Y., Zhu, H., et al. (2019) Phosphorylation of LIFR promotes prostate cancer progression by activating the AKT pathway. *Cancer Lett.* **451**, 110–121
151. Lin, W. H., Chang, Y. W., Hong, M. X., Hsu, T. C., et al. (2021) STAT3 phosphorylation at Ser727 and Tyr705 differentially regulates the EMT–MET switch and cancer metastasis. *Oncogene.* **40**, 791–805
152. Gulluoglu, S., Sahin, M., Tuysuz, E. C., Yaltirik, C. K., et al. (2017) Leukemia inhibitory factor promotes aggressiveness of Chordoma. *Oncol. Res.* **25**, 1177–1188
153. Fitzgerald, J. S., Tsareva, S. A., Poehlmann, T. G., Berod, L., et al. (2005) Leukemia inhibitory factor triggers activation of signal transducer and activator of transcription 3, proliferation, invasiveness, and altered protease expression in choriocarcinoma cells. *Int. J. Biochem. Cell Biol.* **37**, 2284–2296
154. Firulli, A., and Conway, S. (2008) Phosphoregulation of Twist1 provides a mechanism of cell fate control. *Curr. Med. Chem.* **15**, 2641–2647
155. Mertins, P., Mani, D. R., Ruggles, K. V., Gillette, M. A., et al. (2016) Proteogenomics connects somatic mutations to signaling in breast cancer. *Nature.* **534**, 55–62
156. Hong, J., Zhou, J., Fu, J., He, T., et al. (2011) Phosphorylation of Serine 68 of Twist1 by MAPKs Stabilizes Twist1 Protein and Promotes Breast Cancer Cell Invasiveness. *Cancer Res.* **71**, 3980–3990

157. Xu, Y., Hu, B., Qin, L., Zhao, L., et al. (2014) SRC-1 and twist1 expression positively correlates with a poor prognosis in human breast cancer. *Int. J. Biol. Sci.* **10**, 396–403
158. Riaz, M., Sieuwerts, A. M., Look, M. P., Timmermans, M. A., et al. (2012) High TWIST1 mRNA expression is associated with poor prognosis in lymph node-negative and estrogen receptor-positive human breast cancer and is co-expressed with stromal as well as ECM related genes. *Breast Cancer Res.* **14**, 1–15
159. Zeng, H., Qu, J., Jin, N., Xu, J., et al. (2016) Feedback activation of Leukemia Inhibitory Factor Receptor limits response to histone deacetylase inhibitors in breast cancer. *Cancer Cell.* **30**, 459–473
160. Johnson, R., Finger, E., Olcina, M., and Giaccia, A. (2017) Induction of LIFR confers a dormancy phenotype in breast cancer cells disseminated to the bone marrow. *Nat Cell Biol.* **18**, 1078–1089
161. Clements, M. E., Holtslander, L., Edwards, C., Todd, V., et al. (2021) HDAC inhibitors induce LIFR expression and promote a dormancy phenotype in breast cancer. *Oncogene.* **40**, 5314–5326
162. Luo, Q., Wang, C., Jin, G., Gu, D., et al. (2015) LIFR functions as a metastasis suppressor in hepatocellular carcinoma by negatively regulating phosphoinositide 3-kinase/AKT pathway. *Carcinogenesis.* **36**, 1201–1212
163. Rose-John, S. (2018) Interleukin-6 family cytokines. *Cold Spring Harb. Perspect. Biol.* 10.1101/cshperspect.a028415
164. Bian, S. B., Yang, Y., Liang, W. Q., Zhang, K. C., et al. (2021) Leukemia inhibitory factor promotes gastric cancer cell proliferation, migration, and invasion via the LIFR–Hippo–YAP pathway. *Ann. N. Y. Acad. Sci.* **1484**, 74–89
165. Yuan, L., Zhang, H., Liu, J., Malhotra, A., et al. (2022) STAT3 is required for Smo-dependent signaling and mediates Smo-targeted treatment resistance and tumorigenesis in Shh medulloblastoma. *Mol. Oncol.* **16**, 1009–1025
166. Johnson, R. W., Rhoades, J., and Martin, T. J. (2022) *Parathyroid hormone-related protein in breast cancer bone metastasis*, 1st Ed., Elsevier Inc., 10.1016/bs.vh.2022.04.006
167. Armanious, H., Gelebart, P., Mackey, J., Ma, Y., and Lai, R. (2010) STAT3 upregulates the protein expression and transcriptional activity of β -catenin in breast cancer. *Int. J. Clin. Exp. Pathol.* **3**, 654–664
168. Wen, Z., Zhong, Z., and Darnell, J. E. (1995) Maximal activation of transcription by stat1 and stat3 requires both tyrosine and serine phosphorylation. *Cell.* **82**, 241–250
169. Shi, X., Zhang, H., Paddon, H., Lee, G., et al. (2006) Phosphorylation of STAT3 serine-727 by cyclin-dependent kinase 1 is critical for nocodazole-induced mitotic arrest. *Biochemistry.* **45**, 5857–5867
170. Guanyi Huang, Yana, H., Yea, S., Tonga, C., and Yinga, Q.-L. (2014) STAT3 phosphorylation at tyrosine 705 and serine 727 differentially regulates mouse ESC fates. *Stem Cells.* **32**, 1149–1160
171. Lu, C., Xu, W., Shao, J., Zhang, F., et al. (2017) Nrf2 induces lipocyte phenotype via a SOCS3-dependent negative feedback loop on JAK2/STAT3 signaling in hepatic stellate cells. *Int. Immunopharmacol.* **49**, 203–211
172. Sun Honghua, Li Yanglong, Quan Xianglan, Chen Ning, et al. (2021) PIAS3/SOCS1-STAT3 axis responses to oxidative stress in hepatocellular cancer cells. *Am. J. Transl. Res.* **13**, 12395–12409
173. Visan, I. (2015) About STATs. *Nat. Immunol.* **16**, 688–688

174. Chen, X., Vinkemeier, U., Zhao, Y., Jeruzalmi, D., et al. (1998) Crystal structure of a tyrosine phosphorylated STAT-1 dimer bound to DNA. *Cell*. **93**, 827–839
175. McDaniel, J. M., Varley, K. E., Gertz, J., Savic, D. S., et al. (2017) Genomic regulation of invasion by STAT3 in triple negative breast cancer. *Oncotarget*. **8**, 8226–8238
176. Guo, H., Cheng, Y., Martinka, M., and Elwee, K. M. (2015) High LIFr expression stimulates melanoma cell migration and is associated with unfavorable prognosis in melanoma. *Oncotarget*. **6**, 25484–25498
177. Jacob, A., Jing, J., Lee, J., Schedin, P., et al. (2013) Rab40b regulates trafficking of MMP2 and MMP9 during invadopodia formation and invasion of breast cancer cells. *J. Cell Sci.* **126**, 4647–4658
178. Schmidt, U., Heller, G., Timelthaler, G., Heffeter, P., et al. (2021) The FAM3C locus that encodes interleukin-like EMT inducer (ILEI) is frequently co-amplified in MET-amplified cancers and contributes to invasiveness. *J. Exp. Clin. Cancer Res.* 10.1186/s13046-021-01862-5
179. Huang, D. W., Sherman, B. T., and Lempicki, R. A. (2009) Systematic and integrative analysis of large gene lists using DAVID bioinformatics resources. *Nat. Protoc.* **4**, 44–57
180. Huang, D. W., Sherman, B. T., and Lempicki, R. A. (2009) Bioinformatics enrichment tools: Paths toward the comprehensive functional analysis of large gene lists. *Nucleic Acids Res.* **37**, 1–13

Additional Data Tables (Tables 7-9)

Table 7 – List of 490 dysregulated genes from superimposition of three RNA-seq datasets. Alphabetized list of dysregulated genes, their NCBI IDs, symbols, and respective fold-change (FC) values relative to their parental counterpart. Column 7, labeled “Fig. 18B” shows the color corresponding to the exploded pie chart in Figure 21B that indicates gene’s expression “synergy”.

Row #	Gene ID	Gene Symbol	FC: shPCBP1/shSCR	FC: FAM3C KO/shPCBP1	FC: LIFR KO/shPCBP1	Fig. 21B
1	ENSMUSG00000097221.2	1810049J17Rik	1.544	0.239	0.075	Blue
2	ENSMUSG00000025194.6	Abcc2	4.443	3.868	2.365	Red
3	ENSMUSG00000032735.16	Ablim3	24.909	0.285	0.178	Blue
4	ENSMUSG00000075023.12	Accsl	6.030	0.302	0.575	Blue
5	ENSMUSG00000023328.15	Ache	4.861	0.533	0.285	Blue
6	ENSMUSG00000021228.16	Acot3	3.616	0.580	0.167	Blue
7	ENSMUSG00000060923.6	Acyp2	16.238	2.240	2.748	Red
8	ENSMUSG00000059901.13	Adamts14	15.549	3.731	1.616	Red
9	ENSMUSG00000020262.16	Adarb1	2.434	0.620	0.483	Blue
10	ENSMUSG00000020431.6	Adcy1	17.328	1.575	2.636	Red
11	ENSMUSG00000034730.18	Adgrb1	1.022	0.423	0.457	Blue
12	ENSMUSG00000023918.13	Adgrf4	2.236	0.363	0.585	Blue
13	ENSMUSG00000018500.3	Adora2b	2.080	2.188	1.950	Red
14	ENSMUSG00000025083.19	Afap1l2	1.530	1.520	0.595	Yellow
15	ENSMUSG00000019806.14	Aig1	23.364	2.460	1.902	Red
16	ENSMUSG00000035936.7	Aldh5a1	6.470	1.840	1.808	Red
17	ENSMUSG00000028766.11	Alpl	5.370	0.659	0.556	Blue
18	ENSMUSG00000027460.8	Angpt4	2.270	0.529	0.552	Blue
19	ENSMUSG00000052331.15	Ankrd44	2.840	2.981	3.057	Red
20	ENSMUSG00000074968.12	Ano3	16.784	0.127	0.295	Blue
21	ENSMUSG00000054662.9	Ano9	2.562	0.196	0.422	Blue
22	ENSMUSG00000006651.9	Aplp1	3.446	0.476	0.429	Blue
23	ENSMUSG00000040613.15	Apobec1	4.505	0.630	0.186	Blue
24	ENSMUSG00000044217.18	Aqp5	6.883	0.590	0.433	Blue
25	ENSMUSG00000022602.15	Arc	7.754	0.056	0.105	Blue
26	ENSMUSG00000019852.8	Arfgef3	10.050	0.154	0.161	Blue
27	ENSMUSG00000037148.9	Arhgap10	2.117	0.548	0.495	Blue
28	ENSMUSG00000048865.17	Arhgap30	5.088	0.297	0.306	Blue
29	ENSMUSG00000031389.18	Arhgap4	2.063	0.645	0.643	Blue
30	ENSMUSG00000040345.11	Arhgap9	1.429	0.509	0.406	Blue
31	ENSMUSG00000033436.14	Armxc2	3.293	0.298	0.261	Blue
32	ENSMUSG00000049804.10	Armxc4	3.684	1.519	0.652	Yellow
33	ENSMUSG00000005470.9	Asf1b	1.227	0.593	0.666	Blue
34	ENSMUSG00000037621.9	Atoh8	12.445	0.512	0.283	Blue
35	ENSMUSG00000037685.16	Atp8a1	22.907	0.286	0.537	Blue
36	ENSMUSG00000027312.15	Atrn	1.207	0.553	0.526	Blue
37	ENSMUSG00000000142.16	Axin2	6.540	0.495	0.479	Blue
38	ENSMUSG00000040270.17	Bach2	15.523	0.249	0.409	Blue
39	ENSMUSG00000030268.18	Bcat1	13.527	0.002	0.365	Blue
40	ENSMUSG00000021070.7	Bdkrb2	5.181	2.322	1.555	Red
41	ENSMUSG00000042182.17	Bend6	4.653	1.758	1.866	Red
42	ENSMUSG00000048186.15	Bend7	23.915	0.228	0.480	Blue
43	ENSMUSG00000052819.7	Best2	3.132	0.544	0.554	Blue
44	ENSMUSG00000098112.9	Bin2	2.665	0.307	0.244	Blue
45	ENSMUSG00000061132.14	Blnk	2.023	0.539	0.465	Blue
46	ENSMUSG00000028351.6	Brinp1	15.933	0.616	0.556	Blue
47	ENSMUSG00000020042.16	Btbd11	23.583	0.152	0.040	Blue
48	ENSMUSG00000017446.15	C1qtnf1	5.156	0.522	0.462	Blue
49	ENSMUSG00000032120.12	C2cd2l	1.417	0.627	0.470	Blue
50	ENSMUSG00000024164.16	C3	2.634	1.846	1.600	Red
51	ENSMUSG00000024112.17	Cacna1h	16.560	0.202	0.209	Blue
52	ENSMUSG00000054423.15	Cadps	8.682	3.958	1.824	Red
53	ENSMUSG00000029761.17	Cald1	1.427	1.522	1.546	Red
54	ENSMUSG00000060371.13	Caln1	19.253	0.495	3.852	Yellow

55	ENSMUSG00000031654.17	Cbln1	8.981	0.062	0.057	Blue
56	ENSMUSG00000053411.17	Cbx7	12.723	0.646	0.498	Blue
57	ENSMUSG00000036686.17	Cc2d1a	1.242	0.575	0.394	Blue
58	ENSMUSG00000004994.13	Ccdc130	1.071	0.656	0.515	Blue
59	ENSMUSG00000029875.6	Ccdc184	18.382	0.396	0.139	Blue
60	ENSMUSG00000048038.9	Ccdc187	15.092	0.062	0.133	Blue
61	ENSMUSG00000027676.12	Ccdc39	2.031	1.687	2.141	Red
62	ENSMUSG00000025808.18	Ccdc7a	1.609	1.592	1.988	Red
63	ENSMUSG00000030613.14	Ccdc90b	1.710	1.870	1.532	Red
64	ENSMUSG00000032532.8	Cck	2.105	0.389	0.128	Blue
65	ENSMUSG00000035385.6	Ccl2	3.206	1.767	1.593	Red
66	ENSMUSG00000035373.3	Ccl7	7.751	2.205	1.633	Red
67	ENSMUSG00000019122.9	Ccl9	5.166	4.048	2.958	Red
68	ENSMUSG00000044052.4	Ccr10	5.258	0.387	0.286	Blue
69	ENSMUSG00000028076.13	Cd1d1	6.955	0.304	0.373	Blue
70	ENSMUSG0000005763.16	Cd247	1.370	1.512	1.979	Red
71	ENSMUSG00000031871.10	Cdh5	7.669	1.625	0.236	Yellow
72	ENSMUSG00000025497.16	Cdhr5	3.848	0.485	0.468	Blue
73	ENSMUSG00000033966.9	Cdkl4	3.312	2.118	1.505	Red
74	ENSMUSG00000029646.4	Cdx2	1.641	0.584	0.452	Blue
75	ENSMUSG00000054169.8	Ceacam10	1.726	4.839	1.782	Red
76	ENSMUSG00000040729.9	Cep126	3.883	1.762	1.816	Red
77	ENSMUSG00000057074.7	Ces1g	16.526	0.172	0.236	Blue
78	ENSMUSG00000062826.8	Ces2f	1.518	2.035	1.670	Red
79	ENSMUSG00000078490.11	Cfap74	7.911	3.937	3.604	Red
80	ENSMUSG00000079502.9	Cfap77	6.500	5.708	2.896	Red
81	ENSMUSG00000035200.8	Chrb4	6.864	0.543	0.624	Blue
82	ENSMUSG00000027221.6	Chst1	10.999	0.239	0.196	Blue
83	ENSMUSG00000034612.8	Chst11	19.706	0.016	0.003	Blue
84	ENSMUSG00000037347.8	Chst7	19.978	0.184	0.203	Blue
85	ENSMUSG00000051159.17	Cited1	8.916	0.557	0.585	Blue
86	ENSMUSG00000037033.10	Clca3b	8.688	0.312	0.626	Blue
87	ENSMUSG00000047230.7	Cldn2	1.858	0.637	0.656	Blue
88	ENSMUSG00000013921.16	Clip3	9.442	2.799	2.261	Red
89	ENSMUSG00000024059.11	Clip4	7.146	0.607	0.565	Blue
90	ENSMUSG00000042190.13	Cmklr1	16.814	0.535	0.170	Blue
91	ENSMUSG00000001349.6	Cnn1	3.169	0.638	0.591	Blue
92	ENSMUSG00000044288.7	Cnr1	1.764	0.279	0.388	Blue
93	ENSMUSG00000030075.11	Cntn3	20.465	2.585	4.111	Red
94	ENSMUSG00000039419.18	Cntnap2	17.072	4.565	8.859	Red
95	ENSMUSG00000079465.9	Col4a3	2.857	1.803	1.745	Red
96	ENSMUSG00000048126.17	Col6a3	7.446	0.349	0.345	Blue
97	ENSMUSG00000028247.3	Coq3	6.538	0.120	0.364	Blue
98	ENSMUSG0000005220.11	Corin	12.885	1.772	2.722	Red
99	ENSMUSG00000052560.16	Cpne8	1.872	1.604	1.692	Red
100	ENSMUSG00000032060.11	Cryab	3.416	0.571	0.633	Blue
101	ENSMUSG00000071713.7	Csf2rb	17.652	0.360	0.303	Blue
102	ENSMUSG00000032515.9	Csrp1	2.477	0.656	0.420	Blue
103	ENSMUSG00000083282.4	Ctsf	11.189	0.532	0.625	Blue
104	ENSMUSG00000032359.15	Ctsh	10.023	0.645	0.478	Blue
105	ENSMUSG00000040327.17	Cul9	4.306	0.517	0.491	Blue
106	ENSMUSG00000052336.8	Cx3cr1	3.524	1.855	2.291	Red
107	ENSMUSG00000029375.7	Cxcl15	1.928	0.506	0.581	Blue
108	ENSMUSG00000020340.17	Cyfp2	23.145	0.006	0.101	Blue
109	ENSMUSG00000024087.5	Cyp1b1	7.667	3.623	3.842	Red
110	ENSMUSG00000063415.13	Cyp26b1	6.299	0.530	0.334	Blue
111	ENSMUSG0000005547.15	Cyp2a5	27.191	0.069	0.400	Blue
112	ENSMUSG00000025002.6	Cyp2c55	7.729	3.172	2.235	Red
113	ENSMUSG00000048826.8	Dact2	14.570	0.117	0.121	Blue
114	ENSMUSG00000021559.15	Dapk1	2.791	0.626	0.337	Blue
115	ENSMUSG00000041477.15	Dcp1b	20.522	0.158	0.475	Blue
116	ENSMUSG00000026674.10	Ddr2	4.078	6.418	4.624	Red
117	ENSMUSG00000030768.13	Disp1	3.629	1.961	2.548	Red
118	ENSMUSG00000000881.13	Dlg3	23.049	0.017	0.030	Blue
119	ENSMUSG00000047428.15	Dlk2	4.949	0.641	0.331	Blue
120	ENSMUSG00000023391.9	Dlx2	21.880	0.595	0.503	Blue
121	ENSMUSG00000045103.20	Dmd	19.671	0.586	0.621	Blue
122	ENSMUSG00000060962.13	Dmkn	9.276	0.589	0.236	Blue
123	ENSMUSG00000020657.17	Dnajc27	26.021	0.590	0.663	Blue

124	ENSMUSG00000044716.13	Dok7	10.091	0.114	0.095	Blue
125	ENSMUSG00000029168.15	Dpysl5	8.089	0.424	0.332	Blue
126	ENSMUSG00000001804.10	Dsg4	16.799	2.880	3.296	Red
127	ENSMUSG00000018983.10	E2f2	1.937	0.459	0.360	Blue
128	ENSMUSG00000010476.15	Ebf3	22.781	0.019	0.319	Blue
129	ENSMUSG00000053552.15	Ebf4	16.807	1.588	0.572	Yellow
130	ENSMUSG00000022842.19	Ece2	4.412	2.782	1.803	Red
131	ENSMUSG00000021367.9	Edn1	2.784	1.500	1.611	Red
132	ENSMUSG00000093661.2	Eif4e3	27.134	0.650	0.524	Blue
133	ENSMUSG00000028546.18	Elavl4	7.387	2.055	2.354	Red
134	ENSMUSG00000048988.9	Elfn1	10.530	0.144	0.129	Blue
135	ENSMUSG00000043460.8	Elfn2	5.999	6.777	0.649	Yellow
136	ENSMUSG00000001542.8	ElI2	1.067	1.664	1.765	Red
137	ENSMUSG00000041986.17	Elmod1	7.357	1.660	1.637	Red
138	ENSMUSG00000032262.14	Elov14	23.187	0.387	0.352	Blue
139	ENSMUSG00000058070.15	Eml1	5.432	2.760	1.616	Red
140	ENSMUSG00000033857.13	Engase	1.904	0.565	0.425	Blue
141	ENSMUSG00000028024.15	Enpep	1.489	0.520	0.098	Blue
142	ENSMUSG00000022425.17	Enpp2	5.583	1.583	0.511	Yellow
143	ENSMUSG00000019989.9	Enpp3	1.765	2.303	2.209	Red
144	ENSMUSG00000032446.15	Eomes	16.551	0.098	0.165	Blue
145	ENSMUSG00000005958.16	Ephb3	8.561	0.456	0.242	Blue
146	ENSMUSG00000029869.8	Ephb6	1.740	0.658	0.303	Blue
147	ENSMUSG00000038776.14	Ephx1	1.031	0.666	0.541	Blue
148	ENSMUSG00000050248.12	Evc2	20.968	0.025	0.075	Blue
149	ENSMUSG00000028838.12	Extl1	2.769	1.722	0.508	Yellow
150	ENSMUSG00000050147.10	F2r13	1.630	0.403	0.324	Blue
151	ENSMUSG00000023011.9	Faim2	4.074	0.492	0.457	Blue
152	ENSMUSG00000049119.15	Fam110b	22.138	0.171	0.147	Blue
153	ENSMUSG00000035095.12	Fam167a	1.551	0.035	0.060	Blue
154	ENSMUSG00000030207.16	Fam234b	2.393	0.559	0.522	Blue
155	ENSMUSG00000030859.9	Fam24a	2.592	1.608	2.244	Red
156	ENSMUSG00000092518.10	Fam71e2	16.551	1.951	2.238	Red
157	ENSMUSG0000003808.19	Farsa	1.389	0.640	0.555	Blue
158	ENSMUSG00000025738.9	Fbxl16	7.112	0.300	0.358	Blue
159	ENSMUSG00000041556.9	Fbxo2	1.731	0.448	0.460	Blue
160	ENSMUSG00000054200.8	Ffar4	8.795	0.301	0.393	Blue
161	ENSMUSG00000042826.14	Fgf11	7.673	0.639	0.560	Blue
162	ENSMUSG00000054252.19	Fgfr3	1.532	0.536	0.279	Blue
163	ENSMUSG00000047414.7	Flrt2	11.439	1.545	1.509	Red
164	ENSMUSG00000038552.15	Fndc4	20.344	0.440	0.482	Blue
165	ENSMUSG00000018844.7	Fndc8	3.030	0.499	0.457	Blue
166	ENSMUSG00000048721.3	Fndc9	9.280	0.026	0.170	Blue
167	ENSMUSG00000042812.6	Foxf1	25.729	0.018	0.019	Blue
168	ENSMUSG00000052135.9	Foxo6	1.554	0.649	0.301	Blue
169	ENSMUSG00000027238.18	Frmf5	2.687	0.443	0.526	Blue
170	ENSMUSG00000035615.13	Frmf1	3.586	4.381	4.606	Red
171	ENSMUSG00000027344.15	Fsip1	1.175	2.218	1.987	Red
172	ENSMUSG00000032750.14	Gab3	2.102	0.432	0.571	Blue
173	ENSMUSG00000047261.10	Gap43	24.594	0.397	0.432	Blue
174	ENSMUSG00000052957.9	Gas1	17.749	0.109	0.091	Blue
175	ENSMUSG00000015053.15	Gata2	11.550	0.294	0.316	Blue
176	ENSMUSG00000058624.14	Gda	13.831	0.045	0.075	Blue
177	ENSMUSG00000025089.16	Gfra1	17.969	0.149	0.181	Blue
178	ENSMUSG00000095547.2	Gm10719	12.810	1.670	3.747	Red
179	ENSMUSG00000075015.4	Gm10801	2.567	1.702	3.017	Red
180	ENSMUSG00000045699.5	Gm21411	15.107	1.732	2.053	Red
181	ENSMUSG00000034792.9	Gna15	1.605	0.617	0.407	Blue
182	ENSMUSG00000031748.17	Gnao1	14.744	0.530	0.545	Blue
183	ENSMUSG00000043004.14	Gng2	16.822	0.491	0.667	Blue
184	ENSMUSG00000031672.9	Got2	1.054	0.601	0.559	Blue
185	ENSMUSG00000029816.11	Gpnmb	21.706	0.269	0.226	Blue
186	ENSMUSG00000053101.4	Gpr141	5.270	5.965	2.592	Red
187	ENSMUSG00000040836.16	Gpr161	5.243	0.655	0.561	Blue
188	ENSMUSG00000038390.12	Gpr162	2.823	0.471	0.362	Blue
189	ENSMUSG00000040372.3	Gpr63	21.963	0.368	0.665	Blue
190	ENSMUSG00000051043.17	Gprc5c	8.076	0.060	0.082	Blue
191	ENSMUSG00000020656.17	Grhl1	1.947	0.537	0.597	Blue
192	ENSMUSG00000023982.9	Guca1a	5.279	1.640	0.651	Yellow

193	ENSMUSG00000045868.13	Gvin1	15.122	2.753	3.204	Red
194	ENSMUSG00000030074.10	Gxylt2	13.770	0.585	0.537	Blue
195	ENSMUSG00000073411.13	H2-D1	5.015	0.365	0.539	Blue
196	ENSMUSG00000061232.17	H2-K1	3.290	0.630	0.586	Blue
197	ENSMUSG00000079507.11	H2-Q1	2.585	0.635	0.382	Blue
198	ENSMUSG00000067235.15	H2-Q10	1.171	0.538	0.479	Blue
199	ENSMUSG00000060550.17	H2-Q7	2.748	0.624	0.441	Blue
200	ENSMUSG00000075297.11	H60b	2.382	1.522	1.570	Red
201	ENSMUSG00000069917.8	Hba-a2	4.990	0.588	0.350	Blue
202	ENSMUSG00000021730.9	Hcn1	3.763	0.346	0.161	Blue
203	ENSMUSG00000020875.10	Hoxb9	22.184	0.590	0.388	Blue
204	ENSMUSG0000001655.7	Hoxc13	22.570	0.062	0.064	Blue
205	ENSMUSG00000075394.5	Hoxc4	17.625	0.098	0.032	Blue
206	ENSMUSG00000022485.4	Hoxc5	18.640	0.067	0.027	Blue
207	ENSMUSG00000001661.6	Hoxc6	8.420	0.049	0.023	Blue
208	ENSMUSG00000036139.7	Hoxc9	17.024	0.369	0.122	Blue
209	ENSMUSG000000101174.9	Hoxd4	17.262	0.067	0.069	Blue
210	ENSMUSG00000031722.11	Hp	2.942	0.226	0.310	Blue
211	ENSMUSG00000035273.15	Hpse	3.715	0.540	0.542	Blue
212	ENSMUSG00000070407.6	Hs3st3b1	25.697	0.480	0.399	Blue
213	ENSMUSG00000091971.4	Hspa1a	3.788	0.448	0.241	Blue
214	ENSMUSG000000090877.4	Hspa1b	4.341	0.444	0.321	Blue
215	ENSMUSG00000006221.8	Hspb7	15.561	0.055	0.201	Blue
216	ENSMUSG00000021379.3	Id4	22.253	0.427	0.418	Blue
217	ENSMUSG00000078920.4	Ifi47	2.984	4.341	3.284	Red
218	ENSMUSG00000025491.15	Ifitm1	17.808	0.278	0.108	Blue
219	ENSMUSG00000096854.2	Ifnz	2.053	0.466	0.464	Blue
220	ENSMUSG00000048583.17	Igf2	9.749	0.471	0.077	Blue
221	ENSMUSG00000013367.6	Iglon5	1.801	0.422	0.434	Blue
222	ENSMUSG00000025997.14	Ikzf2	2.271	1.668	1.610	Red
223	ENSMUSG00000004371.16	Il11	9.342	1.571	4.149	Red
224	ENSMUSG00000078735.5	Il11ra2	15.561	0.576	0.540	Blue
225	ENSMUSG00000026981.16	Il1rn	5.727	2.313	1.908	Red
226	ENSMUSG00000026288.15	Inpp5d	1.071	2.951	0.587	Yellow
227	ENSMUSG00000034570.13	Inpp5j	1.186	0.489	0.374	Blue
228	ENSMUSG00000020227.11	Irx3	24.145	0.423	0.498	Blue
229	ENSMUSG00000031734.14	Irx3	5.656	0.012	0.152	Blue
230	ENSMUSG00000035692.8	Isg15	2.659	3.407	2.935	Red
231	ENSMUSG00000032318.13	Isl2	11.387	0.593	0.370	Blue
232	ENSMUSG00000037206.16	Islr	17.268	0.548	0.442	Blue
233	ENSMUSG00000051243.15	Islr2	2.928	0.338	0.109	Blue
234	ENSMUSG00000000290.14	Itgb2	5.427	2.318	1.861	Red
235	ENSMUSG00000032702.17	Kank1	1.147	0.538	0.629	Blue
236	ENSMUSG00000040606.15	Kazn	7.214	0.330	0.331	Blue
237	ENSMUSG00000018470.9	Kcnab3	2.165	0.602	0.419	Blue
238	ENSMUSG00000028033.17	Kcnq5	6.882	0.066	0.113	Blue
239	ENSMUSG00000033287.17	Kctd17	16.261	0.597	0.425	Blue
240	ENSMUSG00000072294.6	Klf12	18.247	0.557	0.576	Blue
241	ENSMUSG000000055148.8	Klf2	19.164	0.475	0.266	Blue
242	ENSMUSG00000044041.5	Krt13	18.402	0.241	0.161	Blue
243	ENSMUSG00000019718.9	L3hypdh	1.015	1.568	0.568	Yellow
244	ENSMUSG00000028581.18	Laptm5	8.768	0.665	0.236	Blue
245	ENSMUSG00000035202.9	Lars2	1.561	0.128	0.155	Blue
246	ENSMUSG00000020140.16	Lgr5	24.057	0.292	0.545	Blue
247	ENSMUSG00000042793.14	Lgr6	10.714	0.443	0.545	Blue
248	ENSMUSG00000000247.12	Lhx2	5.488	0.172	0.049	Blue
249	ENSMUSG00000054263.13	Lifr	25.138	0.369	0.498	Blue
250	ENSMUSG00000024395.10	Lims2	6.267	1.561	0.546	Yellow
251	ENSMUSG00000062044.17	Lmtk3	1.180	0.580	0.260	Blue
252	ENSMUSG00000025185.15	Loxl4	4.716	0.497	0.540	Blue
253	ENSMUSG00000090291.4	Lrrc10b	19.587	0.652	0.402	Blue
254	ENSMUSG00000033707.10	Lrrc24	3.073	0.580	0.602	Blue
255	ENSMUSG00000050587.15	Lrrc4c	1.194	2.844	1.912	Red
256	ENSMUSG00000052581.14	Lrrtm4	12.885	1.679	1.807	Red
257	ENSMUSG00000040488.19	Ltbp4	5.634	1.791	0.624	Yellow
258	ENSMUSG00000075602.11	Ly6a	15.628	0.574	0.266	Blue
259	ENSMUSG00000022587.15	Ly6e	7.290	0.534	0.461	Blue
260	ENSMUSG00000022586.12	Ly6i	17.256	0.660	0.338	Blue
261	ENSMUSG00000074622.5	Mafb	17.268	0.055	0.056	Blue

262	ENSMUSG00000062162.3	Mageb1	22.044	2.317	1.760	Red
263	ENSMUSG00000073069.3	Mageb2	22.804	3.860	2.530	Red
264	ENSMUSG00000055407.15	Map6	8.984	0.498	0.424	Blue
265	ENSMUSG00000031442.22	Mcf2l	16.543	0.473	0.378	Blue
266	ENSMUSG00000005410.7	Mcm5	2.266	0.477	0.417	Blue
267	ENSMUSG00000005583.17	Mef2c	6.024	0.040	0.020	Blue
268	ENSMUSG00000024593.16	Megf10	14.551	4.659	0.386	Yellow
269	ENSMUSG00000043289.13	Mei4	19.519	0.239	0.437	Blue
270	ENSMUSG00000031647.11	Mfap3l	3.103	1.799	2.033	Red
271	ENSMUSG00000031790.9	Mmp15	1.060	0.436	0.319	Blue
272	ENSMUSG00000029436.10	Mmp17	2.803	0.513	0.401	Blue
273	ENSMUSG00000031740.9	Mmp2	24.734	0.027	0.074	Blue
274	ENSMUSG00000048450.11	Msx1	24.526	0.103	0.106	Blue
275	ENSMUSG00000031765.9	Mt1	3.087	0.500	0.439	Blue
276	ENSMUSG00000031762.8	Mt2	7.454	0.436	0.402	Blue
277	ENSMUSG00000029651.17	Mtus2	6.121	6.835	4.866	Red
278	ENSMUSG00000020908.15	Myh3	13.881	0.474	0.287	Blue
279	ENSMUSG00000071203.7	Naip5	1.279	1.835	1.646	Red
280	ENSMUSG00000025588.5	Nat1	3.093	0.631	0.507	Blue
281	ENSMUSG00000052512.18	Nav2	5.967	0.352	0.359	Blue
282	ENSMUSG00000020181.19	Nav3	2.926	0.018	0.029	Blue
283	ENSMUSG00000002341.9	Ncan	19.734	0.577	0.546	Blue
284	ENSMUSG00000022488.10	Nckap1l	8.442	0.287	0.470	Blue
285	ENSMUSG00000049001.6	Ndnf	9.341	0.352	0.629	Blue
286	ENSMUSG00000036564.18	Ndrq4	5.417	0.376	0.515	Blue
287	ENSMUSG00000053702.17	Neb1	22.606	0.284	0.120	Blue
288	ENSMUSG00000032012.10	Nectin1	24.812	0.228	0.059	Blue
289	ENSMUSG00000006435.17	Neur1a	6.864	0.608	0.387	Blue
290	ENSMUSG00000001911.17	Nfix	2.850	0.597	0.407	Blue
291	ENSMUSG00000005397.9	Nid1	2.376	1.852	1.528	Red
292	ENSMUSG000000067219.10	Nipal1	5.069	1.692	2.042	Red
293	ENSMUSG00000015579.6	Nkx2-5	18.633	0.190	0.196	Blue
294	ENSMUSG000000074151.14	Nlrc5	5.806	0.449	0.142	Blue
295	ENSMUSG00000016626.11	Nlrp14	20.280	2.351	2.448	Red
296	ENSMUSG000000055994.16	Nod2	7.028	0.213	0.254	Blue
297	ENSMUSG00000027931.13	Npr1	4.493	0.634	0.454	Blue
298	ENSMUSG00000022206.8	Npr3	15.229	1.982	1.612	Red
299	ENSMUSG000000029126.8	Nsg1	3.680	0.645	0.595	Blue
300	ENSMUSG00000061356.14	Nuggc	2.747	3.427	0.619	Yellow
301	ENSMUSG000000057000.13	Nxf3	11.911	3.408	9.909	Red
302	ENSMUSG00000021913.9	Ogdhl	11.365	3.752	2.126	Red
303	ENSMUSG000000081724.5	Olfr129	12.848	1.938	1.931	Red
304	ENSMUSG00000045518.9	Onecut3	3.759	0.414	0.256	Blue
305	ENSMUSG000000026525.10	Opn3	2.942	1.647	1.547	Red
306	ENSMUSG00000022146.13	Osmr	13.831	0.123	0.134	Blue
307	ENSMUSG00000022330.6	Osr2	15.923	0.422	0.309	Blue
308	ENSMUSG00000005917.16	Otx1	8.378	0.470	0.463	Blue
309	ENSMUSG00000036353.14	P2ry12	3.756	2.704	2.825	Red
310	ENSMUSG000000036381.14	P2ry14	6.226	2.285	1.744	Red
311	ENSMUSG00000038168.6	P3h2	9.256	0.648	0.568	Blue
312	ENSMUSG00000025329.4	Padi1	5.646	0.438	0.406	Blue
313	ENSMUSG00000038507.7	Parp12	27.266	0.618	0.616	Blue
314	ENSMUSG00000001497.19	Pax9	1.178	0.411	0.582	Blue
315	ENSMUSG00000035566.8	Pcdh17	13.579	0.046	0.113	Blue
316	ENSMUSG00000051323.17	Pcdh19	16.534	0.069	0.080	Blue
317	ENSMUSG00000047910.7	Pcdhb16	1.800	1.701	1.552	Red
318	ENSMUSG00000044022.6	Pcdhb21	1.945	2.259	2.448	Red
319	ENSMUSG000000103144.2	Pcdhga1	5.353	2.644	1.945	Red
320	ENSMUSG00000022489.7	Pde1b	15.122	0.586	0.250	Blue
321	ENSMUSG00000028525.17	Pde4b	7.881	0.323	0.399	Blue
322	ENSMUSG00000053965.11	Pde5a	1.104	2.697	2.084	Red
323	ENSMUSG00000032006.16	Pdgfd	7.008	0.565	0.430	Blue
324	ENSMUSG00000021846.10	Peli2	1.546	0.380	0.441	Blue
325	ENSMUSG00000050751.15	Pgbd5	1.609	0.633	0.610	Blue
326	ENSMUSG00000050860.7	Phospho1	6.132	0.556	0.323	Blue
327	ENSMUSG00000041482.18	Piezo2	6.608	0.074	0.041	Blue
328	ENSMUSG00000028023.17	Pitx2	4.044	0.343	0.150	Blue
329	ENSMUSG00000026413.13	Pkp1	22.933	5.409	3.172	Red
330	ENSMUSG00000021822.4	Plau	16.161	0.293	0.422	Blue

331	ENSMUSG00000074170.6	Plekhf1	2.665	0.559	0.434	Blue
332	ENSMUSG00000026640.13	Plxna2	1.047	0.640	0.579	Blue
333	ENSMUSG00000018217.13	Pmp22	10.272	2.517	2.315	Red
334	ENSMUSG00000050424.10	Pnma5	5.214	0.394	0.349	Blue
335	ENSMUSG00000012889.9	Podnl1	4.102	0.531	0.427	Blue
336	ENSMUSG00000025608.10	Podxl	7.331	0.616	0.548	Blue
337	ENSMUSG00000048349.10	Pou4f1	16.266	0.034	0.128	Blue
338	ENSMUSG00000062168.13	Ppef1	6.576	1.837	1.572	Red
339	ENSMUSG00000025129.3	Ppp1r27	3.274	0.472	0.293	Blue
340	ENSMUSG00000075028.13	Prdm11	21.492	0.382	0.364	Blue
341	ENSMUSG00000039621.14	Prex1	16.560	0.181	0.221	Blue
342	ENSMUSG0000002688.9	Prkd1	21.067	0.351	0.614	Blue
343	ENSMUSG00000049409.10	Prokr1	4.137	0.543	0.287	Blue
344	ENSMUSG00000034686.9	Prr7	3.062	1.526	0.617	Yellow
345	ENSMUSG00000024114.16	Prss41	2.105	0.435	0.281	Blue
346	ENSMUSG00000039126.11	Prune2	5.726	0.182	0.125	Blue
347	ENSMUSG00000034117.4	Ptgdr2	2.954	0.657	0.423	Blue
348	ENSMUSG00000040016.17	Ptger3	15.923	0.066	0.051	Blue
349	ENSMUSG00000028399.19	Ptprd	3.281	3.103	4.422	Red
350	ENSMUSG00000033278.11	Ptprm	5.294	0.517	0.284	Blue
351	ENSMUSG00000035916.9	Ptprq	3.230	1.616	1.633	Red
352	ENSMUSG00000020674.18	Pxdn	28.527	2.733	1.613	Red
353	ENSMUSG00000032202.12	Rab27a	8.440	0.447	0.367	Blue
354	ENSMUSG00000029576.18	Radil	19.823	0.433	0.664	Blue
355	ENSMUSG00000041046.8	Ramp3	23.147	0.138	0.312	Blue
356	ENSMUSG00000071042.13	Rasgrp3	3.968	1.561	1.819	Red
357	ENSMUSG00000039601.17	Rcan2	18.970	0.118	0.209	Blue
358	ENSMUSG00000089789.2	Rdh1	1.504	0.374	0.393	Blue
359	ENSMUSG00000030110.14	Ret	10.910	0.117	0.099	Blue
360	ENSMUSG00000024186.16	Rgs11	2.920	0.514	0.479	Blue
361	ENSMUSG00000043333.13	Rhbdl2	5.114	0.322	0.228	Blue
362	ENSMUSG00000024143.16	Rhoq	1.160	1.531	1.507	Red
363	ENSMUSG00000093989.2	Rnasek	1.115	0.662	0.491	Blue
364	ENSMUSG00000034177.16	Rnf43	3.652	0.386	0.507	Blue
365	ENSMUSG00000020641.17	Rsad2	14.551	0.479	1.550	Yellow
366	ENSMUSG00000048617.17	Rtbdn	1.978	0.572	0.582	Blue
367	ENSMUSG00000006586.16	Runx111	15.536	0.214	0.348	Blue
368	ENSMUSG00000094018.3	S100a2	3.869	0.667	0.653	Blue
369	ENSMUSG00000063767.5	S100a7a	8.653	0.651	0.666	Blue
370	ENSMUSG00000067586.5	S1pr3	18.382	0.113	0.128	Blue
371	ENSMUSG00000049532.12	Sall2	22.484	0.419	0.295	Blue
372	ENSMUSG00000058656.14	Samd12	2.297	1.618	0.483	Yellow
373	ENSMUSG00000060487.8	Samd5	1.438	4.771	4.007	Red
374	ENSMUSG00000023927.16	Satb1	17.636	0.046	0.227	Blue
375	ENSMUSG00000046056.16	Sbsn	3.466	0.566	0.366	Blue
376	ENSMUSG00000057182.16	Scn3a	1.085	2.611	4.241	Red
377	ENSMUSG00000032511.18	Scn5a	8.893	0.365	0.256	Blue
378	ENSMUSG00000025743.15	Sdc3	2.503	0.467	0.202	Blue
379	ENSMUSG00000026580.17	Selp	6.646	3.488	3.697	Red
380	ENSMUSG00000028883.20	Sema3a	2.540	2.397	2.441	Red
381	ENSMUSG00000000627.16	Sema4f	13.614	0.367	0.235	Blue
382	ENSMUSG00000022231.11	Sema5a	15.933	0.053	0.074	Blue
383	ENSMUSG00000019647.17	Sema6a	22.625	0.018	0.022	Blue
384	ENSMUSG00000023232.18	Serinc2	15.933	0.314	0.608	Blue
385	ENSMUSG00000051029.9	Serpinb1b	6.274	2.416	1.639	Red
386	ENSMUSG00000079049.10	Serpinb1c	5.470	2.074	2.143	Red
387	ENSMUSG00000067001.12	Serpinb7	17.045	0.212	0.156	Blue
388	ENSMUSG00000057726.4	Serpinb9g	21.052	1.650	0.619	Yellow
389	ENSMUSG00000047281.4	Sfn	1.009	0.530	0.328	Blue
390	ENSMUSG00000057719.12	Sh3rf2	6.535	0.301	0.301	Blue
391	ENSMUSG00000030468.13	Siglecg	3.418	4.050	2.143	Red
392	ENSMUSG00000001995.10	Sipa1l2	2.653	0.601	0.305	Blue
393	ENSMUSG00000041920.15	Slc16a6	1.179	0.431	0.476	Blue
394	ENSMUSG00000022199.13	Slc22a17	3.496	0.309	0.380	Blue
395	ENSMUSG00000021509.6	Slc25a48	6.733	0.067	0.044	Blue
396	ENSMUSG00000024600.9	Slc27a6	12.165	12.193	5.568	Red
397	ENSMUSG00000029151.15	Slc30a3	16.551	0.466	0.231	Blue
398	ENSMUSG00000038602.8	Slc35f1	12.848	2.251	3.406	Red
399	ENSMUSG00000042195.10	Slc35f2	11.142	0.253	0.302	Blue

400	ENSMUSG00000057060.9	Slc35f3	1.708	3.497	1.667	Red
401	ENSMUSG00000022464.15	Slc38a4	24.652	0.187	0.598	Blue
402	ENSMUSG00000022756.18	Slc7a4	13.692	0.233	0.235	Blue
403	ENSMUSG00000026062.13	Slc9a2	7.554	0.524	0.375	Blue
404	ENSMUSG00000031129.10	Slc9a9	18.268	0.491	0.589	Blue
405	ENSMUSG00000063975.14	Slco1a5	2.243	1.972	2.212	Red
406	ENSMUSG00000025938.17	Slco5a1	26.103	2.265	1.506	Red
407	ENSMUSG00000027796.3	Smad9	8.851	0.322	0.249	Blue
408	ENSMUSG00000023886.11	Smoc2	22.509	0.356	0.246	Blue
409	ENSMUSG00000038248.9	Sobp	18.848	0.461	0.600	Blue
410	ENSMUSG00000041540.17	Sox5	4.684	0.087	0.513	Blue
411	ENSMUSG00000038560.8	Sp6	10.254	0.169	0.504	Blue
412	ENSMUSG00000068859.6	Sp9	7.037	2.207	1.671	Red
413	ENSMUSG00000026207.17	Speg	10.881	1.829	0.602	Yellow
414	ENSMUSG00000050359.8	Sprr1a	3.122	0.500	0.630	Blue
415	ENSMUSG00000046259.3	Sprr2h	1.908	0.644	0.452	Blue
416	ENSMUSG00000022114.6	Spry2	1.215	0.583	0.642	Blue
417	ENSMUSG00000039860.20	Srrm3	1.764	0.609	0.366	Blue
418	ENSMUSG00000042286.14	Stab1	2.198	3.001	1.511	Red
419	ENSMUSG00000031216.14	Stard8	7.750	0.302	0.208	Blue
420	ENSMUSG00000027030.16	Stk39	21.876	0.509	0.272	Blue
421	ENSMUSG00000028801.15	Stpg1	6.217	0.282	0.194	Blue
422	ENSMUSG00000032327.15	Stra6	4.383	0.620	0.607	Blue
423	ENSMUSG00000006800.15	Sulf2	8.754	0.279	0.170	Blue
424	ENSMUSG0000003271.18	Sult2b1	2.168	0.623	0.448	Blue
425	ENSMUSG00000022340.16	Sybu	7.979	0.643	0.599	Blue
426	ENSMUSG00000043079.18	Synpo	2.210	0.460	0.321	Blue
427	ENSMUSG00000027220.3	Syt13	27.652	0.506	0.629	Blue
428	ENSMUSG00000024339.13	Tap2	3.879	0.428	0.251	Blue
429	ENSMUSG00000031709.16	Tbc1d9	27.812	0.536	0.619	Blue
430	ENSMUSG00000031965.16	Tbx20	24.812	0.415	0.649	Blue
431	ENSMUSG00000051579.11	Tceal8	23.130	0.143	0.178	Blue
432	ENSMUSG00000055799.14	Tcf7l1	3.064	0.238	0.171	Blue
433	ENSMUSG00000052415.6	Tchh	21.056	0.177	0.320	Blue
434	ENSMUSG00000049336.17	Tenm2	8.326	1.934	1.689	Red
435	ENSMUSG00000042386.8	Tex13b	2.747	0.579	0.569	Blue
436	ENSMUSG00000010342.17	Tex14	15.536	0.554	0.617	Blue
437	ENSMUSG00000026380.11	Tfcp2l1	3.294	1.894	1.726	Red
438	ENSMUSG00000027082.16	Tfpi	3.767	0.363	3.256	Yellow
439	ENSMUSG00000039239.15	TGER2	4.385	0.525	0.388	Blue
440	ENSMUSG00000040152.9	Thbs1	1.305	2.461	2.059	Red
441	ENSMUSG00000040413.16	Timd2	8.000	3.250	2.422	Red
442	ENSMUSG00000042246.6	Tmc7	4.573	0.345	0.368	Blue
443	ENSMUSG00000026109.15	Tmeff2	2.894	4.070	4.397	Red
444	ENSMUSG00000043388.9	Tmem130	1.513	2.314	1.948	Red
445	ENSMUSG00000096847.3	Tmem151b	14.532	0.083	0.113	Blue
446	ENSMUSG00000037913.13	Tmem156	4.477	2.904	1.755	Red
447	ENSMUSG00000046157.14	Tmem229b	4.353	0.209	0.302	Blue
448	ENSMUSG00000049692.8	Tmem239	2.258	0.661	0.421	Blue
449	ENSMUSG00000054409.6	Tmem74	20.111	0.620	0.269	Blue
450	ENSMUSG00000010307.8	Tmem86a	1.907	0.569	0.596	Blue
451	ENSMUSG00000016942.7	Tmprss6	1.383	0.634	0.527	Blue
452	ENSMUSG00000030306.15	Tmtc1	1.491	2.298	2.102	Red
453	ENSMUSG00000028965.14	Tnfrsf9	2.598	4.377	2.236	Red
454	ENSMUSG00000031691.15	Tnpo2	1.442	0.647	0.571	Blue
455	ENSMUSG00000017607.10	Tns4	5.833	4.148	3.277	Red
456	ENSMUSG00000033327.19	Tnxb	4.961	0.498	0.368	Blue
457	ENSMUSG00000042870.16	Tom1	2.499	0.528	0.421	Blue
458	ENSMUSG00000026875.15	Traf1	8.560	1.644	0.546	Yellow
459	ENSMUSG00000030921.18	Trim30a	2.626	1.737	3.568	Red
460	ENSMUSG00000056596.9	Trnp1	3.818	0.630	0.611	Blue
461	ENSMUSG0000000244.18	Tspan32	4.344	0.516	0.500	Blue
462	ENSMUSG00000024424.16	Ttc39c	20.720	0.660	0.418	Blue
463	ENSMUSG00000046782.15	Ttc6	11.114	4.614	2.418	Red
464	ENSMUSG00000042734.7	Ttc9	11.290	0.320	2.769	Yellow
465	ENSMUSG00000035799.7	Twist1	19.964	0.032	0.033	Blue
466	ENSMUSG00000007805.5	Twist2	9.782	0.501	0.488	Blue
467	ENSMUSG00000032020.16	Ubash3b	22.506	0.242	0.066	Blue
468	ENSMUSG00000074502.5	Ubtfl1	4.396	2.246	3.381	Red

469	ENSMUSG00000006313.6	Upk1a	1.556	0.608	0.440	Blue
470	ENSMUSG00000045288.11	Ush1g	5.271	0.602	0.234	Blue
471	ENSMUSG00000021256.6	Vash1	6.897	0.589	0.412	Blue
472	ENSMUSG00000034777.3	Vax2	2.774	0.426	0.225	Blue
473	ENSMUSG00000091635.3	Vmn2r13	5.553	0.200	0.209	Blue
474	ENSMUSG00000091491.3	Vmn2r97	3.669	0.574	0.463	Blue
475	ENSMUSG00000059355.14	Wdr83os	1.076	0.499	0.487	Blue
476	ENSMUSG00000041245.14	Wnk3	1.638	7.608	3.018	Red
477	ENSMUSG00000027022.15	Xirp2	4.452	0.224	0.179	Blue
478	ENSMUSG00000073125.11	Xlr3b	4.967	3.035	1.938	Red
479	ENSMUSG00000058147.2	Xlr3c	8.967	2.842	2.506	Red
480	ENSMUSG00000044646.16	Zbtb7c	4.615	0.136	0.116	Blue
481	ENSMUSG00000034265.9	Zdhhc14	16.791	0.403	0.444	Blue
482	ENSMUSG00000068962.8	Zfp114	8.938	0.247	0.245	Blue
483	ENSMUSG00000062012.15	Zfp13	2.919	1.915	0.553	Yellow
484	ENSMUSG00000073176.5	Zfp449	3.261	1.535	1.768	Red
485	ENSMUSG00000068855.13	Zfp467	20.340	0.102	0.033	Blue
486	ENSMUSG00000039081.11	Zfp503	19.678	0.028	0.166	Blue
487	ENSMUSG00000062518.8	Zfp534	4.078	1.675	2.443	Red
488	ENSMUSG00000043456.18	Zfp536	18.394	0.112	0.068	Blue
489	ENSMUSG00000074194.5	Zfp791	2.067	0.529	0.601	Blue
490	ENSMUSG00000002266.18	Zim1	4.059	0.247	0.431	Blue

Table 8 – List of 58 dysregulated transcription factor genes. Alphabetized list of dysregulated transcription factor genes derived from Table 7. Column 7, labeled “Fig. 21B” shows the color corresponding to the exploded pie chart in Figure 21B that indicates gene’s expression “synergy”.

Row #	Gene ID	Gene Symbol	FC: shPCBP1/ shSCR	FC: FAM3C KO/ shPCBP1	FC: LIFR KO/ shPCBP1	Fig. 21B
1	ENSMUSG00000037621.9	Atoh8	12.445	0.512	0.283	Blue
2	ENSMUSG00000040270.17	Bach2	15.523	0.249	0.409	Blue
3	ENSMUSG00000029646.4	Cdx2	1.641	0.584	0.452	Blue
4	ENSMUSG00000032515.9	Csmp1	2.477	0.656	0.420	Blue
5	ENSMUSG00000023391.9	Dlx2	21.880	0.595	0.503	Blue
6	ENSMUSG00000018983.10	E2f2	1.937	0.459	0.360	Blue
7	ENSMUSG00000010476.15	Ebf3	22.781	0.019	0.319	Blue
8	ENSMUSG00000053552.15	Ebf4	16.807	1.588	0.572	Yellow
9	ENSMUSG00000032446.15	Eomes	16.551	0.098	0.165	Blue
10	ENSMUSG00000052135.9	Foxo6	1.554	0.649	0.301	Blue
11	ENSMUSG00000015053.15	Gata2	11.550	0.294	0.316	Blue
12	ENSMUSG00000020656.17	Grhl1	1.947	0.537	0.597	Blue
13	ENSMUSG00000020875.10	Hoxb9	22.184	0.590	0.388	Blue
14	ENSMUSG00000001655.7	Hoxc13	22.570	0.062	0.064	Blue
15	ENSMUSG00000075394.5	Hoxc4	17.625	0.098	0.032	Blue
16	ENSMUSG00000022485.4	Hoxc5	18.640	0.067	0.027	Blue
17	ENSMUSG00000001661.6	Hoxc6	8.420	0.049	0.023	Blue
18	ENSMUSG00000021379.3	Id4	22.253	0.427	0.418	Blue
19	ENSMUSG00000025997.14	Ikzf2	2.271	1.668	1.610	Red
20	ENSMUSG00000031734.14	Irx3	5.656	0.012	0.152	Blue
21	ENSMUSG00000032318.13	Isl2	11.387	0.593	0.370	Blue
22	ENSMUSG00000072294.6	Klf12	18.247	0.557	0.576	Blue
23	ENSMUSG000000055148.8	Klf2	19.164	0.475	0.266	Blue
24	ENSMUSG00000000247.12	Lhx2	5.488	0.172	0.049	Blue
25	ENSMUSG00000074622.5	Mafb	17.268	0.055	0.056	Blue
26	ENSMUSG00000005583.17	Mef2c	6.024	0.040	0.020	Blue
27	ENSMUSG00000048450.11	Msx1	24.526	0.103	0.106	Blue
28	ENSMUSG00000001911.17	Nfix	2.850	0.597	0.407	Blue
29	ENSMUSG00000015579.6	Nkx2-5	18.633	0.190	0.196	Blue
30	ENSMUSG00000045518.9	Onecut	3.759	0.414	0.256	Blue
31	ENSMUSG00000022330.6	Osr2	15.923	0.422	0.309	Blue
32	ENSMUSG00000005917.16	Otx1	8.378	0.470	0.463	Blue
33	ENSMUSG00000038507.7	Parp12	27.266	0.618	0.616	Blue
34	ENSMUSG00000001497.19	Pax9	1.178	0.411	0.582	Blue
35	ENSMUSG00000028023.17	Pitx2	4.044	0.343	0.150	Blue
36	ENSMUSG00000048349.10	Pou4f1	16.266	0.034	0.128	Blue
37	ENSMUSG00000075028.13	Prdm11	21.492	0.382	0.364	Blue
38	ENSMUSG00000006586.16	Runx1t	15.536	0.214	0.348	Blue
39	ENSMUSG00000049532.12	Sall2	22.484	0.419	0.295	Blue
40	ENSMUSG00000023927.16	Satb1	17.636	0.046	0.227	Blue
41	ENSMUSG00000027796.3	Smad9	8.851	0.322	0.249	Blue
42	ENSMUSG00000041540.17	Sox5	4.684	0.087	0.513	Blue
43	ENSMUSG00000038560.8	Sp6	10.254	0.169	0.504	Blue
44	ENSMUSG00000068859.6	Sp9	7.037	2.207	1.671	Red
45	ENSMUSG00000031965.16	Tbx20	24.812	0.415	0.649	Blue
46	ENSMUSG000000055799.14	Tcf7l1	3.064	0.238	0.171	Blue
47	ENSMUSG00000026380.11	Tfcp2l1	3.294	1.894	1.726	Red
48	ENSMUSG00000035799.7	Twist1	19.964	0.032	0.033	Blue
49	ENSMUSG00000007805.5	Twist2	9.782	0.501	0.488	Blue
50	ENSMUSG00000034777.3	Vax2	2.774	0.426	0.225	Blue
51	ENSMUSG00000044646.16	Zbtb7c	4.615	0.136	0.116	Blue
52	ENSMUSG00000062012.15	Zfp13	2.919	1.915	0.553	Yellow
53	ENSMUSG00000073176.5	Zfp449	3.261	1.535	1.768	Red
54	ENSMUSG00000068551.13	Zfp467	20.340	0.102	0.033	Blue
55	ENSMUSG00000039081.11	Zfp503	19.678	0.028	0.166	Blue
56	ENSMUSG00000043456.18	Zfp536	18.394	0.112	0.068	Blue
57	ENSMUSG00000074194.5	Zfp791	2.067	0.529	0.601	Blue
58	ENSMUSG00000002266.18	Zim1	4.059	0.247	0.431	Blue

Table 9 – Nucleotide sequences. This table represents the oligonucleotide sequences synthesized for the various experiments described in the preceding sections.

Row #	Description	Sequence (5' - 3')
1	FAM3C sgRNA: Exon 3, guide 1	GACCTGAGACGCCTGTCTAGGGG
2	FAM3C sgRNA: Exon 3, guide 2	TGCAAAGTTGGTAGTGCCG
3	FAM3C sgRNA: Exon 5, guide 1	CCTCCGAGGTACAAGTGTGGGAT
4	FAM3C sgRNA: Exon 5, guide 2	CGTGGGACCCAAGATCTGCCTGG
5	FAM3C Exon 3 Nested PCR primer FOR	ATCCCTTGACTTGGTGGGTATC
6	FAM3C Exon 3 Nested PCR primer REV	GGCAGAAGCAACTCAGCATG
7	FAM3C Exon 3 Flanking PCR primer FOR	TCCTGTAGACTTGGCAGTGTTT
8	FAM3C Exon 3 Flanking PCR primer REV	GAATAACAACGCAATGCGGGCA
9	FAM3C Exon 5 Nested PCR primer FOR	GTACAAGTGTGGGATCTCAAAGG
10	FAM3C Exon 5 Nested PCR primer REV	CACGACATTGGCTGCTCCAC
11	FAM3C Exon 5 Flanking PCR primer FOR	ATGCTCACCAGTGTGTTCC
12	FAM3C Exon 5 Flanking PCR primer REV	CTGTCACTCAATCCAGACC
13	LIFR sgRNA: Exon 2, guide 1	TTATTGTCTACCATCCACGA
14	LIFR sgRNA: Exon 2, guide 2	CATCTGACGATGCATGCAAA
15	LIFR sgRNA: Exon 6, guide 1	GTAAAGATACCGTTCAGCAC
16	LIFR sgRNA: Exon 6, guide 2	TACAGACCCTTGGTTCACATGGG
17	LIFR Exon 2 Nested PCR primer FOR	GATGGTAGACAATAAAGATCGAGG
18	LIFR Exon 2 Nested PCR primer REV	ATGCATCGTCAGATGCAGGAG
19	LIFR Exon 2 Flanking PCR primer FOR	GAGATCTAGGCTTCAGTCTCAATC
20	LIFR Exon 2 Flanking PCR primer REV	GTCAAAACTCAGAGAACTGTATCC
21	LIFR Exon 6 Nested PCR primer FOR	ACCTGCCCTTGCATGTGC
22	LIFR Exon 6 Nested PCR primer REV	CTTACAGGAGATGTTCTTCAGCG
23	LIFR Exon 6 Flanking PCR primer FOR	ATGATCGTGTGGTGTCACTTCC
24	LIFR Exon 6 Flanking PCR primer REV	CATCTCTCTGTTAGAGGAGTTGT
25	mLifr qPCR primer FOR	GGCTCATCACCACCTTCGAAAA
26	mLifr qPCR primer REV	CCAGGTGAGGAAGATCCTGTT
27	hFAM3C qPCR primer FOR	CAAGATCAGCATTGGACACAGC
28	hFAM3C qPCR primer REV	GCAAATGCTTCTCAGGGCAA
29	hLIFR qPCR primer FOR	AGTACTGGAGCCCTGTGAA
30	hLIFR qPCR primer REV	CACAACAAAATGTTATGTCTGAGCC
31	mLIFR promoter ChIP-qPCR primer FOR	GCCGATTTGCAAATTGCTGTAGA
32	mLIFR promoter ChIP-qPCR primer REV	AGAAATGTGCCAGACGGAGC
33	mTwist1 qPCR primer FOR	CAGCGGGTCATGGCTAACG
34	mTwist1 qPCR primer REV	AGACTGTCCATTTTCTCCTTCTCTG
35	mTwist1 promoter ChIP-qPCR primer FOR	ACCGCTGCCCCCAAATTT
36	mTwist1 promoter ChIP-qPCR primer REV	CGAGGTCCAAAAGAAGGCG
37	mStat3 qPCR primer FOR	AAGAGTCTCGCCTCCTCCAGA
38	mStat3 qPCR primer REV	ATCTGCTGCTTCTGTCACTAC
39	mMyc qPCR primer FOR	GCAGCGACTCTGAAGAAGAGC
40	mMyc qPCR primer REV	CGACCTCTTGGCAGGGGTTT
41	hFAM3C shRNA sequence	ATGTTGGAAGAGGGATCAATGCTCGAGC ATTGATCCCTTCCACCTTTTTT
42	hFAM3C shRNA reference (Sigma)	TRCN0000298583
43	non-human/mouse shRNA sequence (SCR)	CCGGCAACAAGATGAAGACCAACTC GAGTTGGTGCTTTCATCTTGTGTTTT
44	mLifr promoter region	GRCm38.p6 (15:7128390-7129810)
45	mTwist1 promoter region	GRCm38.p6 (12:33957107-33957916)